NASA TECHNICAL NOTE

NASA TN D-6573

NASA TN D-6573

FULL-SCALE WIND-TUNNEL TESTS OF A SMALL UNPOWERED JET AIRCRAFT WITH A T-TAIL

by Paul T. Soderman and Thomas N. Aiken

Ames Research Center
and
U.S. Army Air Mobility R&D Laboratory
Moffett Field, Calif. 94035

NATIONAL AERONAUTICS AND SPACE ADMINISTRATION • WASHINGTON, D. C. • NOVEMBER 1971

1. Report No.	2. Government Accession No.	3. Recipient's Catalog No.
NASA TN D-6573		

4. Title and Subtitle	5. Report Date
FULL-SCALE WIND-TUNNEL TESTS OF A SMALL UNPOWERED JET AIRCRAFT WITH A T-TAIL	November 1971
	6. Performing Organization Code
7. Author(s)	8. Performing Organization Report No.
Paul T. Soderman and Thomas N. Aiken	A-3135
9. Performing Organization Name and Address	10. Work Unit No.
Ames Research Center, NASA Moffett Field, Calif., 94035	126-13-01-43-00-21
	11. Contract or Grant No.
12. Sponsoring Agency Name and Address	13. Type of Report and Period Covered
National Aeronautics and Space Administration Washington, D. C., 20546	Technical Note
	14. Sponsoring Agency Code

15. Supplementary Notes

16. Abstract

The aerodynamic characteristics of a full-scale executive type jet transport aircraft with a T-tail were investigated in the Ames 40- by 80-Foot (12.2- by 24.4-meter) Wind Tunnel (subsonic). Static longitudinal and lateral stability and control characteristics were determined at angles of attack from -2° to +42°.

The aircraft wing had 13° of sweep and an aspect ratio of 5.02. The aircraft was tested power off with various wing leading- and trailing-edge high-lift devices. The basic configuration was tested with and without such components as engine nacelles, wing tip tanks and empannage. Hinge-moment data were obtained and downwash angles in the horizontal-tail plane location were calculated. The data were obtained at Reynolds numbers of 4.1×10^6 and 8.7×10^6 based on wing mean aerodynamic chord.

The model had static longitudinal stability through initial stall. Severe tail buffet occurred near the angle of attack for maximum lift. Above initial stall the aircraft had pronounced pitch-up, characteristic of T-tail configurations. A stable trim point was possible at angles of attack between 30° and 40° (depending on c.g. location and flap setting).

Hinge-moment data showed no regions that would result in adverse effects on stick force. Comparisons of wind-tunnel data and flight-test data are presented.

17. Key Words (Suggested by Author(s))	18. Distribution Statement
Deep stall T-tail aircraft General aviation	Unclassified – Unlimited

19. Security Classif. (of this report)	20. Security Classif. (of this page)	21. No. of Pages	22. Price*
Unclassified	Unclassified	99	$3.00

*For sale by the National Technical Information Service, Springfield, Virginia 22151

NOTATION

b	wing span, 10.40 m (34.1 ft)
c	wing chord measured parallel to the plane of symmetry, m (ft)
$\bar{c}$	mean aerodynamic chord, $\frac{2}{S}\int_0^{b/2} c^2\,dy$, 2.14 m (7.04 ft)
C_D	drag coefficient (wind axes), $\frac{\text{drag}}{q_\infty S}$
C_l	rolling-moment coefficient about stability axis, $\frac{\text{rolling moment}}{q_\infty S b}$
C_{l_β}	$\frac{\partial C_l}{\partial \beta}$ lateral stability parameter, per deg
$C_{l_{\delta_a}}$	$\frac{\partial C_l}{\partial \delta_a}$ aileron effectiveness parameter, per deg
C_L	lift coefficient (wind axes), $\frac{\text{lift}}{q_\infty S}$
C_{L_δ}	$\frac{\partial C_L}{\partial \delta_f}$ flap effectiveness parameter, per deg
C_m	pitching-moment coefficient about $\frac{\bar{c}}{4}$ (stability axes), $\frac{\text{pitching moment}}{q_\infty S \bar{c}}$
C_{m_α}	$\frac{\partial C_m}{\partial \alpha}$ longitudinal stability parameter, per deg
C_n	yawing-moment coefficient about moment center shown in figure 2(a) (stability axes), $\frac{\text{yawing moment}}{q_\infty S b}$
C_{n_β}	$\frac{\partial C_n}{\partial \beta}$ directional stability parameter, per deg
$C_{n_{\delta_r}}$	$\frac{\partial C_n}{\partial \delta_r}$ rudder effectiveness parameter, per deg
C_y	side-force coefficient (wind axes), $\frac{\text{side force}}{q_\infty S}$
i_t	horizontal-tail incidence angle, deg
q	dynamic pressure, N/m^2 (lb/sq ft)
R	Reynolds number, $\frac{V_\infty \bar{c}}{\nu}$
S	wing area, 21.50 m^2 (231.77 ft^2)
V_∞	free-stream velocity, m/sec (ft/sec)

y	spanwise distance perpendicular to the plane of symmetry, m (ft)
α	angle of attack of fuselage, deg
β	angle of sideslip, deg; positive – nose to left
δ_a	trailing-edge aileron deflection angle, deg; positive – left aileron trailing edge down
δ_e	elevator deflection angle, deg; positive – trailing edge down
δ_f	trailing-edge flap deflection measured from wing chord line, deg
δ_r	rudder deflection angle, deg; positive - trailing edge left
δ_s	spoiler deflection angle, deg
ϵ	average downwash at the tail location with respect to free stream, deg
η	wing semispan station, $\frac{y}{b/2}$
$\Lambda_{c/4}$	sweep angle of quarter-chord line, 13°
ν	free-stream kinematic viscosity, m^2/sec (ft^2/sec)
l	leading-edge contours defined on figure 2(d)

Subscripts

L	left
max	maximum
R	right
t	tail
u	uncorrected
Δ	change
∞	free stream

Hinge Moments

Positive hinge moments tend to move the control surface in the direction of positive deflection. The average chord aft of the hinge line was used for the reference length.

Aileron

$$C_{h_a} = \frac{\text{hinge moment}}{qS_a\bar{c}_a}$$ where $S_a = 0.544\ m^2\ (5.85\ ft^2)$, $\bar{c}_a = 0.38\ m\ (1.24\ ft)$

Rudder

$$C_{h_r} = \frac{\text{hinge moment}}{qS_r\bar{c}_r}$$ where $S_r = 0.609\ m^2\ (6.56\ ft^2)$, $\bar{c}_r = 0.46\ m\ (1.51\ ft)$

Elevator

$$C_{h_e} = \frac{\text{hinge moment}}{qS_e\bar{c}_e}$$ where $S_e = 0.635\ m^2\ (6.83\ ft^2)$, $\bar{c}_e = 0.29\ m\ (0.96\ ft)$

Horizontal stabilizer

$$C_{h_h} = \frac{\text{hinge moment}}{qS_h\bar{c}_h}$$ where $S_h = 5.02\ m^2\ (54.0\ ft^2)$, $\bar{c}_h = 1.17\ m\ (3.83\ ft)$

Note: S_e is the area of the right or left elevator; S_h is the total area of the horizontal stabilizer.

FULL–SCALE WIND–TUNNEL TESTS OF A SMALL UNPOWERED JET AIRCRAFT WITH A T–TAIL

Paul T. Soderman and Thomas N. Aiken

Ames Research Center
and
U.S. Army Air Mobility R&D Laboratory
Moffett Field, California 94035

SUMMARY

The aerodynamic characteristics of a full-scale executive type jet transport aircraft with a T-tail were investigated in the Ames 40- by 80-Foot (12.2- by 24.4-m) Wind Tunnel (subsonic). Static longitudinal and lateral stability and control characteristics were determined at angles of attack from -2° to +42°.

The aircraft wing had 13° of sweep and an aspect ratio of 5.02. The aircraft was tested power off with various wing leading- and trailing-edge high-lift devices. The basic configuration was tested with and without such components as engine nacelles, wing tip tanks, and empennage. Hinge-moment data were obtained and downwash angles in the horizontal-tail plane location were calculated. The data were obtained at Reynolds numbers of 4.1×10^6 and 8.7×10^6 based on wing mean aerodynamic chord.

The model had static longitudinal stability through initial stall. Severe tail buffet occurred near the angle of attack for maximum lift. Above initial stall the aircraft had pronounced pitch-up, characteristics of T-tail configurations. A stable trim point was possible at angles of attack between 30° and 40° (depending on c.g. location and flap setting).

Hinge-moment data showed no regions that would result in adverse effects on stick force. Comparisons of wind-tunnel data and flight-test data are presented.

INTRODUCTION

Most small aircraft, including executive jet transports, are designed with a minimum of wind-tunnel data. Furthermore, flight tests are likely to be qualitative rather than quantitative. As a result, the designer has little opportunity to verify his design predictions.

Therefore, to aid designers the present investigation was conducted to determine the static longitudinal and lateral stability and control characteristics through deep stall of a full-scale executive jet aircraft. The deep stall testing was conducted to see if the aircraft exhibited unfavorable characteristics at high angles of attack because of its T-tail. Some of these problems and

related research can be found in references 1 through 4. Unfortunately, it cannot be determined from wind-tunnel tests of unpowered aircraft whether the powered aircraft can become locked in deep stall.

AIRCRAFT AND APPARATUS

In figures 1(a) and (b) the model is shown mounted in the Ames 40- by 80-Foot (12.2- by 24.4-m) Wind Tunnel. Pertinent dimensions of the basic model configurations are given in figures 2(a) and (b).

Wing

The wing had a quarter chord sweep of 13°, an aspect ratio of 5.02, a taper ratio of 0.507, and a dihedral angle of 2.5°. The airfoil section was an NACA 64A–109 modified by increased camber and chord at the leading edge (fig. 2(d)) which was minimum at the root and maximum at the wing-tip tank junction.

High Lift Devices

Flap details- The basic wing had a single slotted, extendable (Fowler) flap (fig. 2(c)) located from the edge of the fuselage at 7.1 percent to 61.2 percent η. Maximum flap angle was 40° at the lower Reynolds number and 38° at the higher Reynolds number because of air load effects. A center section flap that extended under the fuselage was tested (fig. 1(b)). There were no gaps between the sides of the center section flap and the main flaps.

Leading-edge contours- The drooped leading edges of the basic wing were removed, part way through the test, and replaced by various leading-edge contours (fig. 2(d)). The dimensions of the leading edges varied linearly from root to tip.

Wing planform modification- In an attempt to delay the stalling of the wing tip region, fences were placed first on the tops and then on the sides of the tip tanks (fig. 2(e)).

Lateral Controls

Ailerons- The ailerons (fig. 2(b)) had relatively blunt leading edges and balance tabs to decrease stick force. As the ailerons were moved, the balance tabs moved in the opposite direction such that

$$\alpha_{tab} = -(5/6)\delta_a$$

where α_{tab} is the tab angle relative to the aileron chord and δ_a is the aileron angle relative to the wing chord.

Spoilers- The chords of the spoilers were 10.25 percent of the wing chord at midspoiler and were located from 22.2 percent to 49.4 percent semispan (see fig. 2(b)). Spoiler angles ranged from 0° to 42°. In addition to the basic wing spoilers, dummy spoilers were tested outboard (fig. 2(f)).

Tail

The geometry of the horizontal and vertical tails is described in figure 2(g). Pitch control was provided by an all-movable tail that had an available deflection range of 0.4° to -7.0° and by a 32 percent chord elevator with balance horn. The elevator angle was variable from 15° to -15°. The rudder (25 percent chord) had a deflection range of 30° to -30° and had a trim tab that was locked at 0°. The horizontal stabilizer was used for aircraft trim.

Nacelles

Engine nacelle detail and location are shown in figure 2(h). A constant-area circular duct was installed in each nacelle to allow mass flow conditions of 4.81 kg/sec (10.6 lb/sec) of air at standard conditions, similar to that of the jet engines for idle airflow at a Mach number of 0.2. Static and total pressures were measured with rakes at the aft ends of the ducts to determine the actual dynamic pressure of the nacelle flow and the internal nacelle drag (which was removed from the data). The nacelles were removed from the pylons during a part of the test.

Tip Tanks

Wing tip tank detail and location are shown in figure 2(b). All data are presented with the tip tanks on unless stated otherwise.

TESTING AND PROCEDURE

Forces and moments were measured for the model through an angle-of-attack range from -2° to 42°. Pitching-moment data were computed about a moment center location at 25 percent $\bar{c}$. The center-of-gravity range for this aircraft is 16 percent $\bar{c}$ to 31.5 percent $\bar{c}$. Tests were conducted at Reynolds numbers of 4.1×10^6 and 8.7×10^6 based on a mean aerodynamic chord of 2.14 m (7.04 ft) and speeds of 27.8 m/sec (54.2 knots) and 59.0 m/sec (115.0 knots), respectively. These speeds correspond to dynamic pressures of 478.8 N/m^2 (q = 10 psf) and 2156 N/m^2 (q = 45 psf).

Tests were conducted with the basic configuration[1] at several tail incidences with variable elevator, rudder, aileron, spoiler, and flap settings. Data were also obtained with landing gear down. The maximum angle of attack at $R = 8.7 \times 10^6$ was 16° (tail on) because of tail buffet load limitations. Most data, tail on, at angles of attack higher than 16° were taken at a Reynolds number of 4.1×10^6.

[1] Basic configuration refers to the airplane as shown in figure 1(a) with engine nacelles, tip tanks, and empennage on model. Control surfaces were at zero angle unless stated otherwise.

DATA ACQUISITION AND REDUCTION

Forces and moments were measured on the wind-tunnel six-component balance. Torque tubes in the elevators and rudder were gaged to provide hinge-moment data.

All data were corrected for strut tares, nacelle internal flow drag, and wind-tunnel wall effects. Nacelle internal flow drag was calculated from pressure measurements in the nacelle ducts, and $\Delta C_D = 0.0005 \cos \alpha$ was subtracted from model drag. Corrections added for wind-tunnel wall effects were

$$\Delta\alpha = 0.506\, C_{Lu}$$

$$\Delta C_D = 0.0088\, C_{Lu}^2$$

$$\Delta C_m = 0.0171\, C_{Lu} \text{ (tail on runs only)}$$

ACCURACY OF MEASUREMENT

The various quantities measured were accurate within the following limits, which include error limits involved in calibrating, reading, and reducing the data.

Angle of attack	±0.2°
Angle of sideslip	±0.5°
Free-stream dynamic pressure	±0.5 percent
Control surface settings	±0.5°

	Force or moment	Coefficients at $R = 8.7 \times 10^6$
Lift	±22.4 N (±5 lb)	±0.0005
Drag	±13.4 N (±3 lb)	±.0003
Side force	±13.4 N (±3 lb)	±.0003
Pitching moment	±271 J (±200 ft-lb)	±.0027
Yawing moment	±136 J (±100 ft-lb)	±.0003
Rolling moment	±475 J (±350 ft-lb)	±.0010

RESULTS

Table 1 is the index to the figures. The longitudinal data are presented in figures 3 to 18 and the lateral data in figures 19 to 30. Downwash and hinge-moment data are given in figures 31 and 32, respectively.

DISCUSSION

Longitudinal Characteristics

Flap effectiveness- The longitudinal characteristics of the basic airplane at $R = 8.7 \times 10^6$ with three flap settings are shown in figure 3(a). The flap effectiveness parameter, C_{L_δ}, was 0.015/deg for the 20° flap setting and 0.013/deg for the 38° flap setting. A theoretical flap effectiveness estimate was made using the simplified lifting-surface theory of reference 5, which gave the value of C_{L_δ} as 0.022/deg, almost 60 percent higher than measured. This discrepancy was probably due to a nonoptimum gap setting for the single-slotted, Fowler type flaps. A comparison of small-scale with full-scale wind-tunnel data to be discussed in a later section shows that small-scale flap effectiveness is closer to the theoretical value. This suggests that the flap gap choice was based on small-scale test data and not corrected properly for full-scale Reynolds number effects.

Maximum lift- Figure 3(a) shows the basic stall characteristics of the aircraft at $R = 8.7 \times 10^6$. Because of severe buffet on the tail as it penetrated the wing wake, the tail was guy-wired as shown in figure 1(a).[2] In addition, some of the data were taken at a reduced Reynolds number of 4.1×10^6. The tail buffet acted as a strong stall warning. Figure 3(b) shows the longitudinal characteristics at $R = 4.1 \times 10^6$. Increasing the Reynolds number from 4.1×10^6 to 8.7×10^6 caused an increase in maximum lift coefficient of 0.19 (flaps down) and 0.20 (flaps up) as shown in figure 4. The high Reynolds number condition is closer to actual flight conditions. Observation of tufts on the left wing indicated that a region of separated flow developed near the wing leading edge tip tank junction at 8° angle of attack (this did not happen with tip tanks off). As angle of attack was increased the region of separated flow spread aft and inboard. Near $C_{L_{max}}$ the wing root began to stall. Both regions grew with angle of attack until most of the wing stalled and lift dropped.

Static stability- A study of the variation of the stick-fixed pitching-moment coefficient with angle of attack (fig. 5(a)) shows that the airplane was stable through maximum lift (even for aft c.g. limit of 31.5 percent $\bar{c}$). Above maximum lift, the classic deep stall situation occurred that will be discussed later. The data presented for c.g. at 25 percent $\bar{c}$ give $C_{m_\alpha} = -0.0186$/deg. At stall the aircraft experienced a slight nose down pitching moment. The stick-free static stability characteristics, determined from hinge-moment and pitching-moment curves, are shown in figure 5(b) (data are shown for c.g. at 25 percent $\bar{c}$). Freeing the elevator reduced the stability, but the aircraft did not become unstable. For the aft c.g. case (31.5 percent $\bar{c}$), $\delta_f = 0°$, $\alpha = 0°$, C_{m_α} was reduced from -0.0185 to -0.005/deg.

Deep stall- As illustrated in figure 6, the airplane was unstable above maximum lift (stick-fixed) with the center of gravity at the quarter chord, and maximum nose-down trim until an angle of attack of 32° was reached at which point static stability was again attained. Furthermore, the pitching moments became zero or slightly positive above $\alpha = 28°$ flaps down. Thus it may be possible (at low Reynolds number) for the airplane to reach a region of positive pitching moment and pitch up to $\alpha = 32°$, a trim condition (power off) if the pilot does not take corrective action. However, aircraft rolloff may preclude this possibility, as will be discussed in a later section. As shown by the axes superimposed on figure 6(b), at forward c.g. the pitching moments do not become positive, but at the aft c.g. the aircraft would reach the positive pitching-moment region

[2] The wires had very little effect on the data.

sooner and could pitch up to trim at $\alpha = 39°$ (flaps up or down) while completely stalled. Figure 6(c) shows that while the effect of sideslip was beneficial, 8° of sideslip changed the pitching moment only 0.06 at $\alpha = 32°$.

With the flaps up, elevator effectiveness was maintained at all angles of attack but pitching-moment increment due to full elevator deflection at angles of attack greater than 24° is approximately one fourth that at angles of attack below stall (see fig. 7(a)). Therefore, recovery from deep stall (flaps up, c.g. at 25 percent $\bar{c}$) would be possible using the elevator, but the time it takes to rotate the nose down may be long. With the c.g. in the aft location there is insufficient elevator effectiveness to recover from deep stall. With the flaps full down (fig. 7(b)) there was an almost complete loss of elevator control power above $\alpha = 24°$. Since the data (flaps up and down) were taken with the horizontal stabilizer leading edge full up, any movement of that control surface would only make the pitching moments more positive.

Figures 8 and 9 illustrate the effects of horizontal stabilizer incidence and removal of the empennage, respectively, on the longitudinal characteristics.

Effect of wing tip tanks, engine nacelles, and landing gear- Figure 10 shows that the wing tip tanks caused an increase in lift coefficient and lift curve slope primarily because of the increased wing area and aspect ratio (reference area was not changed). The drag change was small up to $C_{L_{max}}$. The addition of the tip tanks made the aircraft slightly more stable in pitch.

The engine nacelles caused a decrease in lift, especially with flaps down (fig. 11). This decrease was probably due to interference with flow around the wing that reduced wing lift since the nacelles did not develop negative lift or reduce tail lift. This explanation is substantiated by the increase in nose-down pitching moment with the nacelles on the aircraft. If the nacelles had developed negative lift or if the tail lift had been reduced, the pitching-moment change would have been nose up. The fact that the wing tips were probably not affected by the nacelles accounts for the nose-down pitching-moment change (i.e., the lift loss was inboard).

The landing gear effect on the longitudinal characteristics is small (fig. 12).

High-lift devices- The effects of four wing leading edges are given in figures 13(a) and (b), flaps up and down. For the flap down case the leading edge l_4, which had the greatest droop, increased maximum lift beyond the value achieved by l_3, the basic configuration leading edge.

In an attempt to improve the $C_{L_{max}}$ of the airplane, fences were placed on the tops and, later, sides of the tip tanks to alleviate flow separation at the junction of the tip tank and wing. Fences on the sides of the tip tanks caused an increase in lift due to the increased wing area and aspect ratio (fig. 14). In no case was the flow separation alleviated near the tip.

The center body flap (fig. 1(b)) caused a very small reduction in lift and drag of the model and a very slight change in pitching moment (fig. 15). The reason for the reduction in lift and drag is unknown.

Drooping the ailerons 13.7° increased maximum lift coefficient by 0.1 (fig. 16). Since drooped ailerons reduce roll control, outboard spoilers were tested. These will be discussed in the lateral control section.

Effect of spoilers- Runs were made with various right and left spoiler deflections (see figs. 17(a) and (b)). The deflection of one or both spoilers 42° caused a nose-down pitching-moment change probably because of an induced increase of tail angle of attack. This supposition checks with figure 17(c) that shows very little change in pitching moment with outboard spoiler deflection. It was expected that the flow field of the tail would not be affected greatly by deflection of the outboard spoilers. The drag was increased 80 percent with full spoiler deflection.

Comparison of wind-tunnel and flight-test data- A comparison of Ames 40- by 80-Foot (12.2- by 24.4-m) Wind Tunnel data, Wichita State University 7- by 10-Foot (2.1- by 3.1-m) Wind Tunnel data and Lear Jet flight-test data is made in reference 6. Two figures from that paper are presented in this report as figures 18(a) and (b). Results show good agreement between full-scale wind-tunnel and flight-test data. Reynolds number effects account for most of the difference between small-scale and full-scale results.

Lateral and Directional Stability and Control

The lateral characteristics of the airplane are shown in figures 19 to 23, and lateral and directional control effectiveness in figures 24 to 29. Stability derivatives C_{n_β} and C_{l_β} are plotted versus angle of attack in figure 30. These data show that the airplane had positive effective dihedral ($-C_{l_\beta}$) over the normal operating range and was directionally stable statically (positive C_{n_β}). With the tail removed (fig. 22) the nonzero rolling moment and side force at $\beta = 0°$ were probably due to flap misalinement. The flaps had been removed and reinstalled on the model prior to these runs. The data in figure 23 show that as the model stalled with flaps up, it tried to roll left (left wind down) and with flaps down, it tried to roll right (right wing down). The change in roll direction at stall was probably caused by asymmetric deflection of the flaps. The rolling moment, flaps down, was greater than that produced by full opposite aileron deflection. This severe rolloff in stall would complicate recovery, but it might prevent a deep stall condition.

Control effectiveness- Aileron roll power was fairly constant below stall but decreased rapidly in stall (fig. 24). The airplane had slight favorable yaw due to aileron above 6° angle of attack. Figures 24(b)–(d) show the control power due to one aileron. The nonzero side force was probably due to model misalinement in the test section. Figure 25 is a summary plot of $C_{l_{\delta_a}}$ versus angle of attack.

Rudder deflection affected the longitudinal characteristics very little. Figure 26 shows the lateral effects of rudder deflection. The rudder was capable of holding the airplane in sideslip between $-15° \leqslant \beta \leqslant 15°$.

The control power of the basic spoiler is shown in figure 28(a) as plots of C_y, C_n, and C_l versus left spoiler angle (right spoiler full down). Figure 28(b) shows the effectiveness of dummy outboard spoilers S_1, S_2, and S_3. These spoilers were more effective than ailerons or inboard spoilers for lateral control. The lateral characteristics of the airplane with the landing gear extended are shown in figure 29. Comparison with the results in figure 19(a) (landing gear retracted) indicates that the landing gear had a small effect on C_y vs. β but only a slight effect on C_n and C_l vs. β.

Downwash at the Horizontal Tail

An average downwash angle at the horizontal stabilizer was estimated from curves of C_m vs. α for several tail incidence angles. The intersection of the tail-on curves with the tail-off curve are points where tail lift is zero; and for a symmetrical horizontal stabilizer

$$\epsilon = \alpha + i_t$$

Figure 31 shows the results of the above calculation, which were identical for both Reynolds number cases.

Hinge Moments

Typical curves of hinge-moment coefficient C_h versus angle of attack and C_h versus control position are presented in figures 32(a)–(h) for aileron, elevator, rudder, and horizontal stabilizer. The data were obtained at $R = 8.7 \times 10^6$ to approximate actual flight conditions. These results show no control force reversal for any of the controls within the normal operating range.

CONCLUSIONS

A full-scale wind-tunnel investigation was made of a small jet aircraft with a T-tail to determine the longitudinal and lateral stability and control characteristics through deep stall, power off. The following conclusions were drawn from the results of the investigation:

1. The airplane had stick-fixed static longitudinal stability at angles of attack up to stall for the full c.g. range. With the stick free, stability was reduced but the aircraft did not become unstable.

2. Before stall the tail experienced severe buffet as it penetrated the wing wake, and, in stall, the airplane tended to roll right wing down or left wing down depending on flap angle. The tail buffet acted as a strong stall warning, that might prevent deep stall entry during actual flight conditions. However, the rolling moment in stall, flaps down, was greater than that produced by full opposite aileron deflection.

3. Above stall, the airplane was unstable in pitch, and the pitching moments could become positive, depending on c.g. A trim condition in deep stall ($\alpha = 39°$) with a large reduction in elevator control was possible. With the c.g. in the aft position, elevator control and horizontal stabilizer control were insufficient for recovery from deep stall trim.

4. The airplane was directionally stable, below stall, and had positive effective dihedral.

Ames Research Center
National Aeronautics and Space Administration
Moffett Field, Calif., 94035, July 6, 1971

REFERENCES

1. Aoyagi, Kiyoshi; and Tolhurst, William H., Jr.: Large-Scale Wind-Tunnel Tests of a Subsonic Transport With Aft Engine Nacelles and High Tail. NASA TN D–3797, 1967.

2. Ray, Edward J.; and Taylor, Robert T.: Effect of Configuration Variables on the Subsonic Longitudinal Stability Characteristics of a High-Tail Transport Configuration. NASA TM X–1165, 1965.

3. Trubshaw, E. B.: Low Speed Handling With Special Reference to the Super Stall. J. Roy. Aeronaut. Soc., vol. 70, no. 667, pp. 695–704, July 1966.

4. Thomas, H. H. B. M.: A Study of the Longitudinal Behavior of an Aircraft Near-Stall and Post-Stall Conditions. R.A.E. TM Aero 953, 1966.

5. DeYoung, John: Theoretical Symmetric Span Loading Due to Flap Deflection for Wings of Arbitrary Plan Form at Subsonic Speeds. NASA Rep. 1071, 1952.

6. Neal, Ronald D.: Correlation of Small-Scale and Full-Scale Wind-Tunnel Data With Flight–Test Data on the Lear Jet Model 23. Paper 700237 presented at SAE National Business Aircraft Meeting (Wichita, Kansas), March 1970.

TABLE 1.– INDEX TO FIGURES

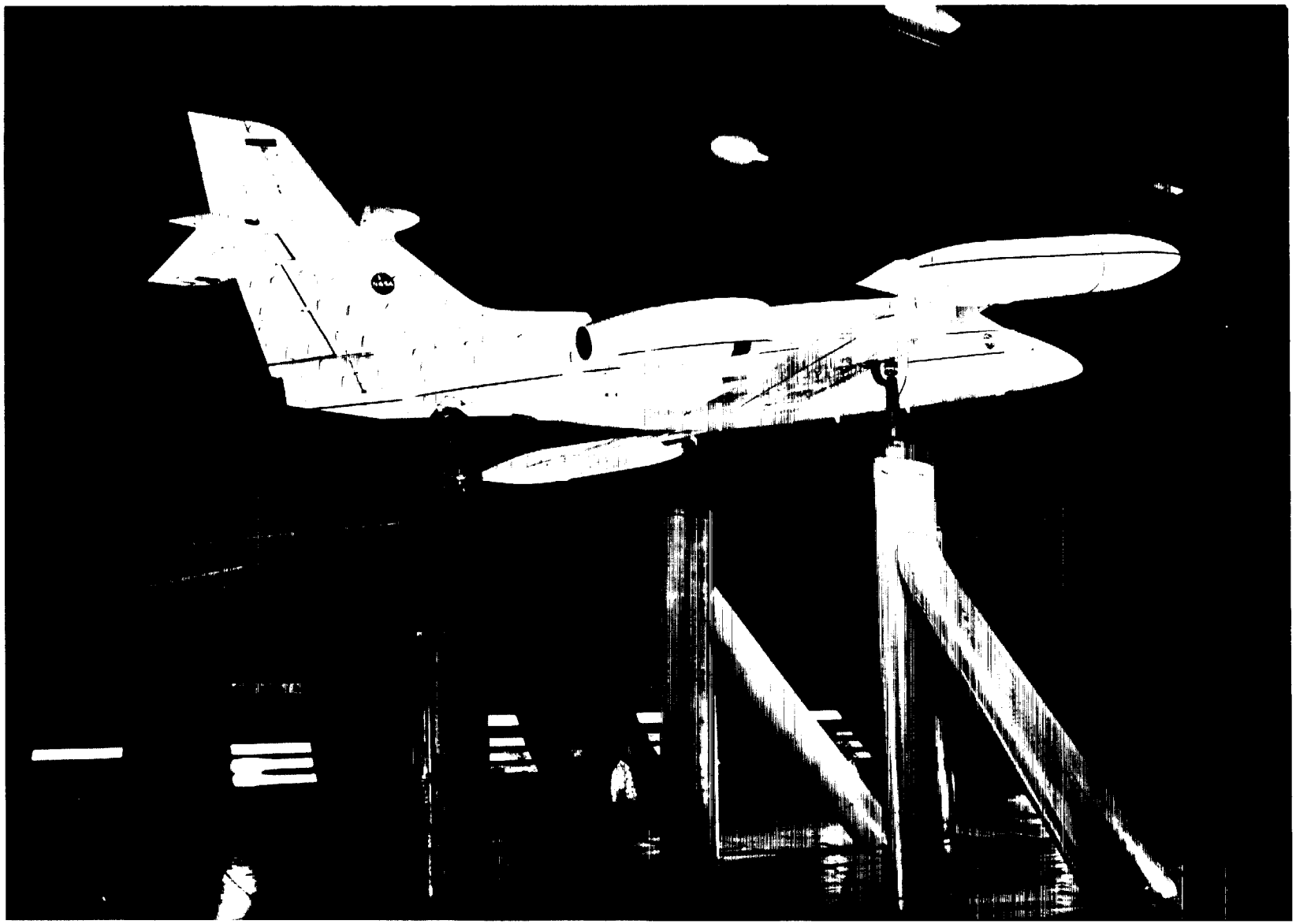

(a) Basic configuration.

Figure 1.- The model mounted in the Ames 40- by 80-Foot (12.2- by 24.4-m) Wind Tunnel.

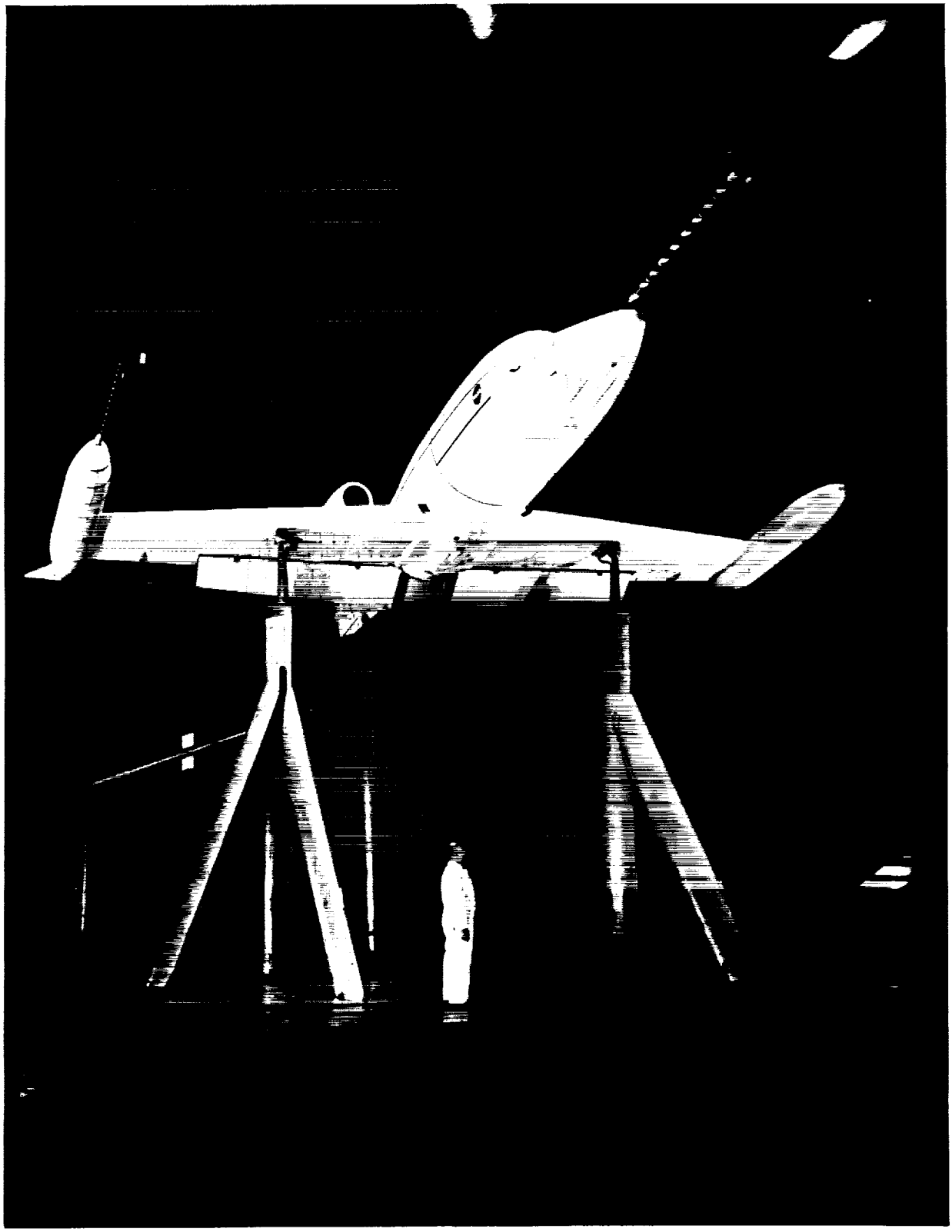

(b) Center section flap, nose and tip booms on model.

Figure 1.- Concluded.

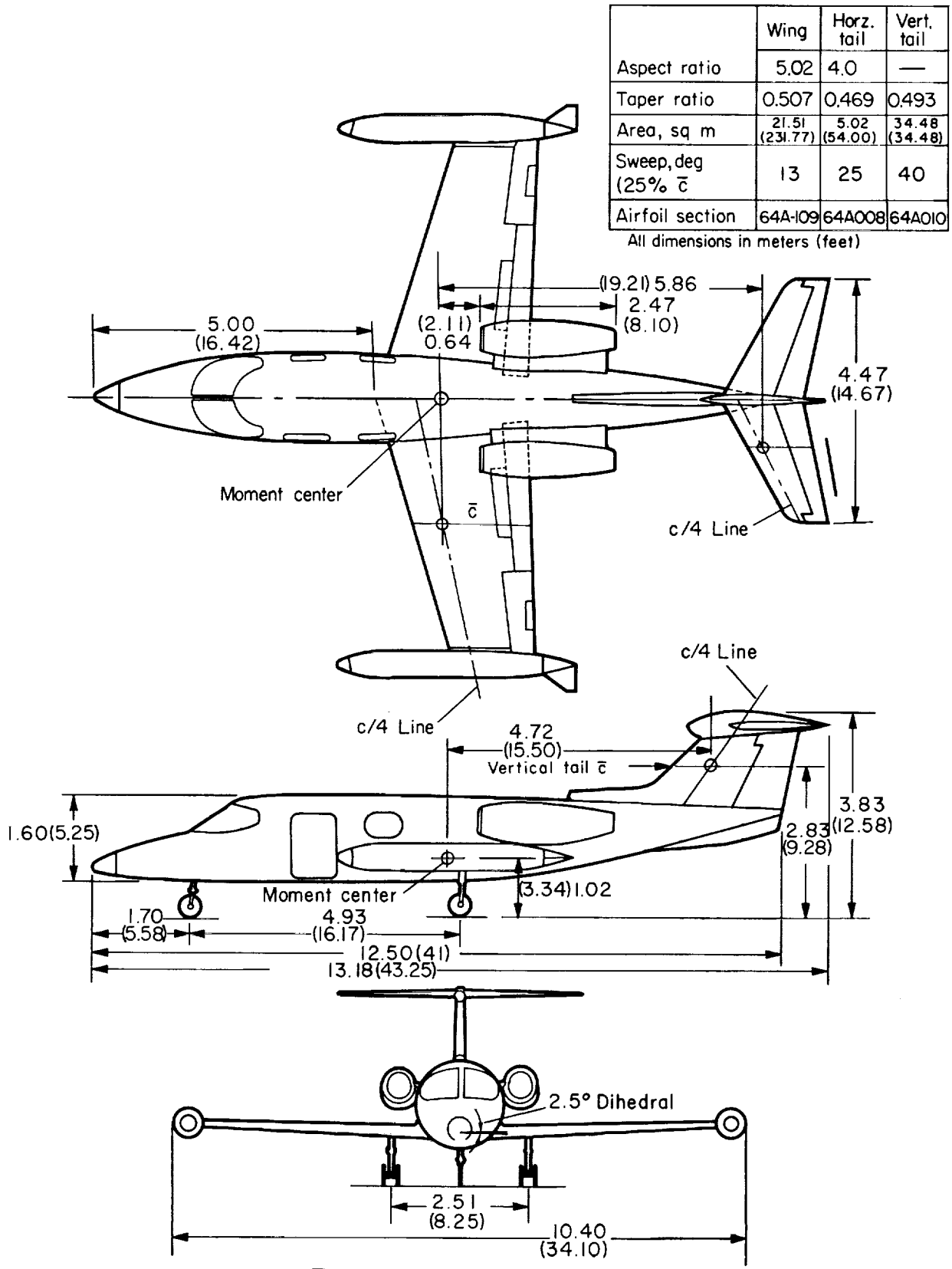

(a) General arrangement of model.

Figure 2.- Geometric details of the model.

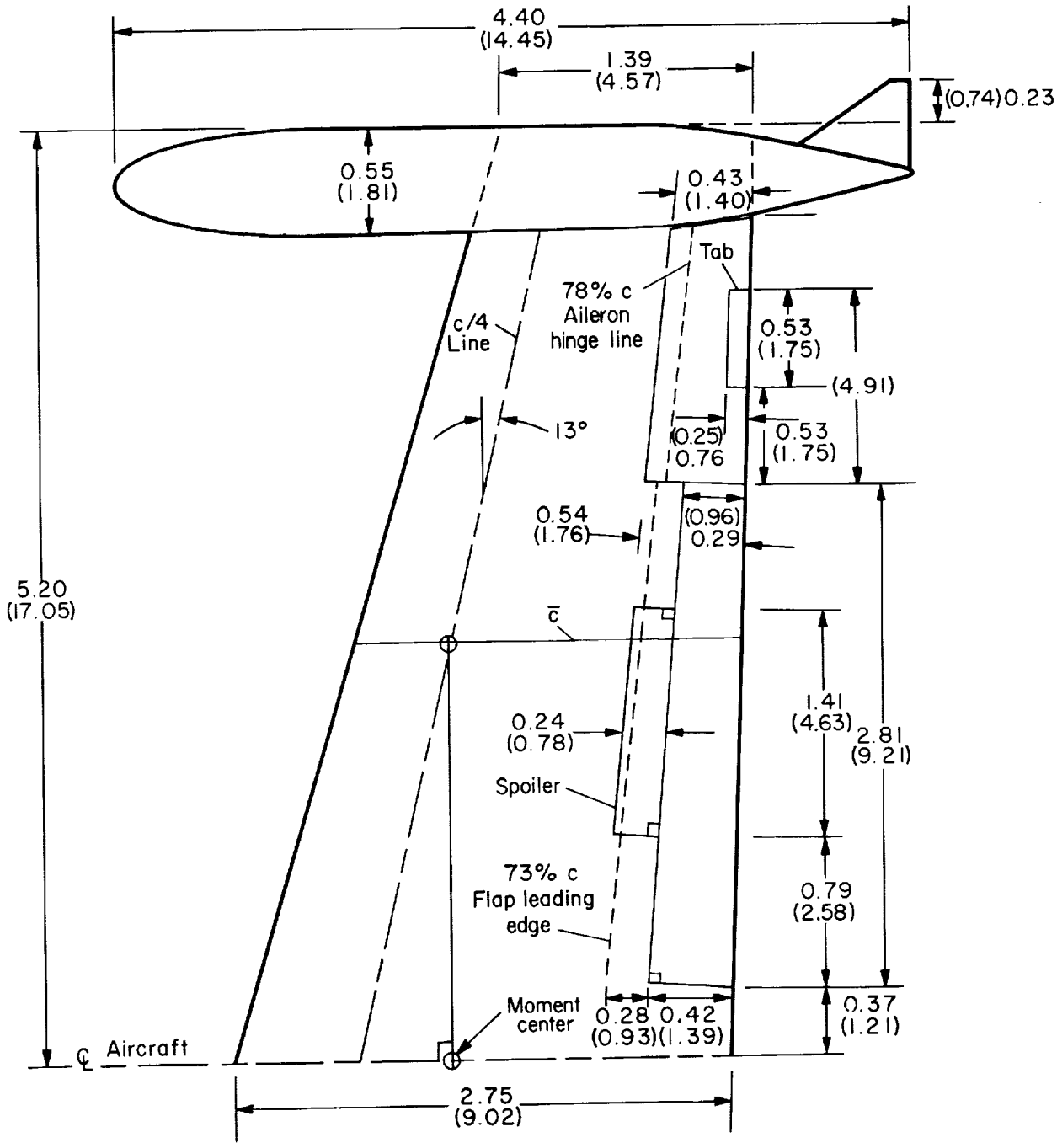

(b) Basic wing detail.

Figure 2.- Continued.

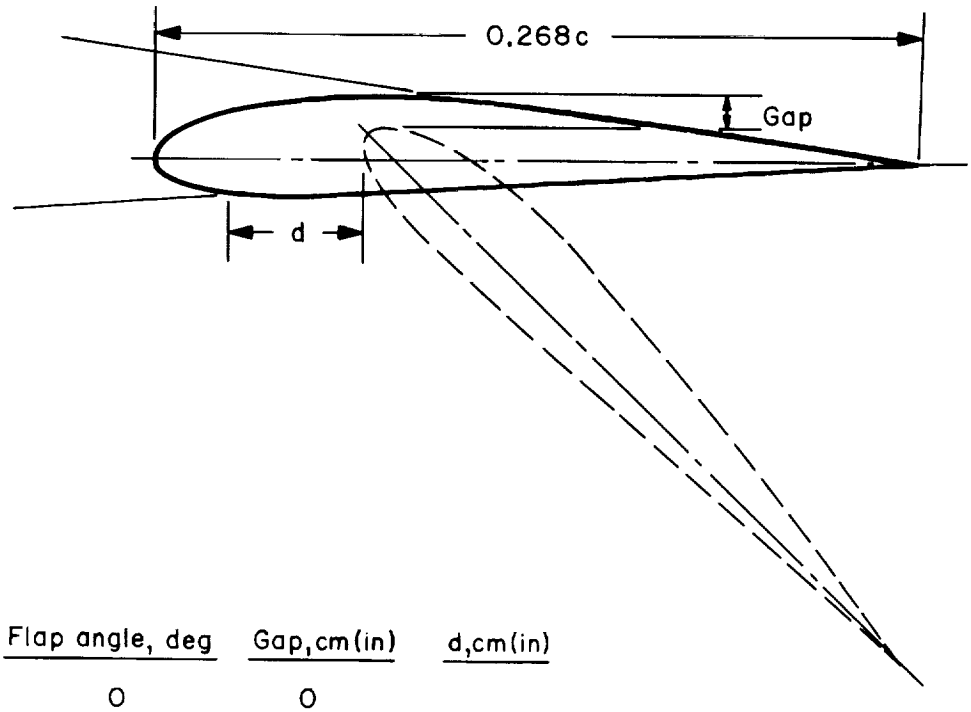

Flap angle, deg	Gap, cm (in)	d, cm (in)
0	0	
20	1.57 (0.62)	13.97 (5.5)
38	2.46 (0.97)	18.55 (7.3)
40	2.46 (0.97)	18.80 (7.4)

(c) Trailing-edge flap.

Figure 2.- Continued.

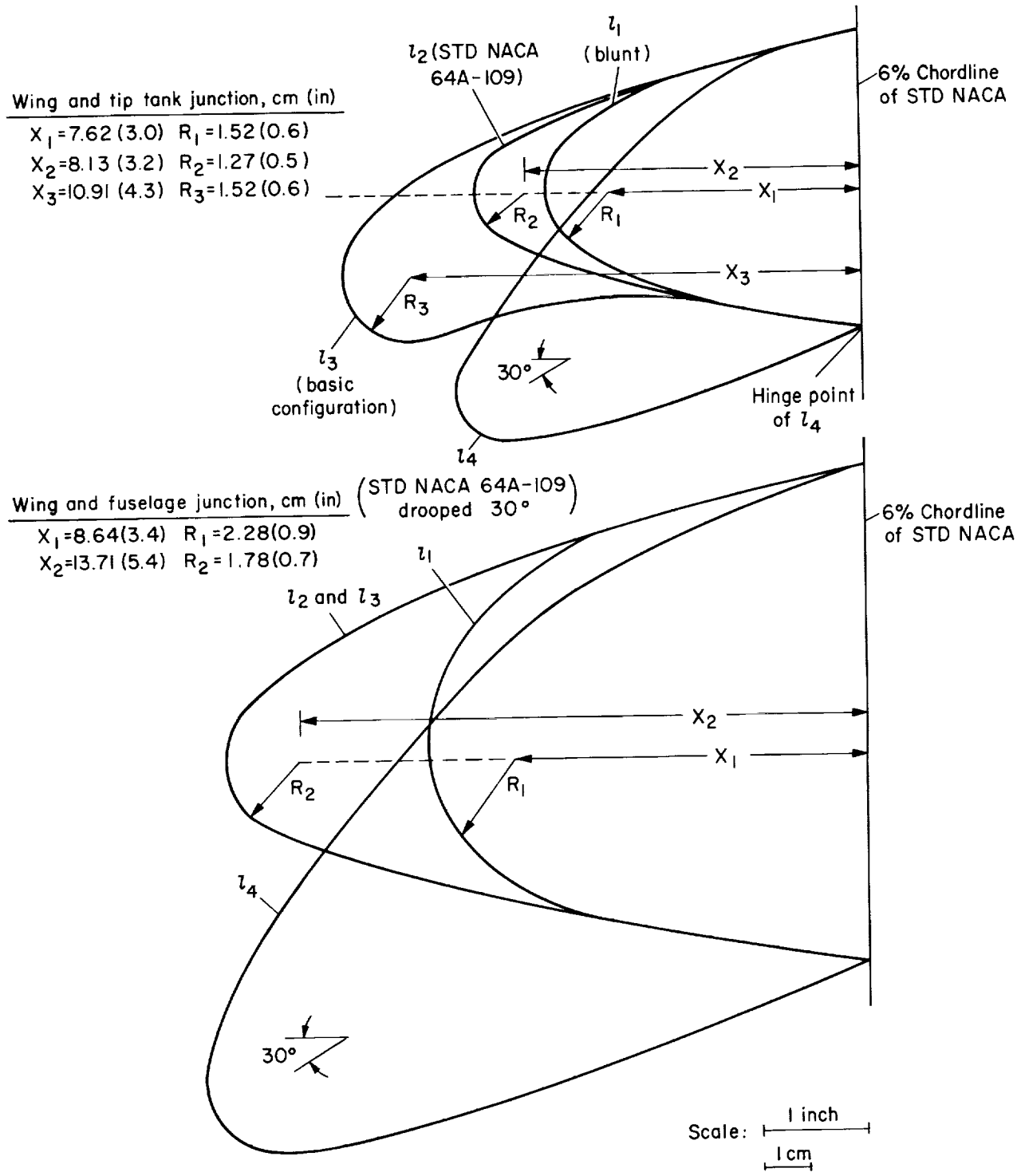

(d) Leading-edge modifications.

Figure 2.- Continued.

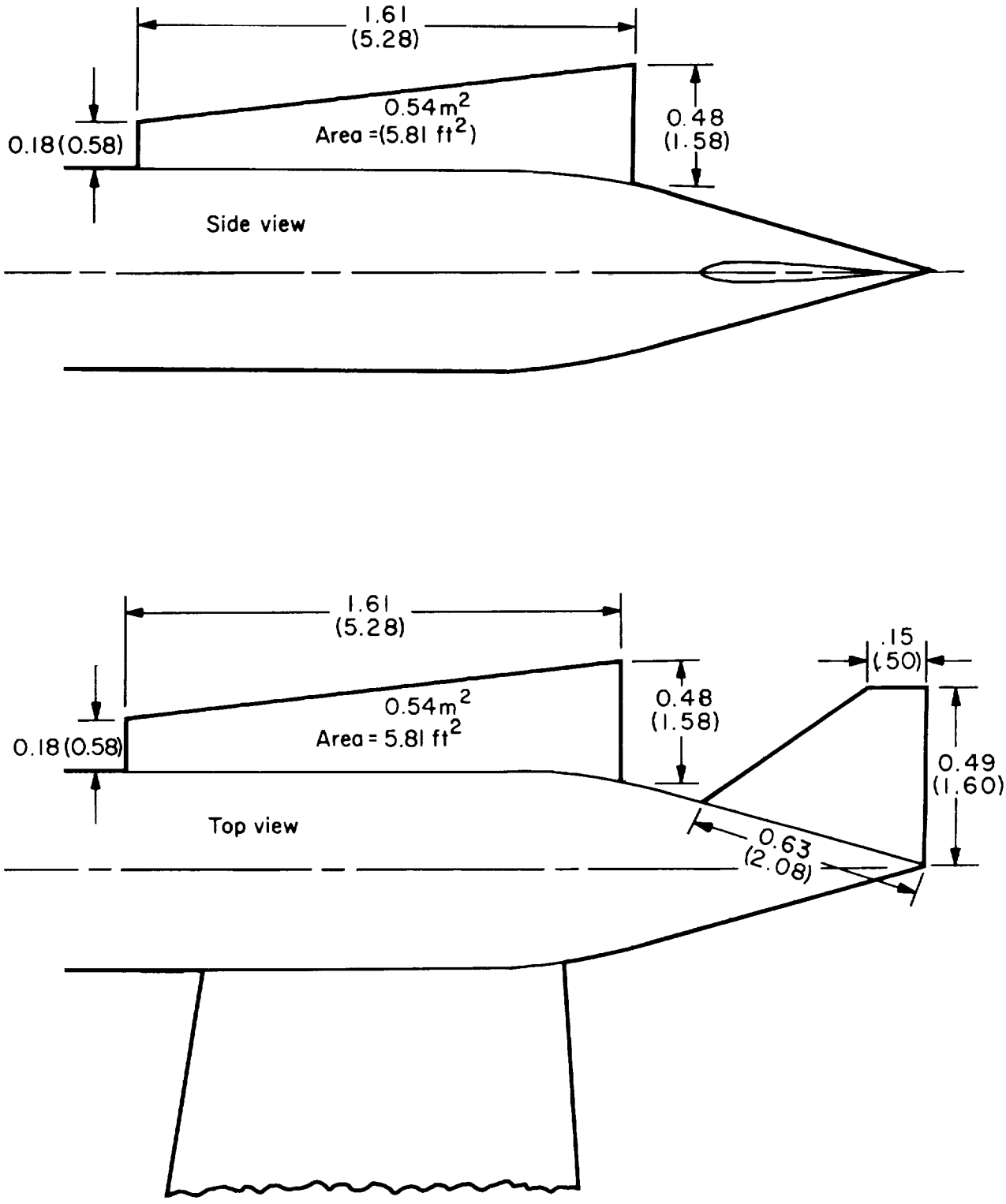

(e) Fence located on side and top of tip tank.

Figure 2.- Continued.

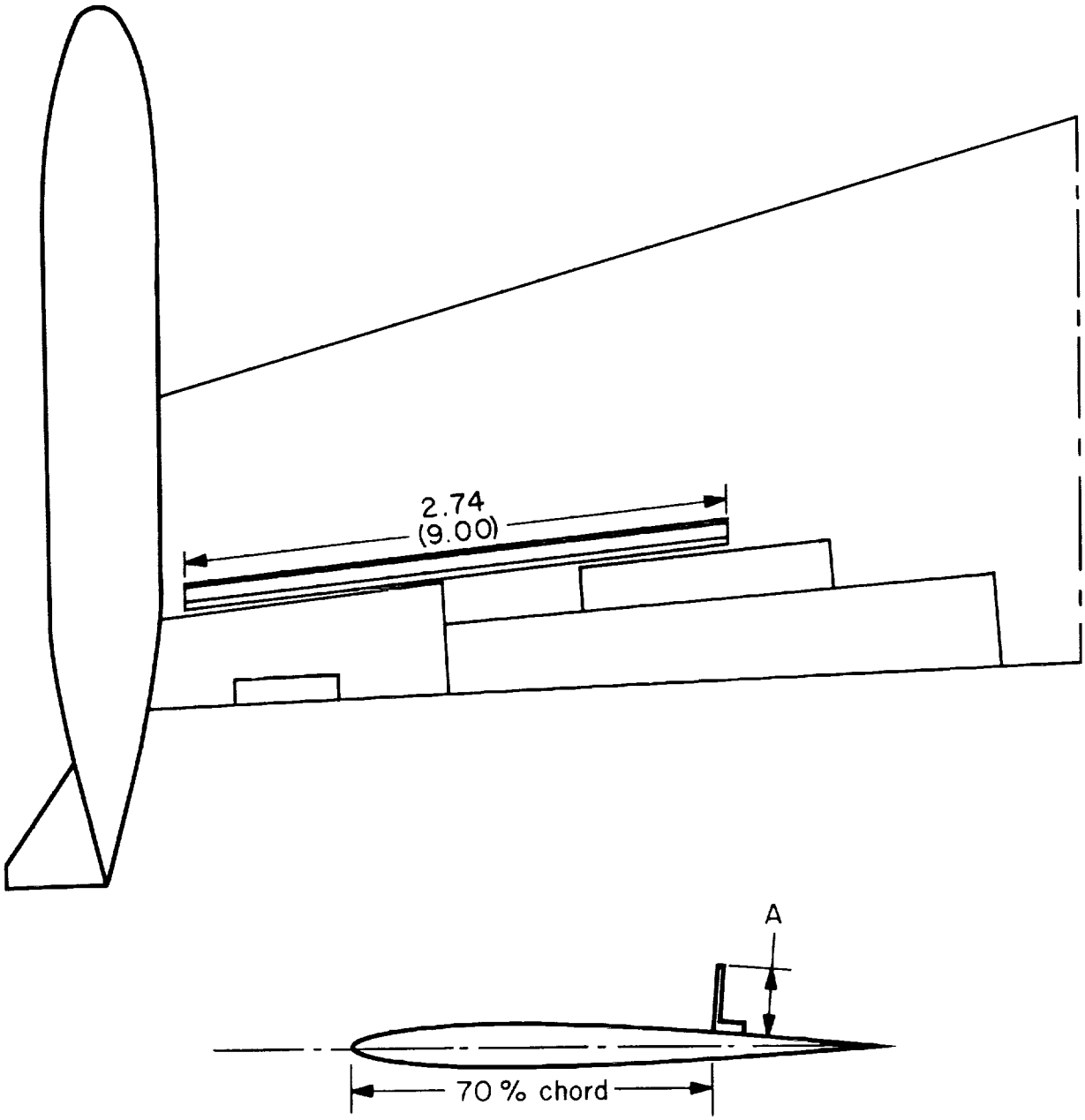

Symbol	"A" dimension, (in) cm
S_1	(2.25)5.71
S_2	(5.50)13.98
S_3	(6.75)17.15

(f) Outboard spoiler.

Figure 2.- Continued.

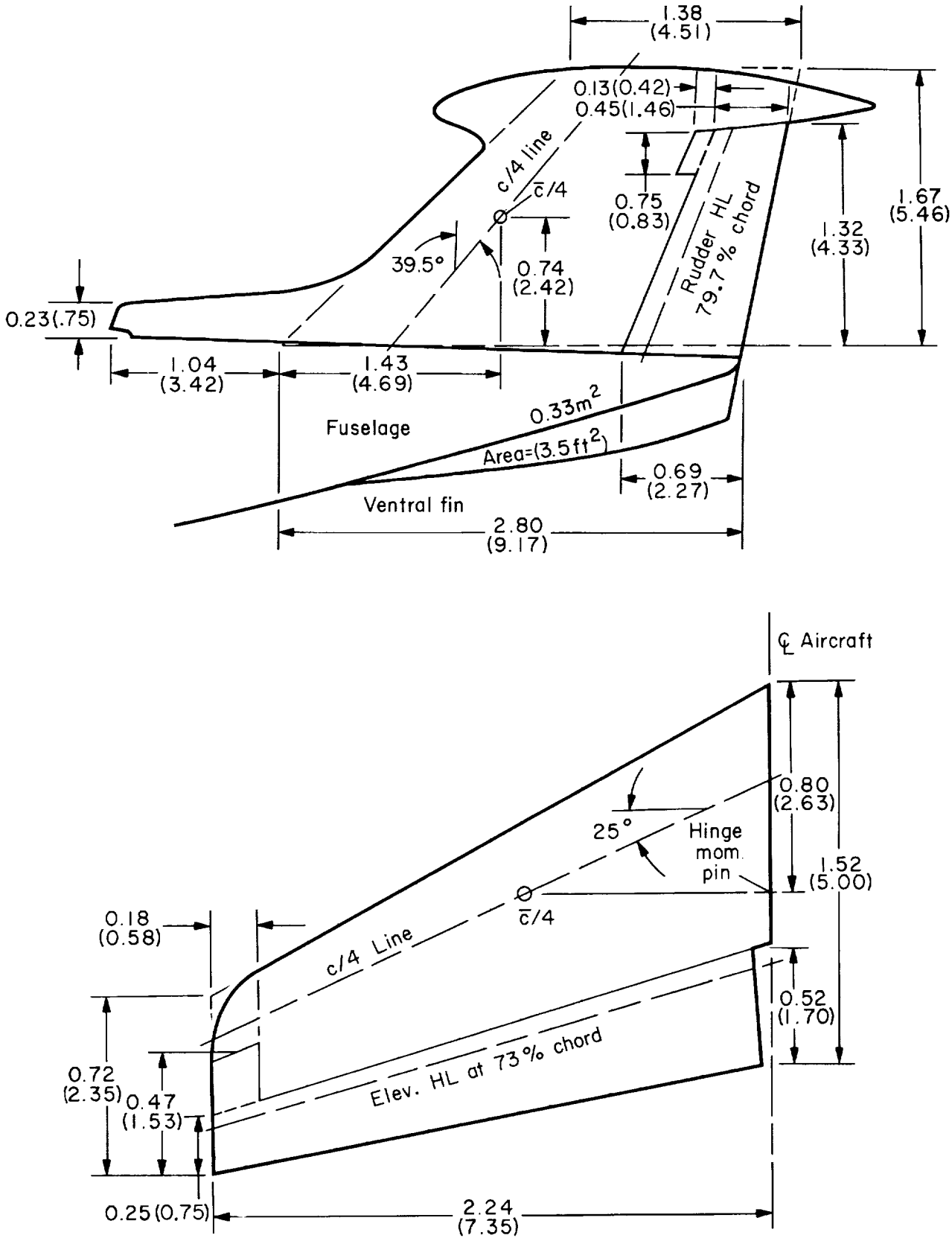

(g) Horizontal and vertical stabilizer.

Figure 2.- Continued.

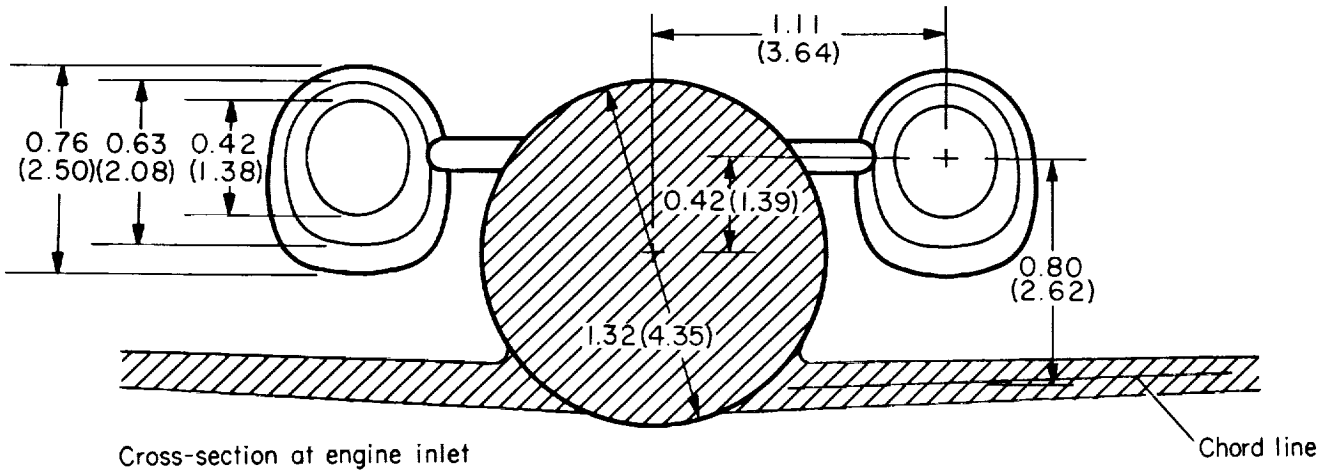

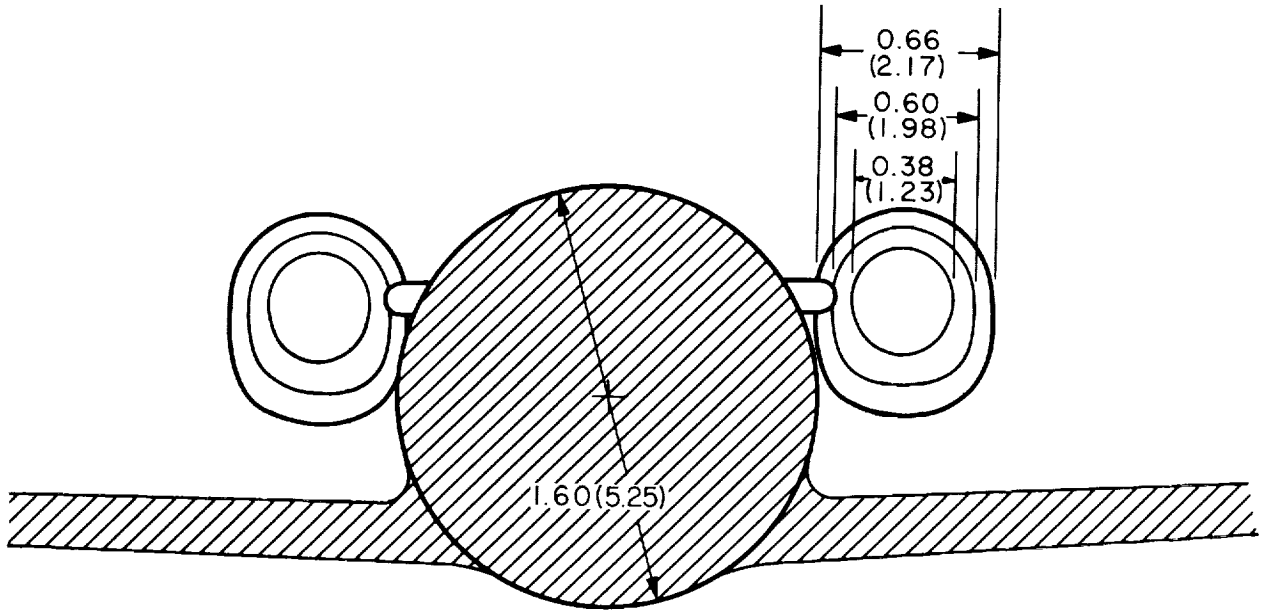

(h) Fuselage-wing cross section at two locations.

Figure 2.- Concluded.

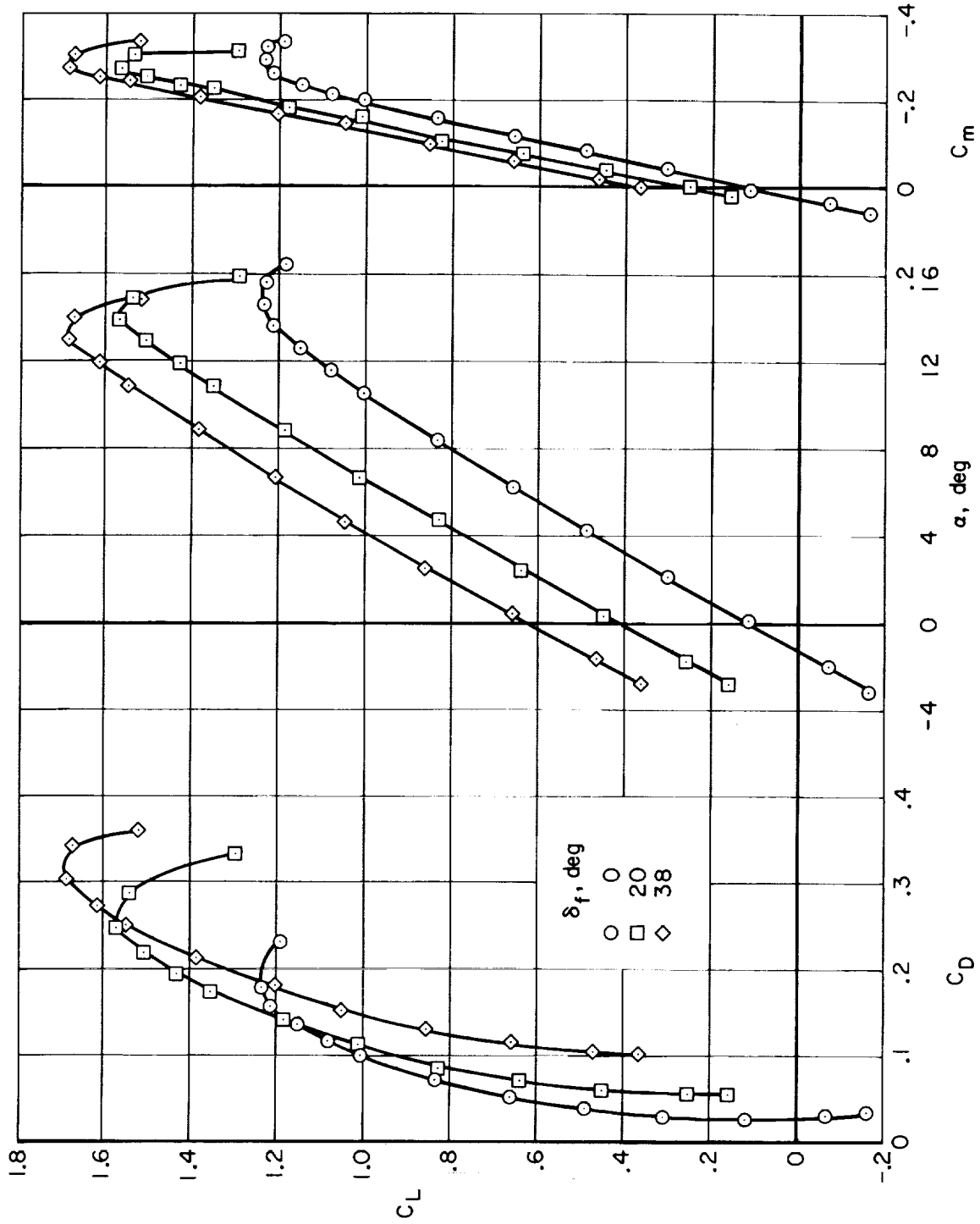

(a) R = 8.7X10^6, i_t = 0.4°

Figure 3.- Longitudinal characteristics of the basic configuration for three flap angles.

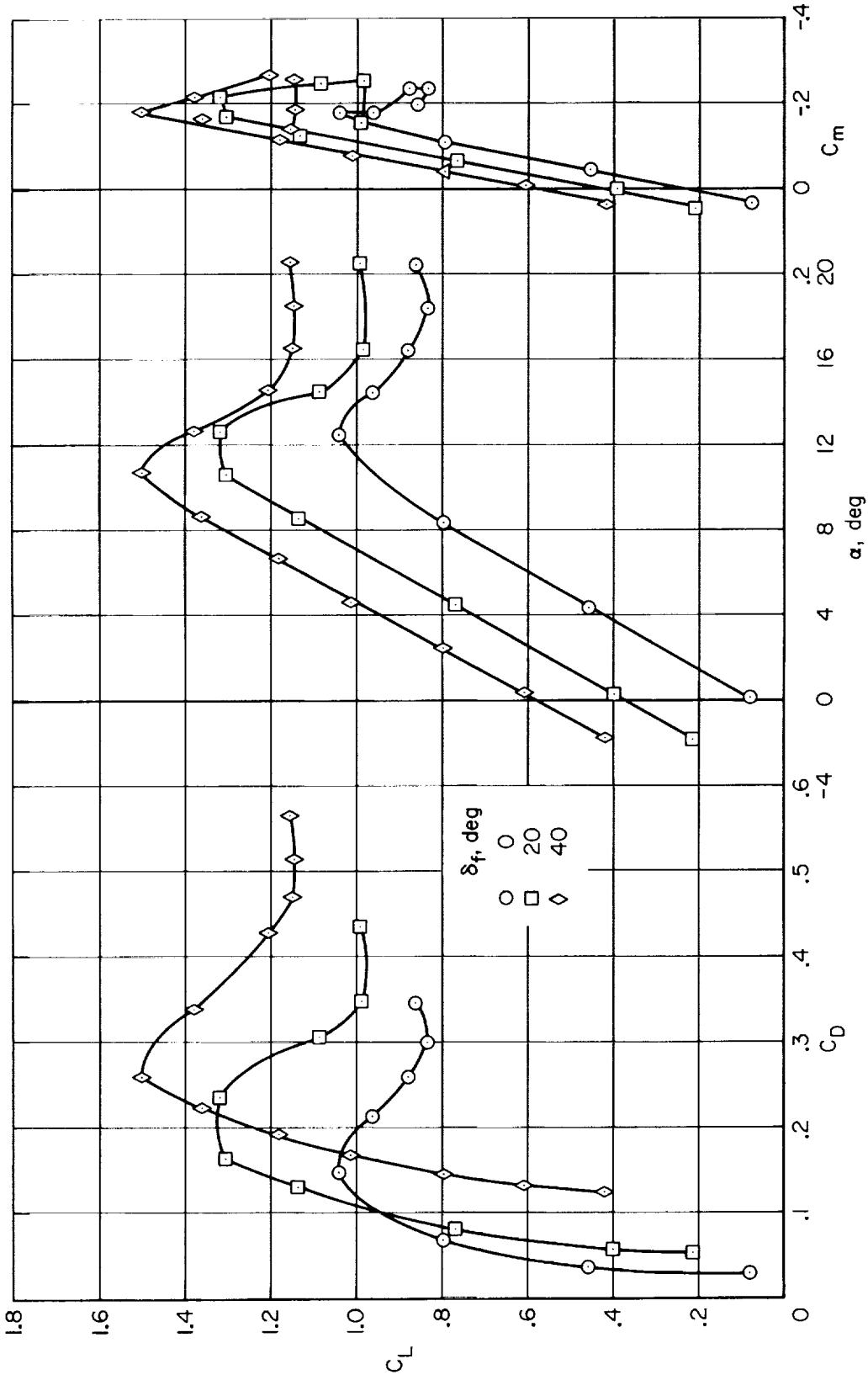

(b) R = 4.1X10^6, i_t = 0.4°

Figure 3.- Concluded.

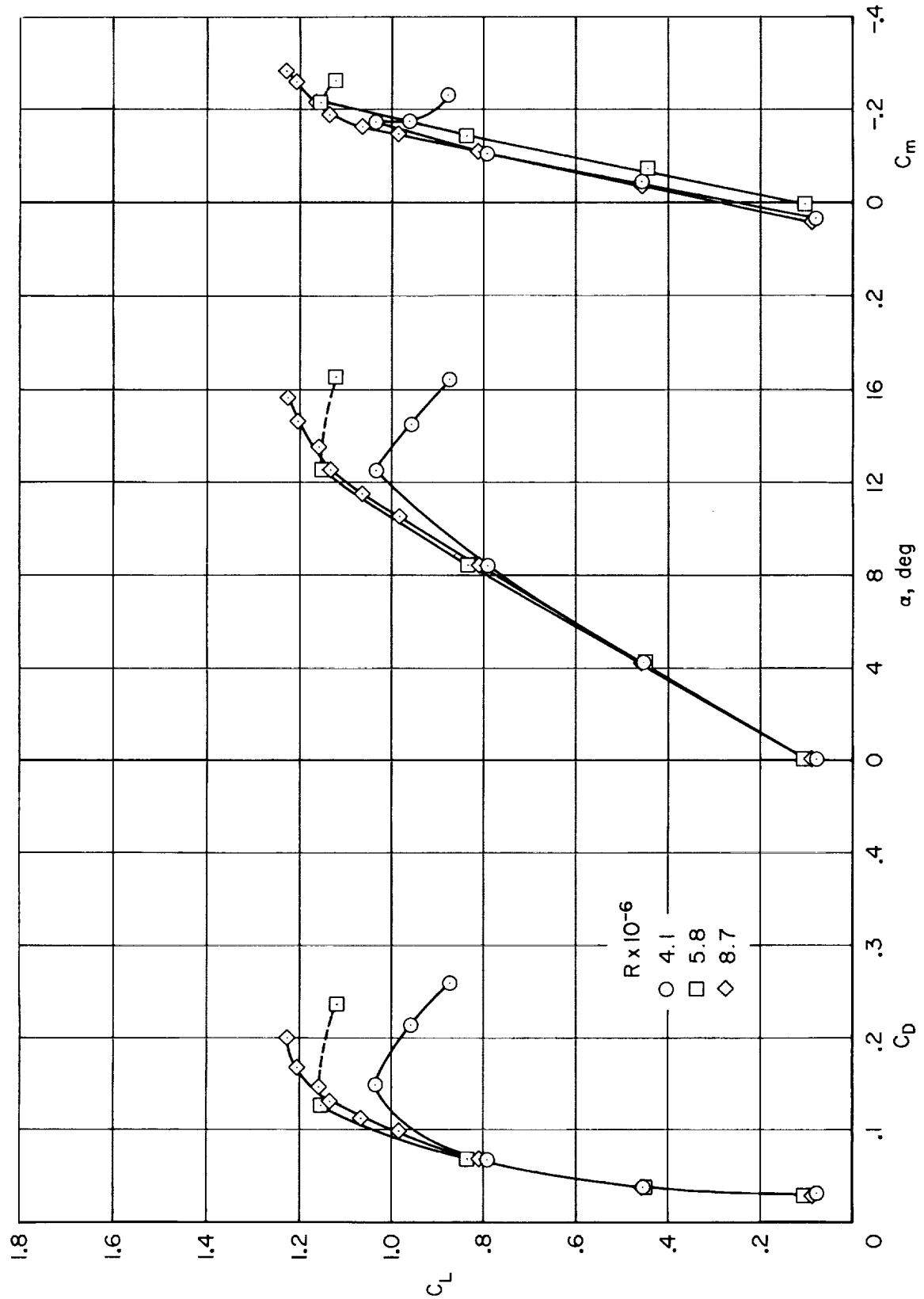

(a) $\delta_f = 0°$

Figure 4.- Effect of Reynolds number on longitudinal characteristics; $i_t = 0.4°$.

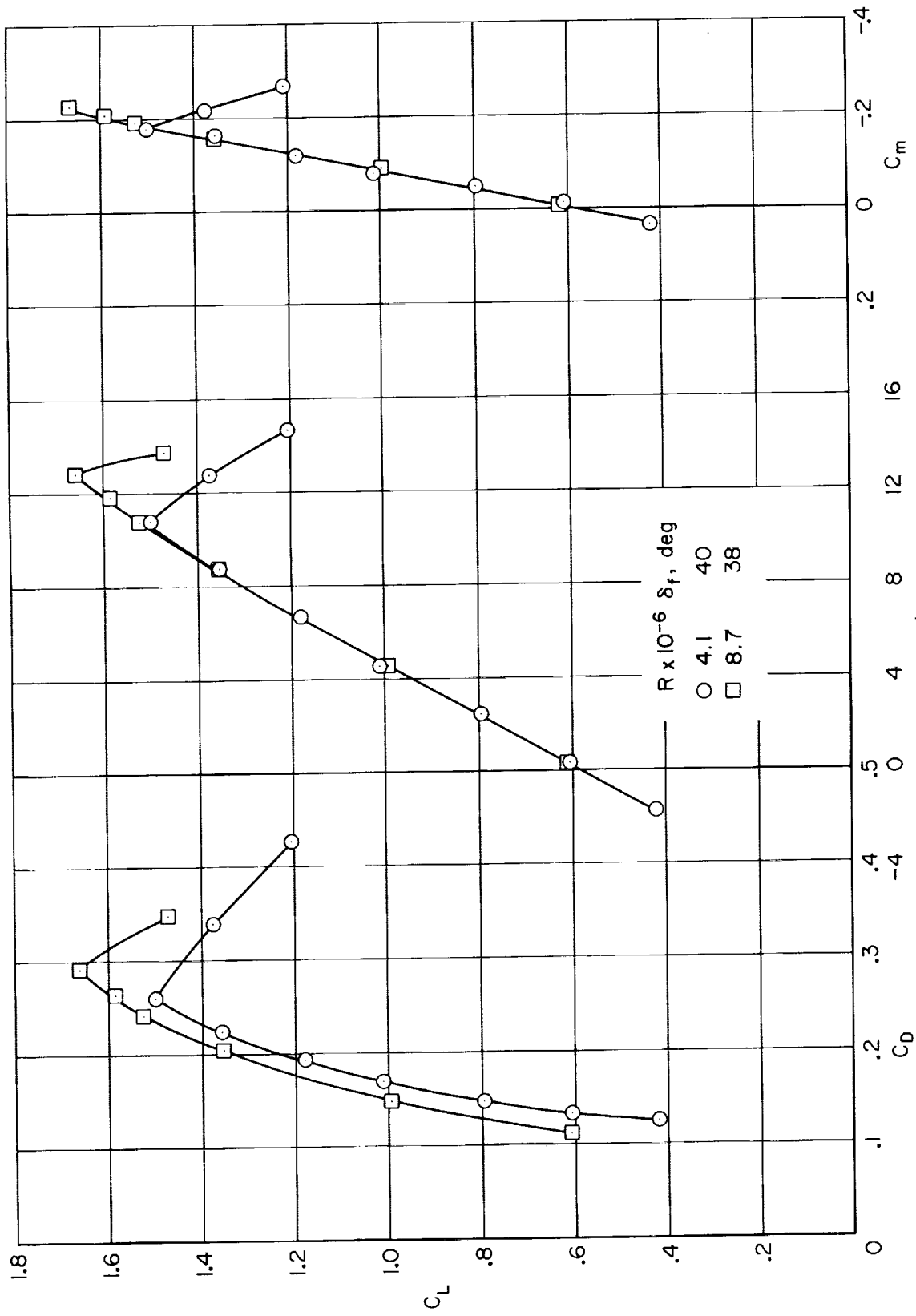

(b) Flaps down.

Figure 4.- Concluded.

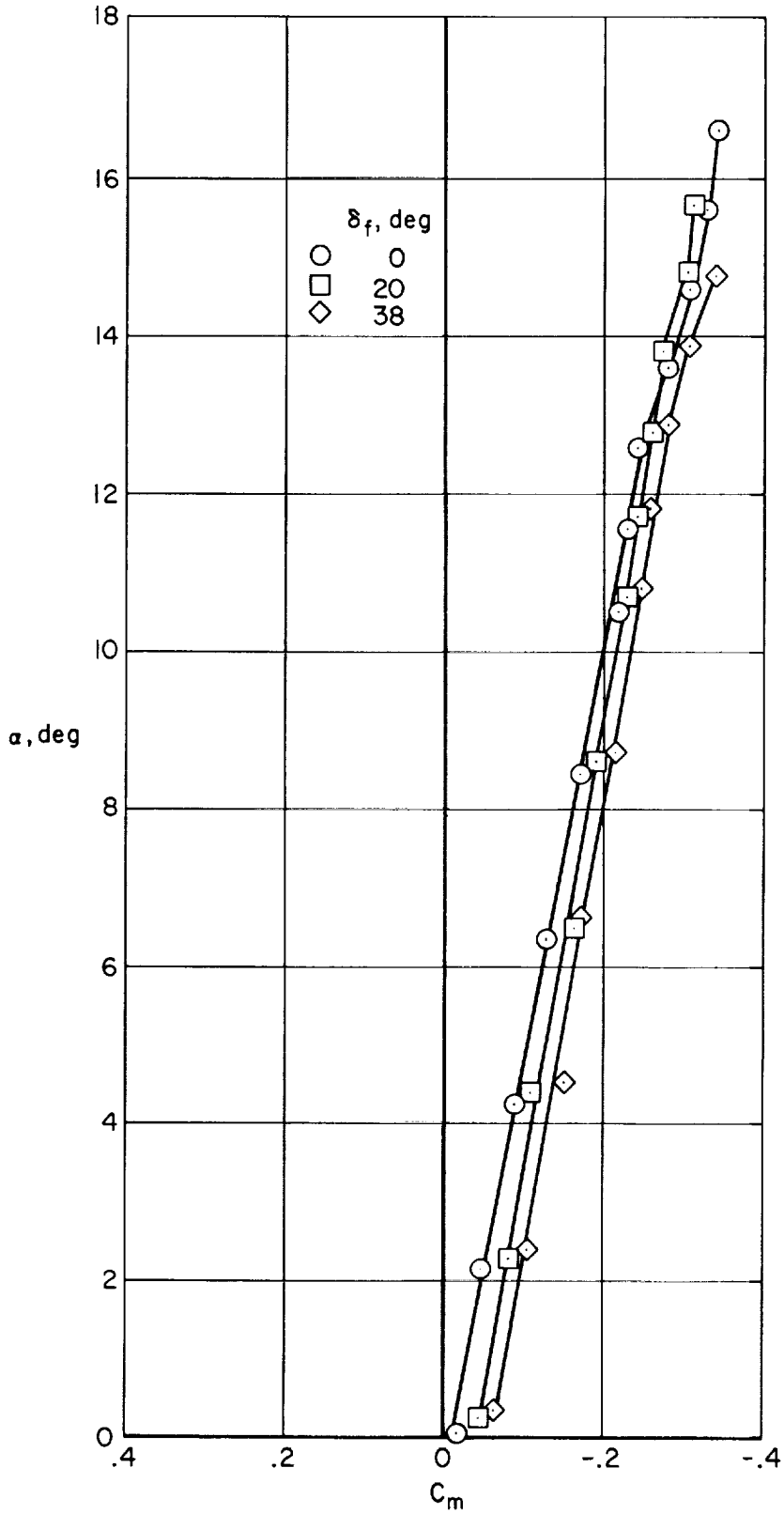

(a) Stick fixed.

Figure 5.- Variation of pitching-moment coefficient with angle of attack; $R = 8.7 \times 10^6$, $i_t = 0.4°$.

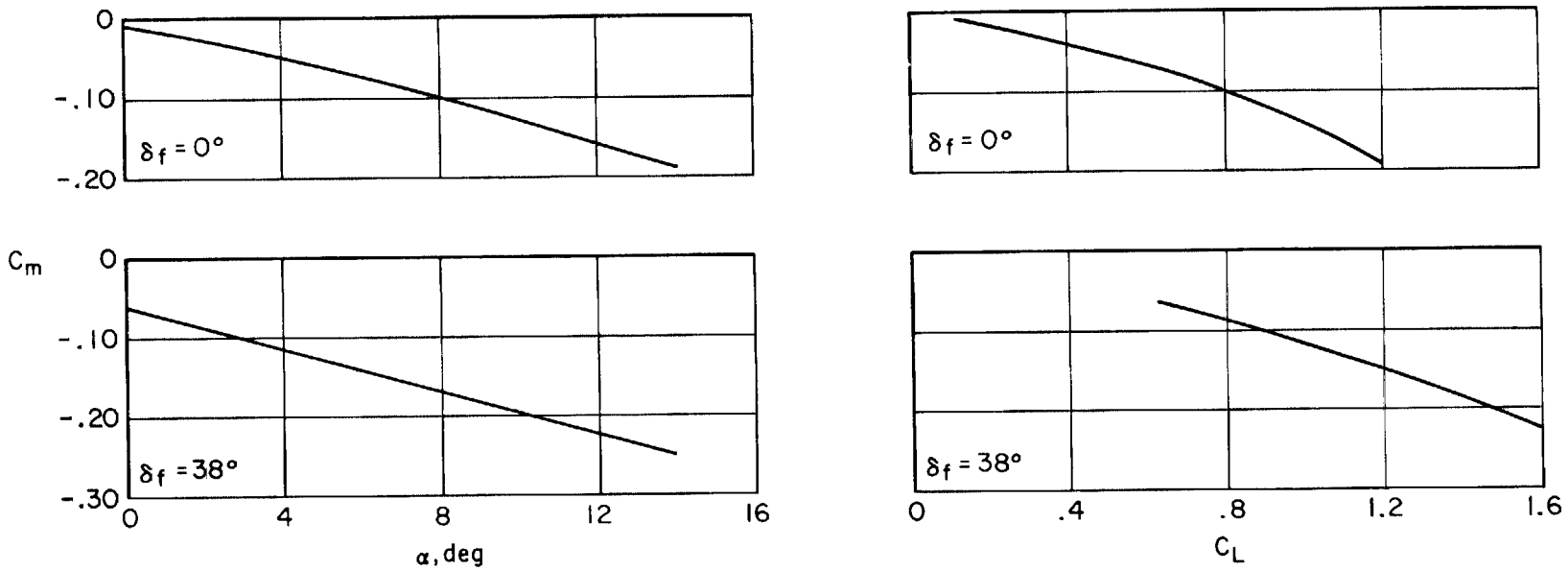

(b) Stick free.

Figure 5.- Concluded.

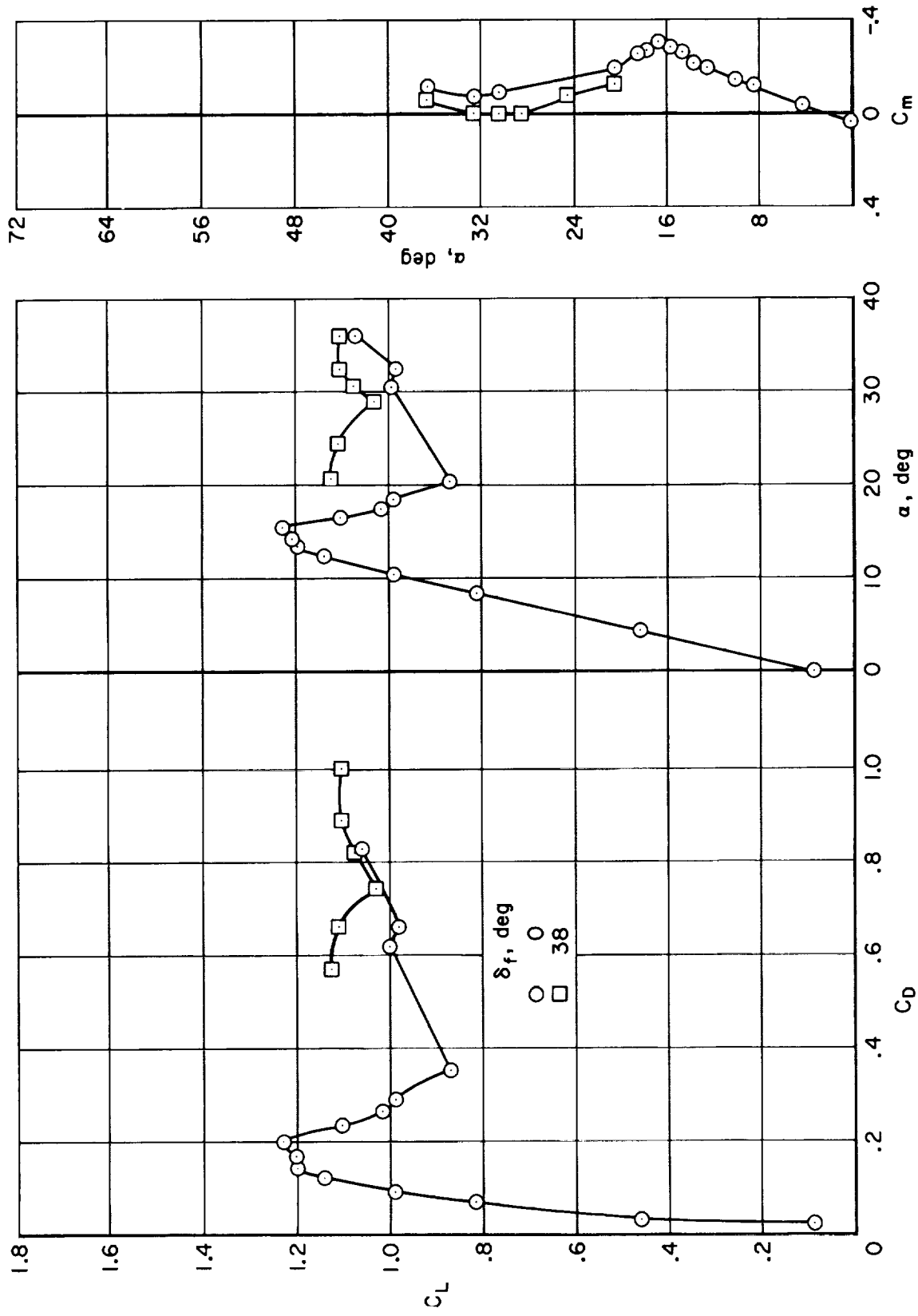

(a) R = 8.7X10^6; i_t = 0.4°

Figure 6.- Longitudinal characteristics through deep stall.

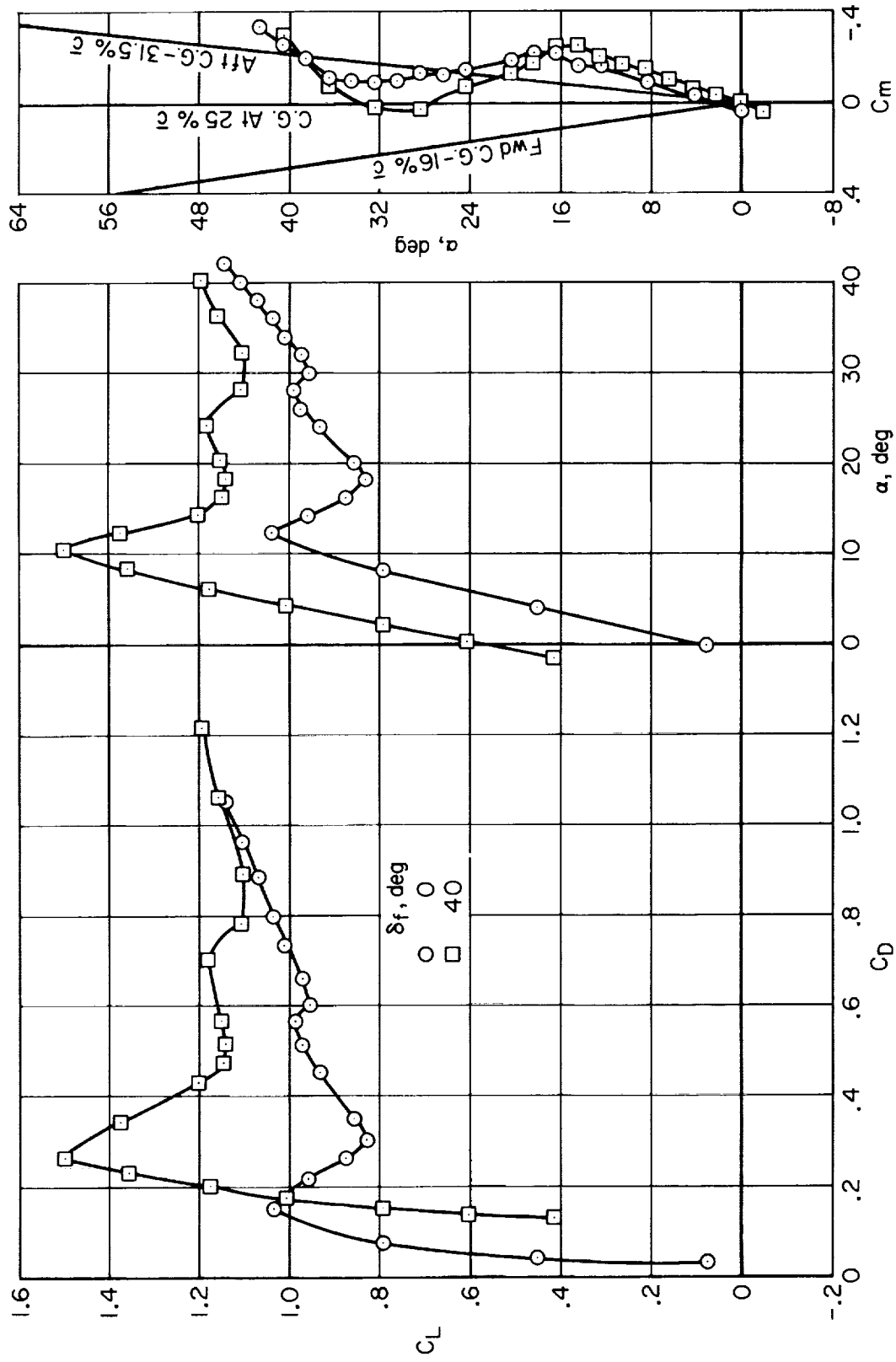

(b) R = 4.1X10^6, i_t = 0.4°

Figure 6.- Continued.

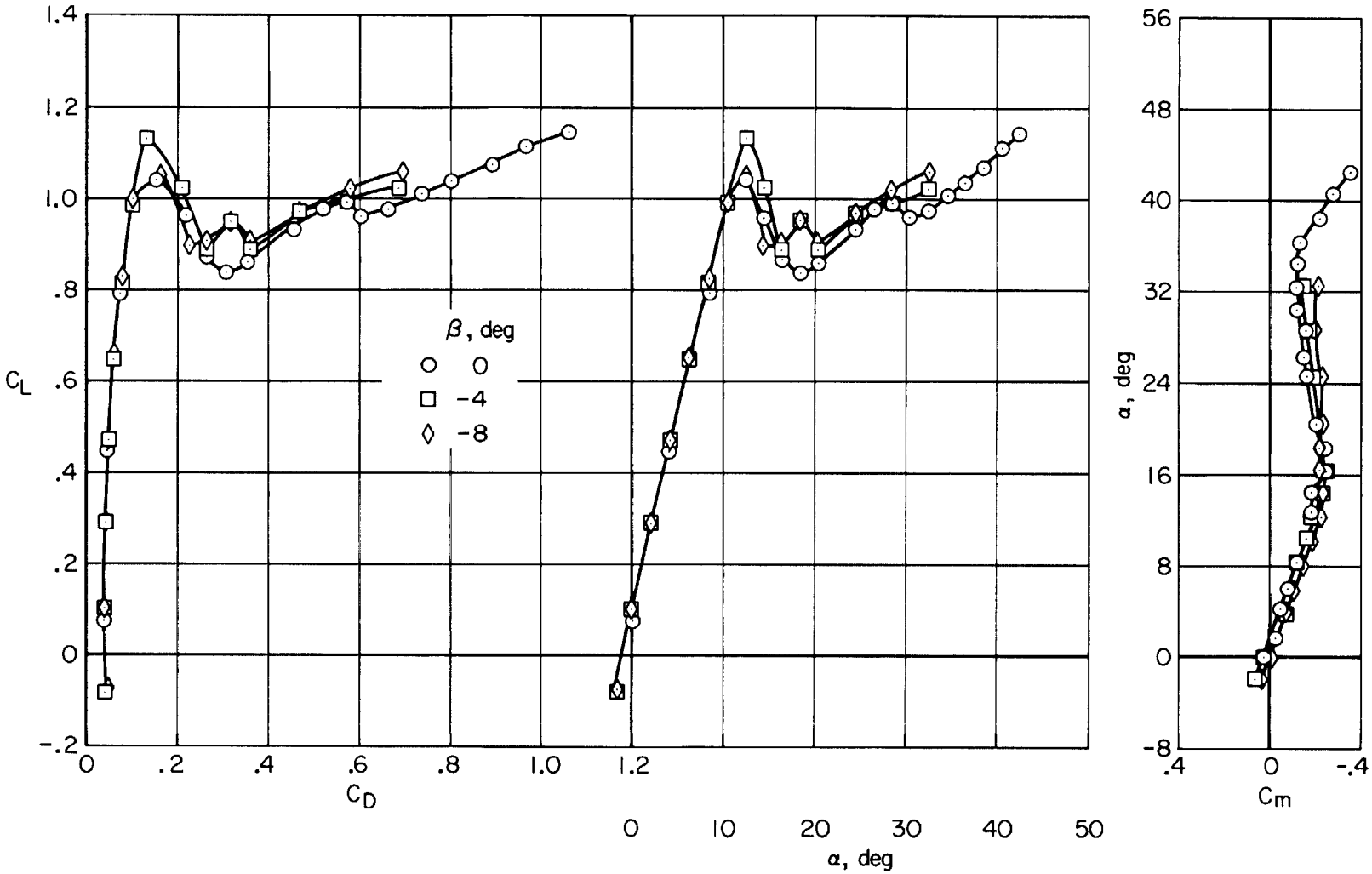

(c) $\delta_f = 0°$, $R = 4.1 \times 10^6$, $i_t = 0.4°$, in sideslip

Figure 6.- Concluded.

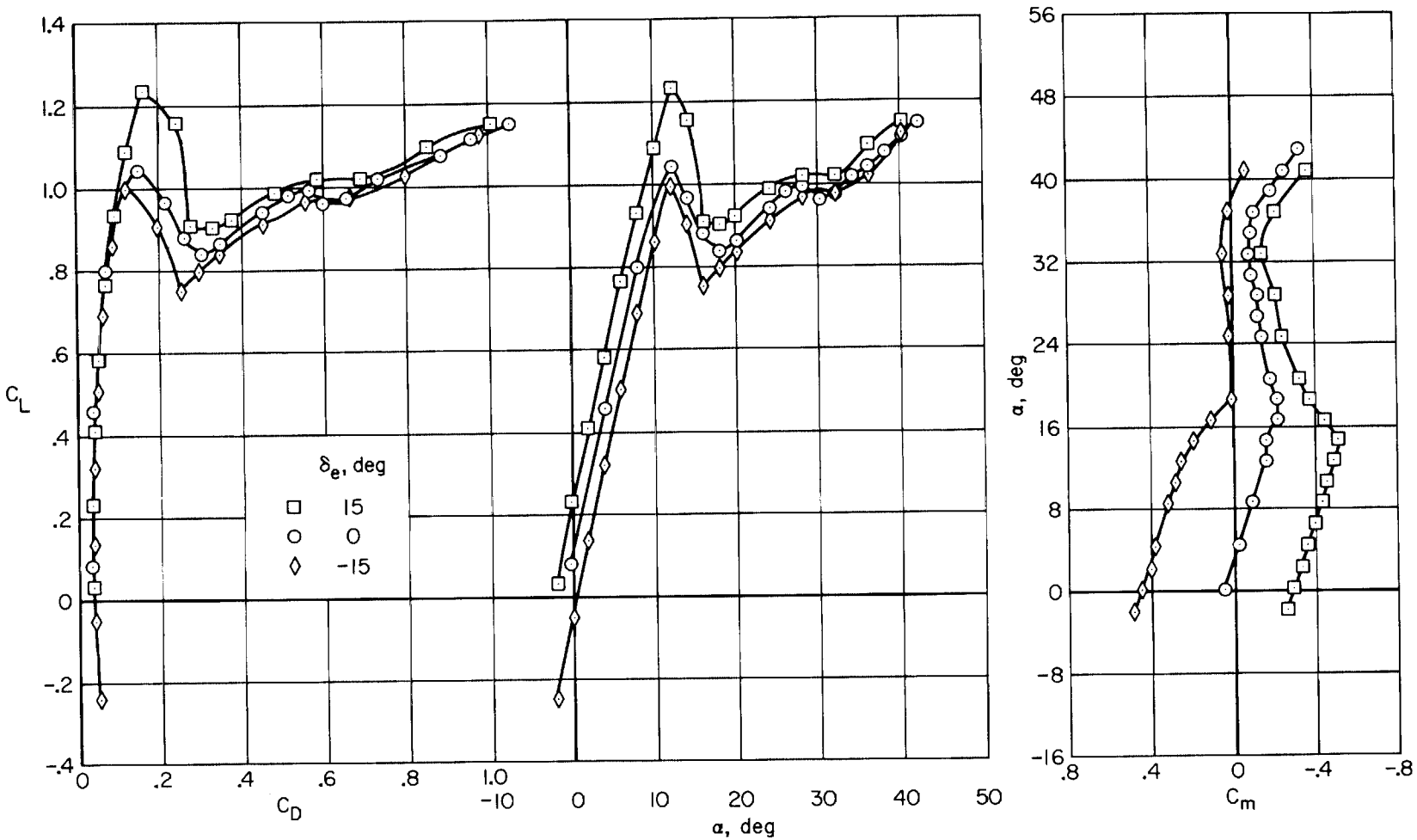

(a) $\delta_f = 0°$, $R = 4.1 \times 10^6$, $i_t = 0.4°$

Figure 7.- Elevator effectiveness.

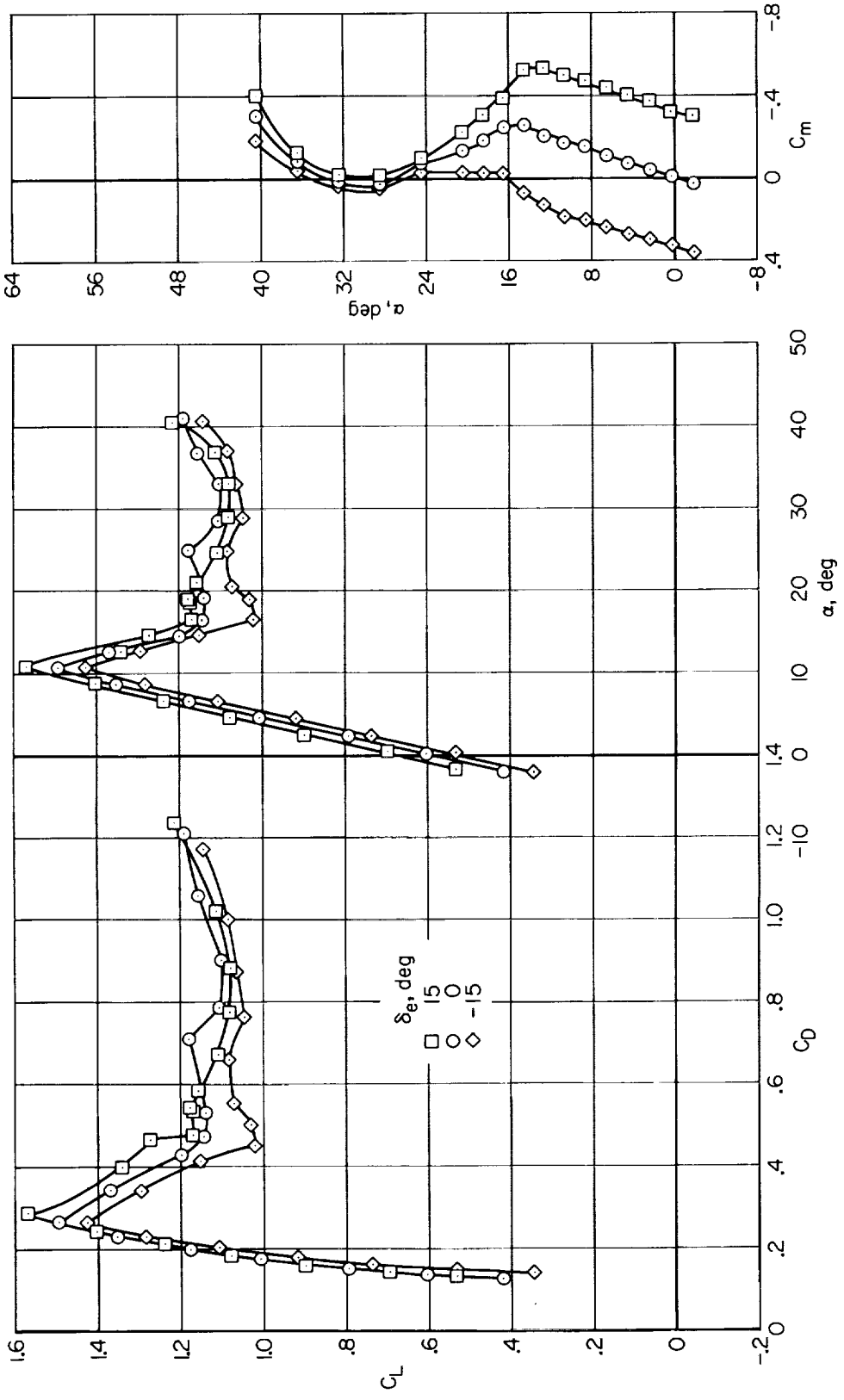

(b) $\delta_f = 40°$, R = 4.1X10^6, $i_t = 0.4°$

Figure 7.- Continued.

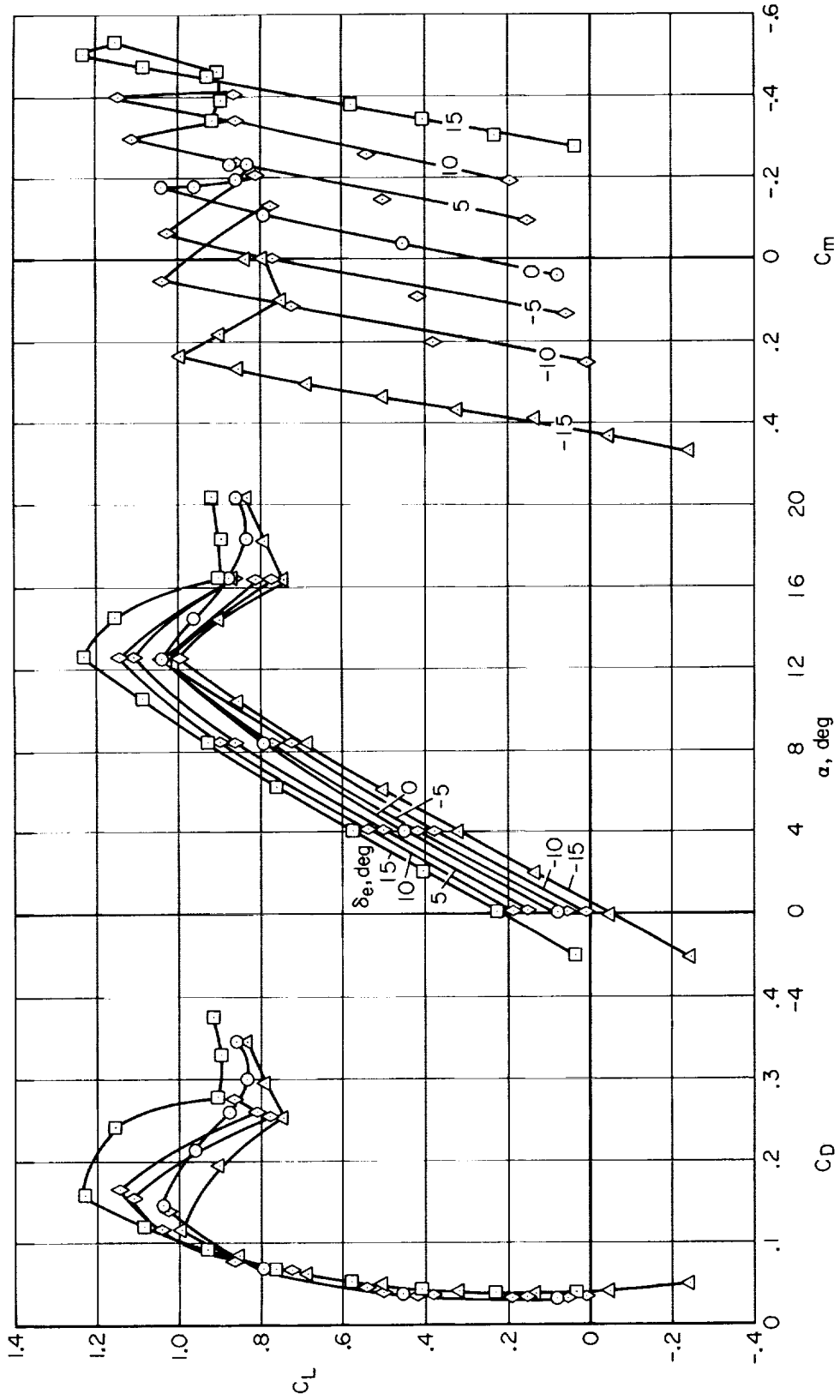

(c) $\delta_f = 0°$, $R = 4.1 \times 10^6$, $i_t = 0.4°$

Figure 7.- Continued.

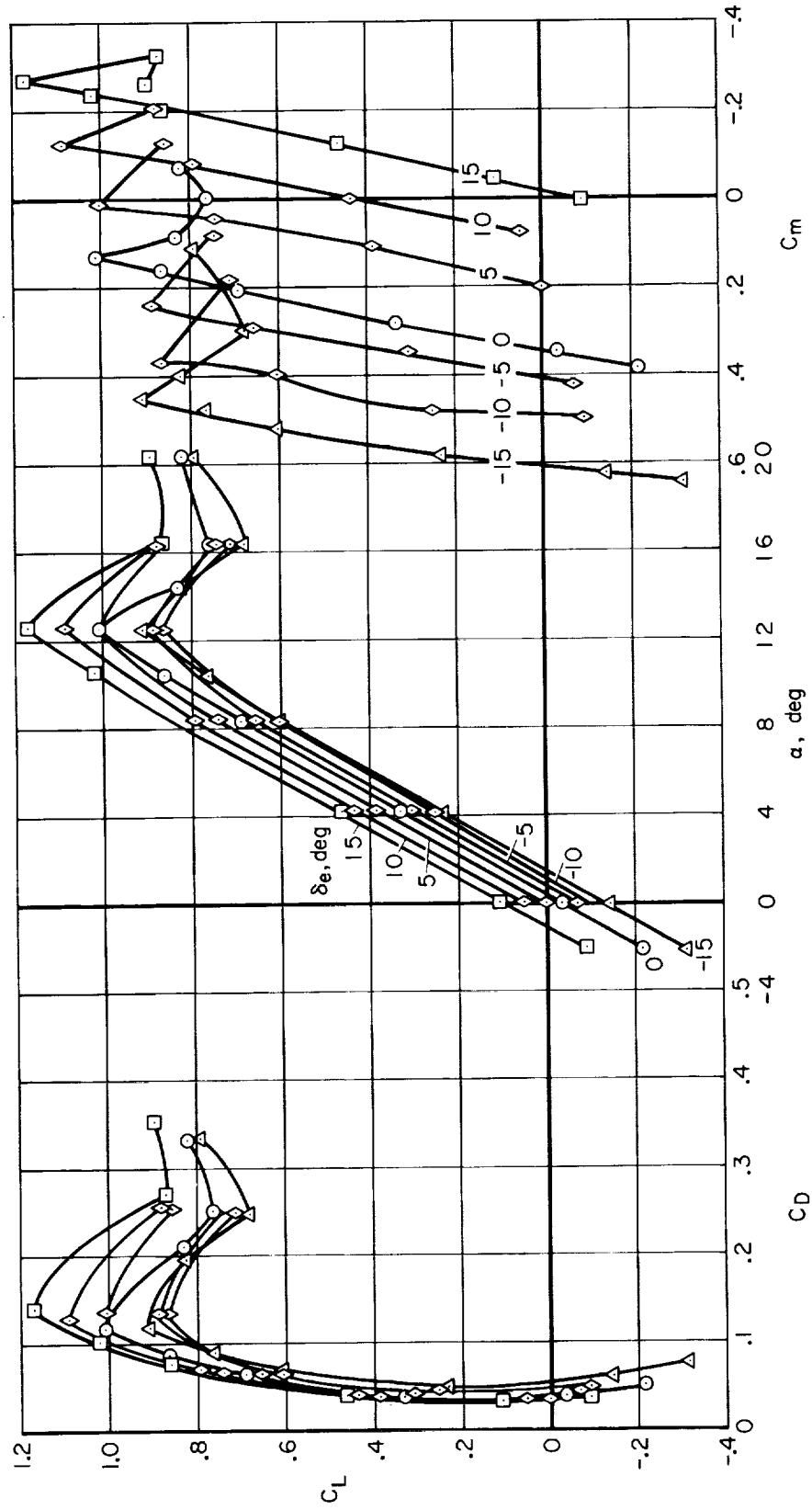

(d) $\delta_f = 0°$, $R = 4.1 \times 10^6$, $i_t = -7°$

Figure 7.- Continued.

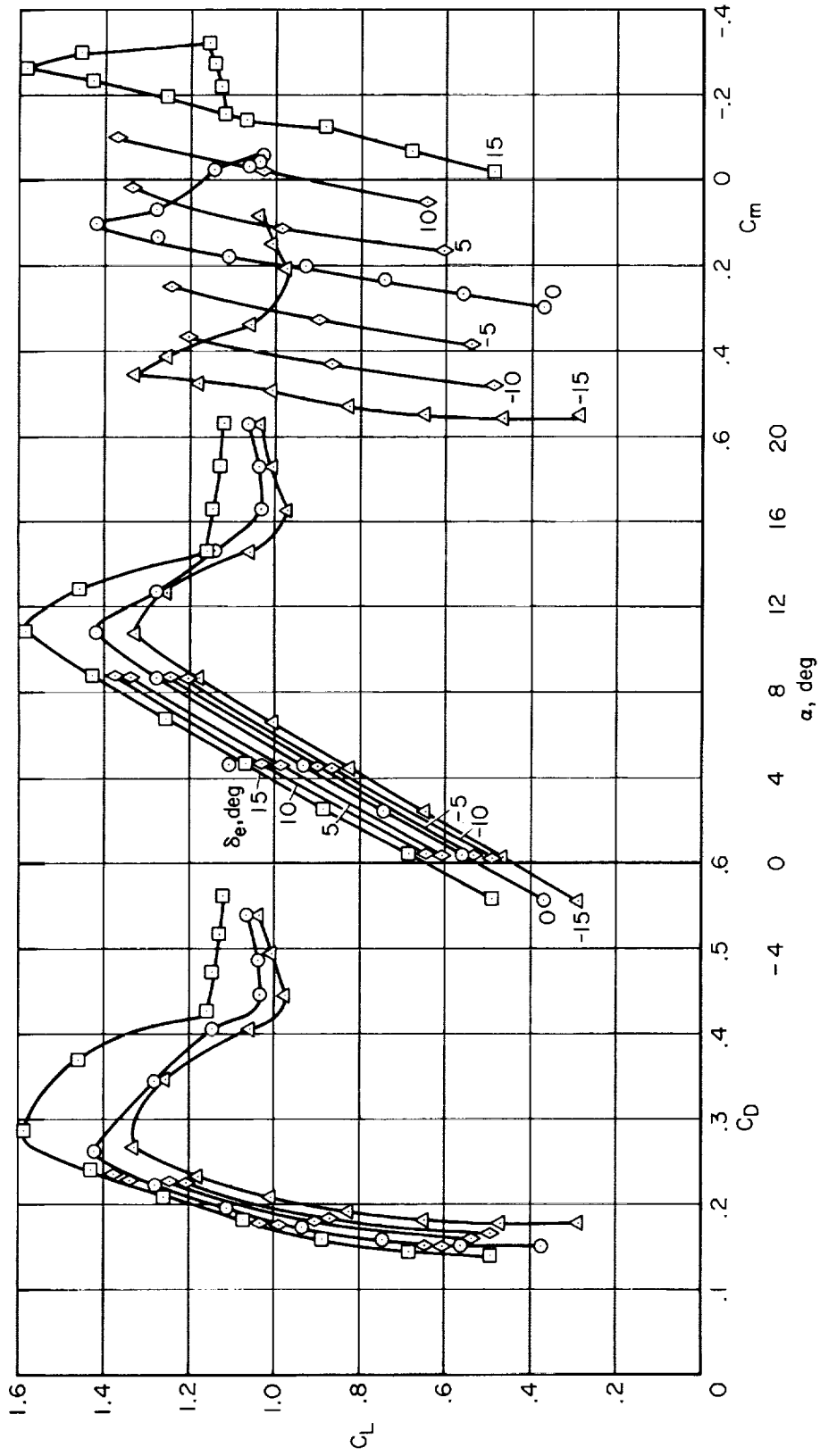

(e) $\delta_f = 40°$, $R = 4.1 \times 10^6$, $i_t = -7°$

Figure 7.- Continued.

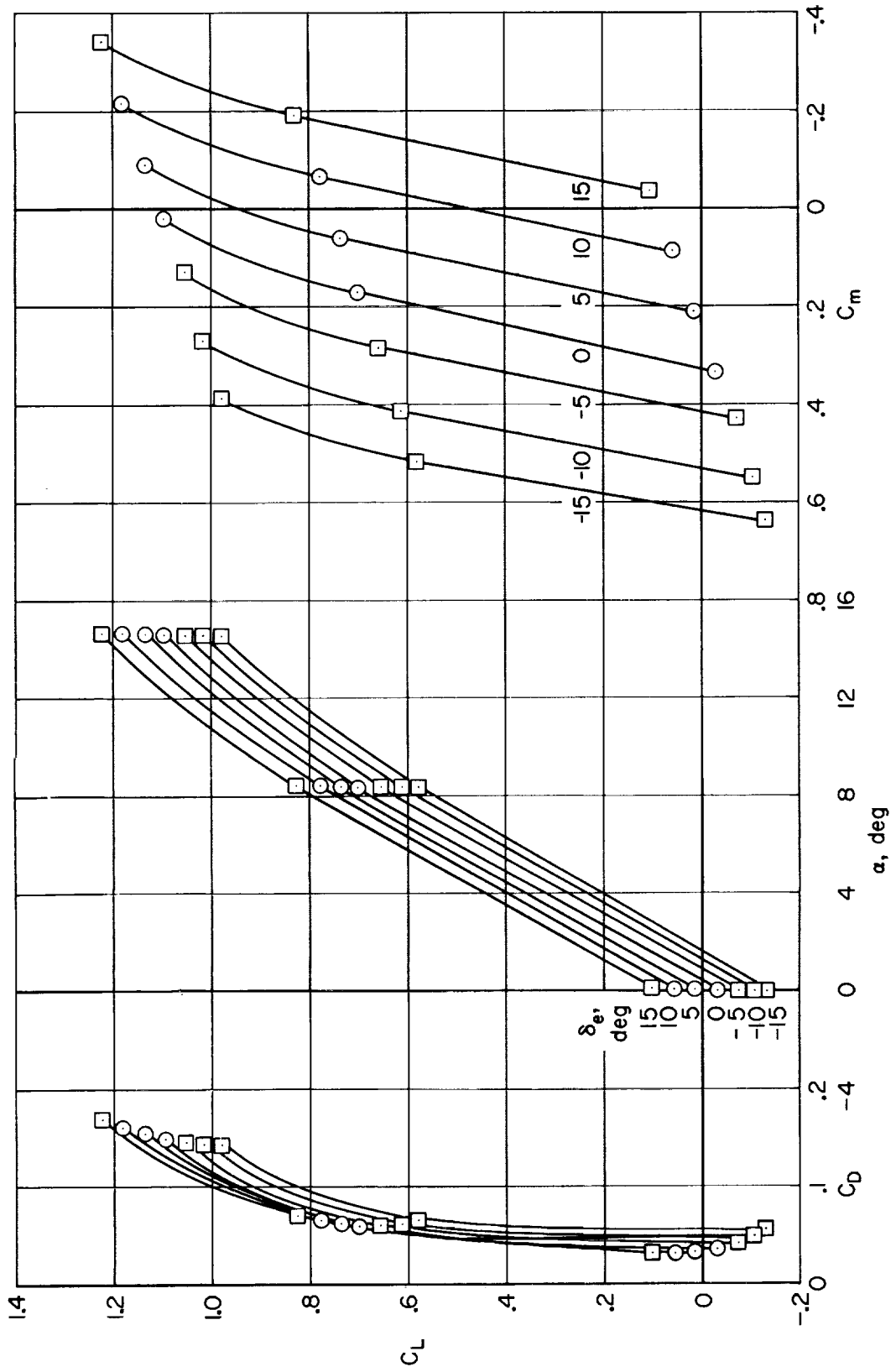

(f) $i_t = -7°$, $\delta_f = 0°$, R = 8.7X10⁶

Figure 7.- Concluded.

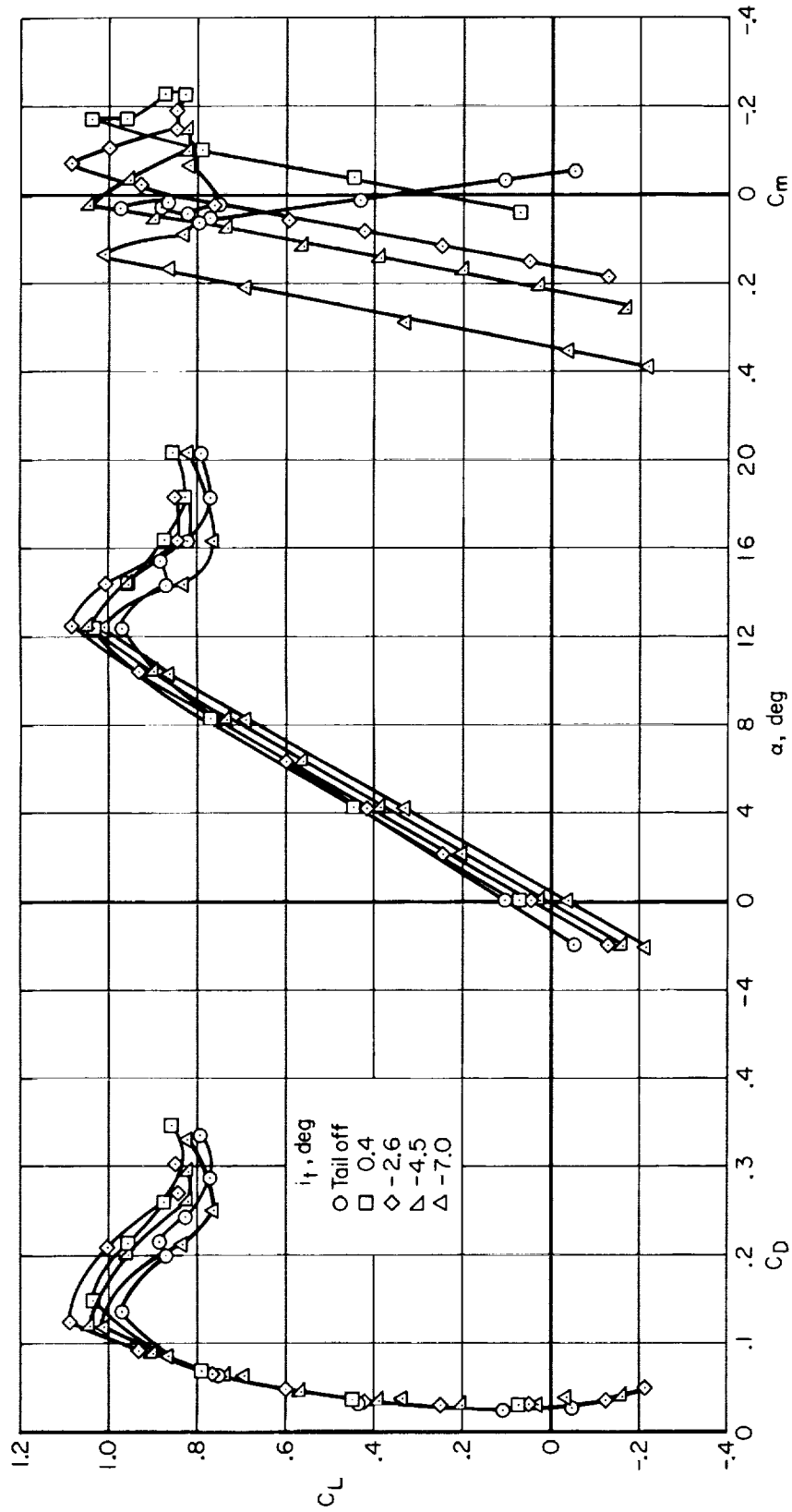

(a) $\delta_f = 0°$, $R = 4.1 \times 10^6$

Figure 8.- Effect of horizontal stabilizer incidence on longitudinal characteristics.

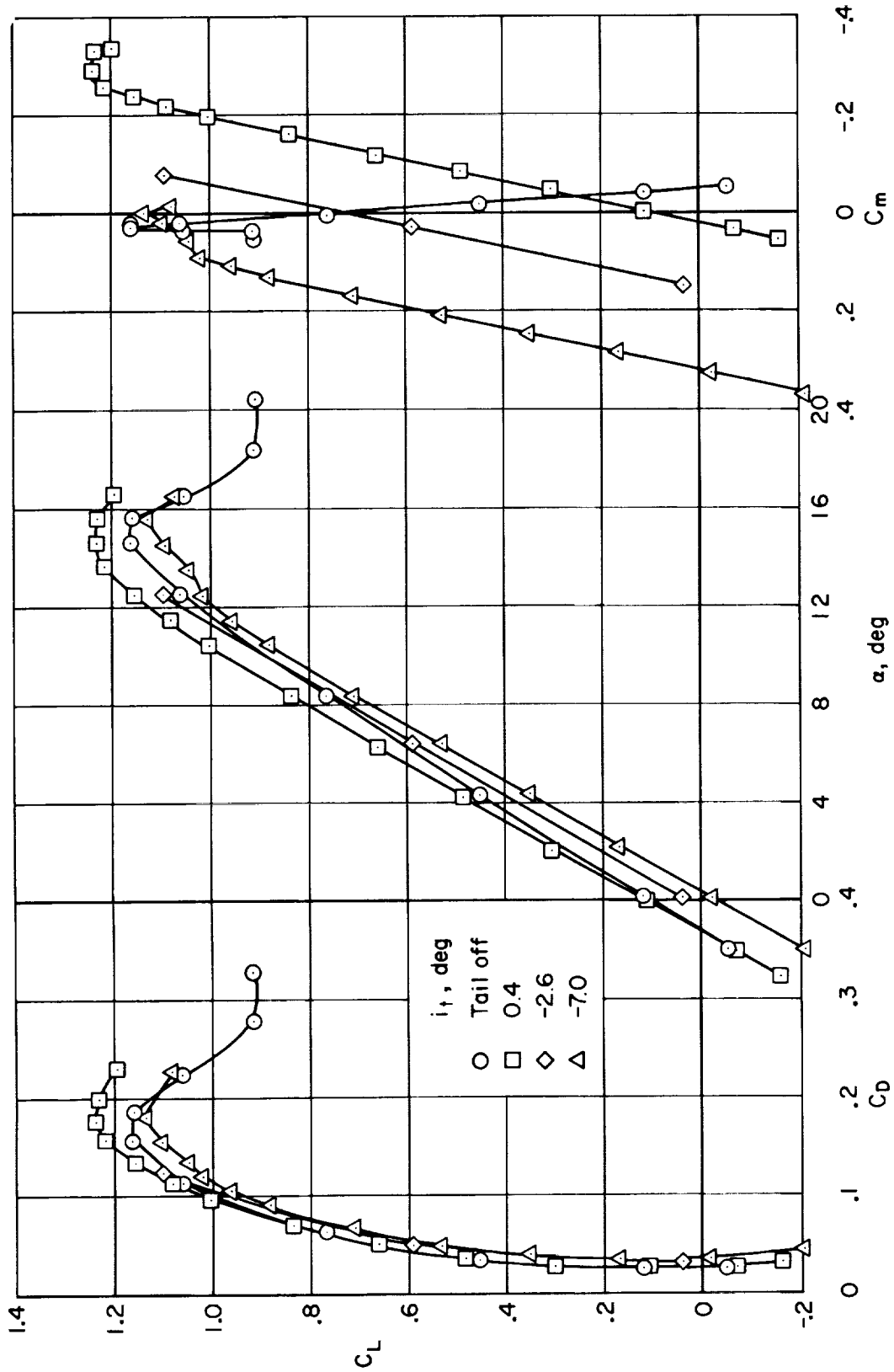

(b) $\delta_f = 0°$, R = 8.7X10^6

Figure 8.- Continued.

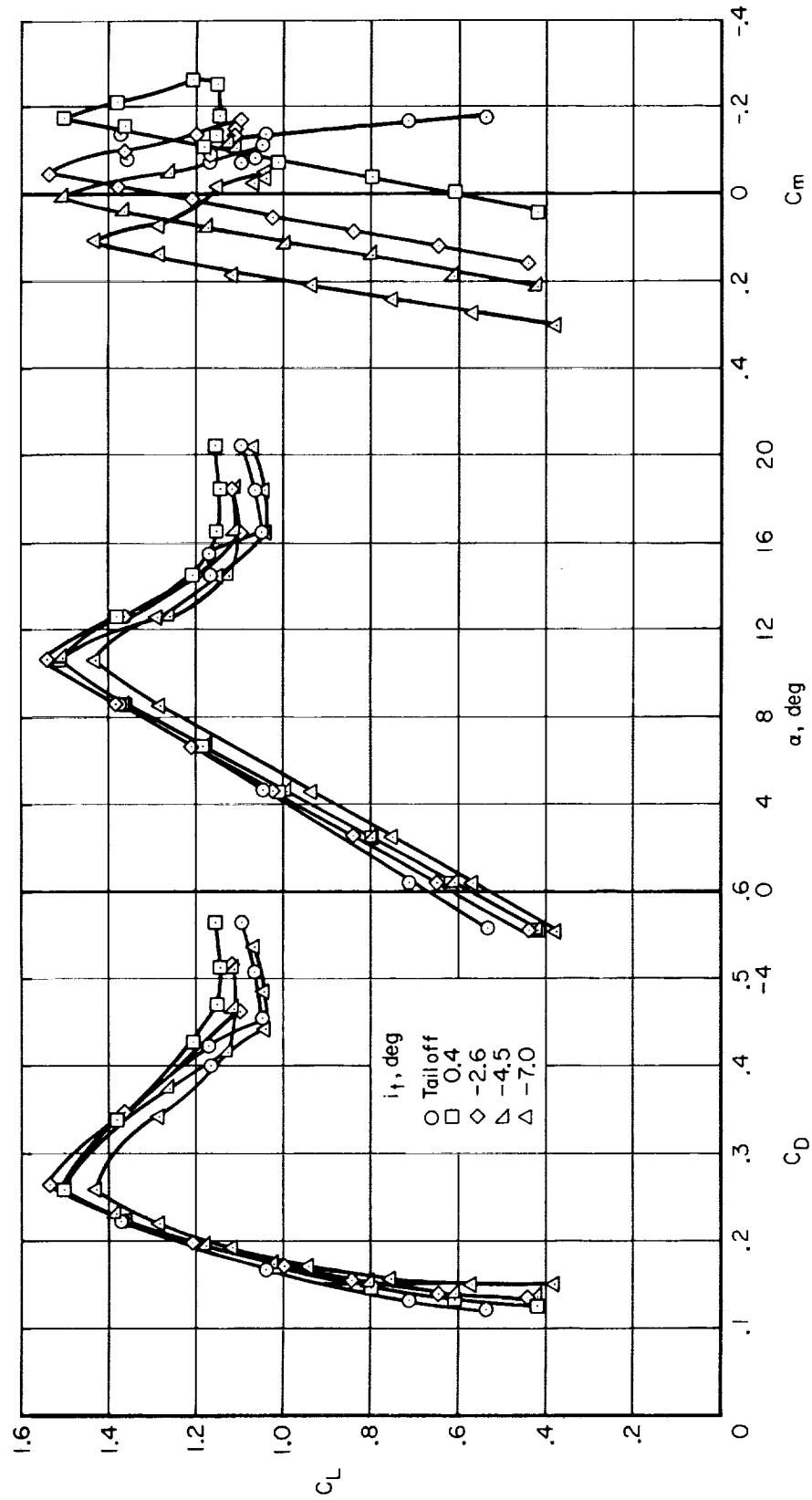

(c) $\delta_f = 40°$, R = 4.1X10^6

Figure 8.- Concluded.

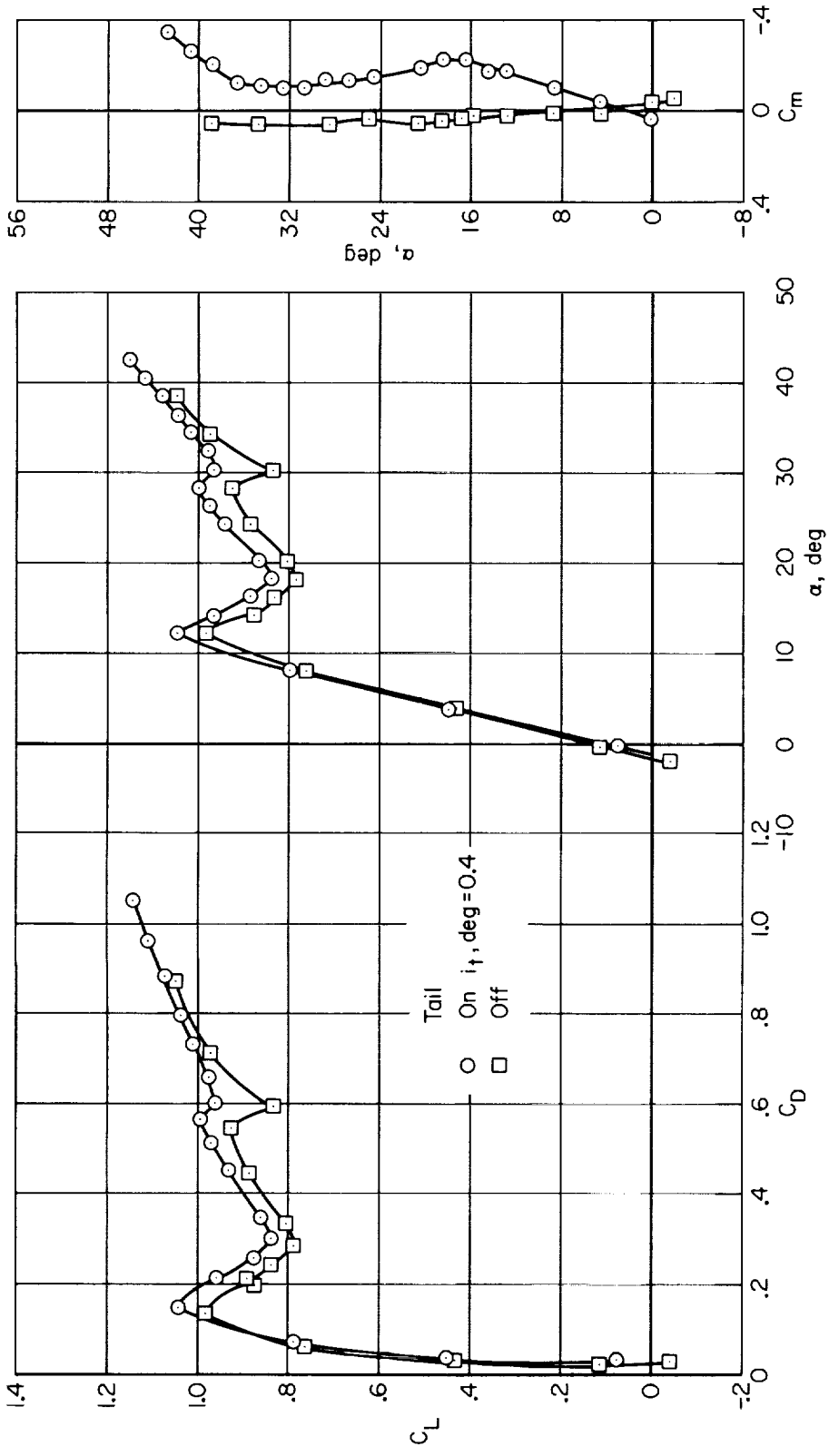

(a) $\delta_f = 0°$, $R = 4.1 \times 10^6$

Figure 9.- Effect of empennage on longitudinal characteristics.

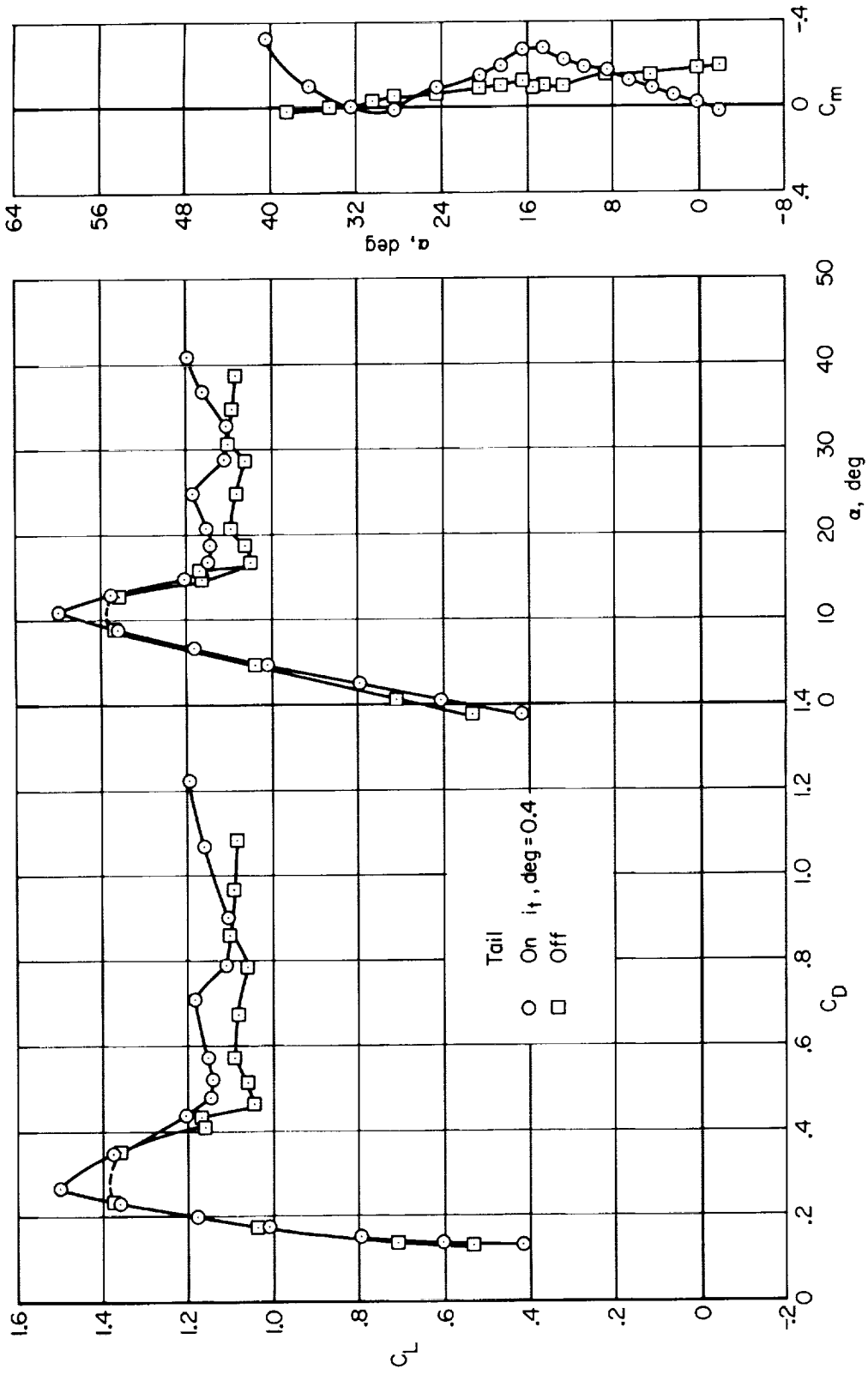

(b) $\delta_f = 40°$, R = 4.1X10⁶

Figure 9.- Continued.

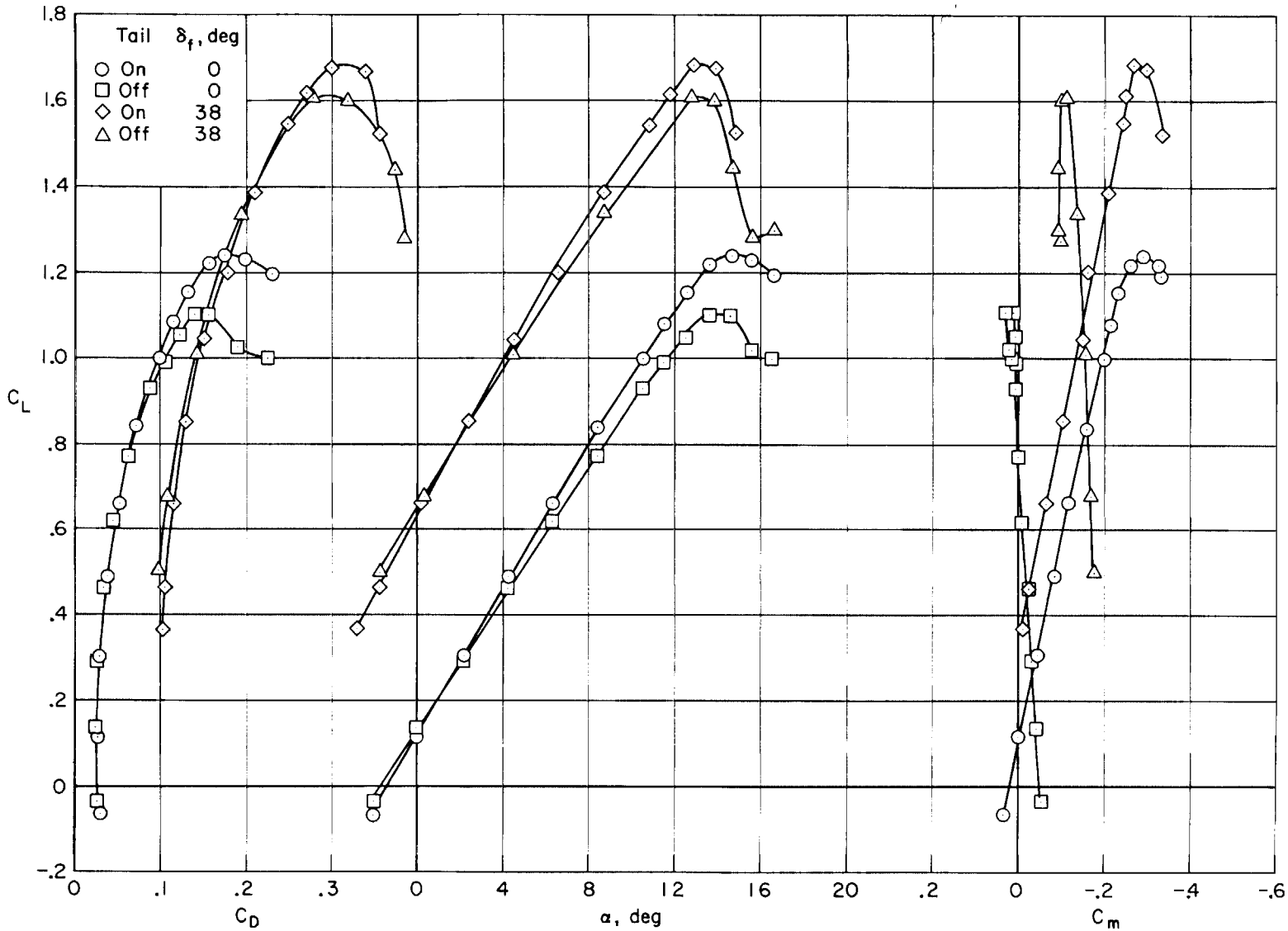

(c) R = 8.7X10⁴

Figure 9.- Concluded.

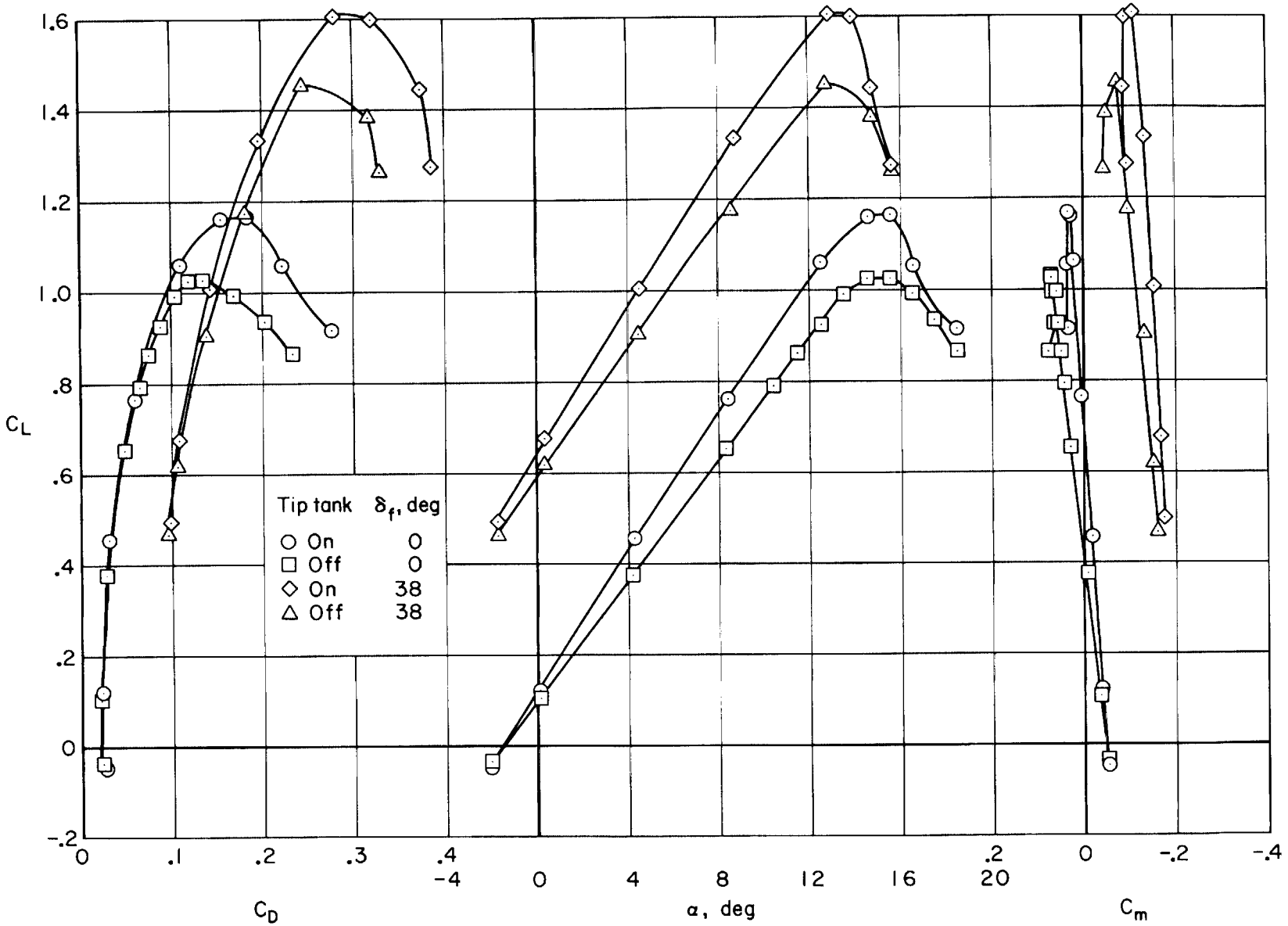

Figure 10.- Effect of removing wing tip tanks, tail off; R = 8.7×10^6.

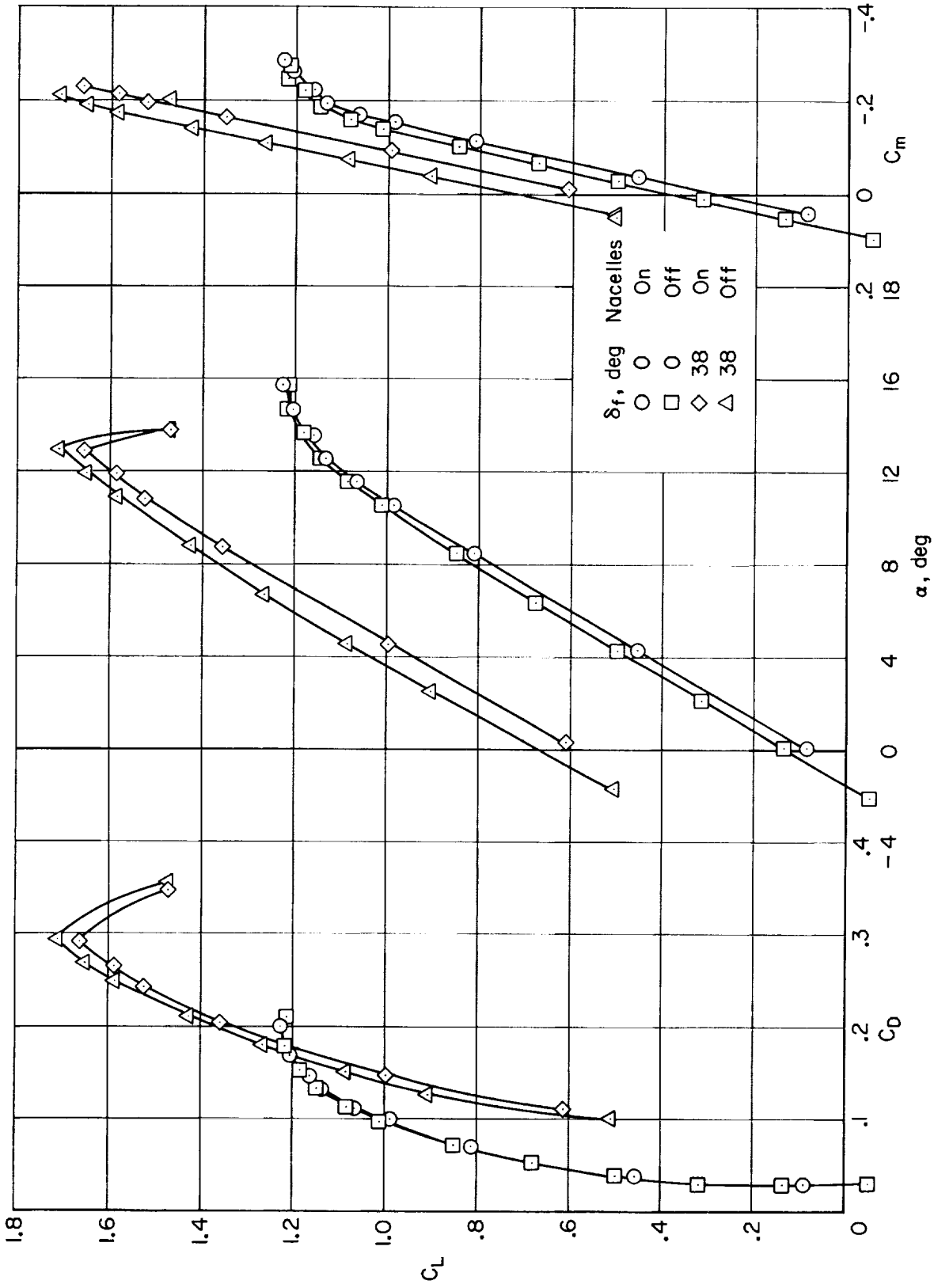

Figure 11.- Effect of engine nacelles on longitudinal characteristics; $R = 8.7 \times 10^6$, $i_t = 0.4°$.

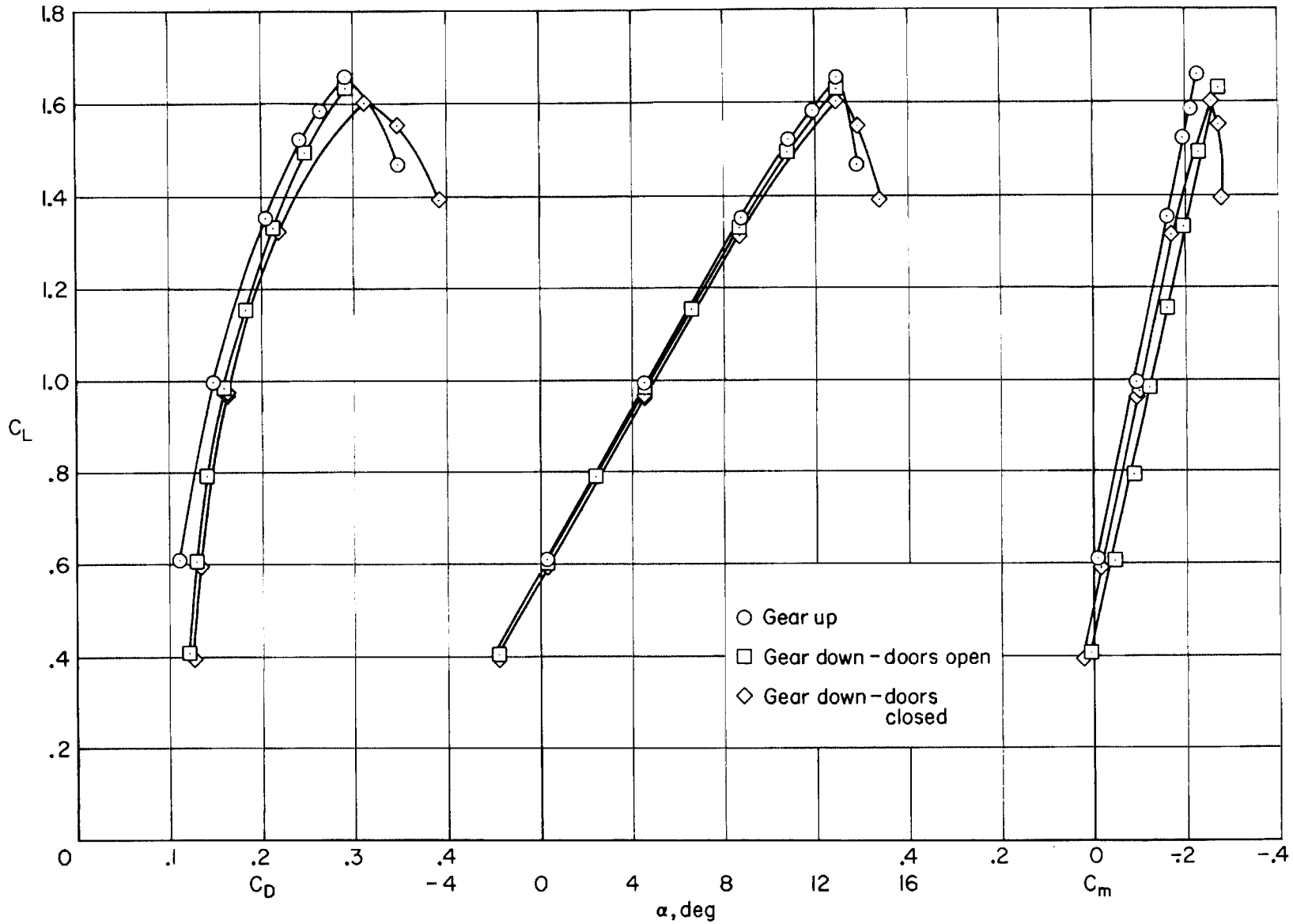

Figure 12.- Effect of landing gear and landing gear doors on longitudinal characteristics; $\delta_f = 38°$, $R = 8.7 \times 10^6$, $i_t = 0.4°$.

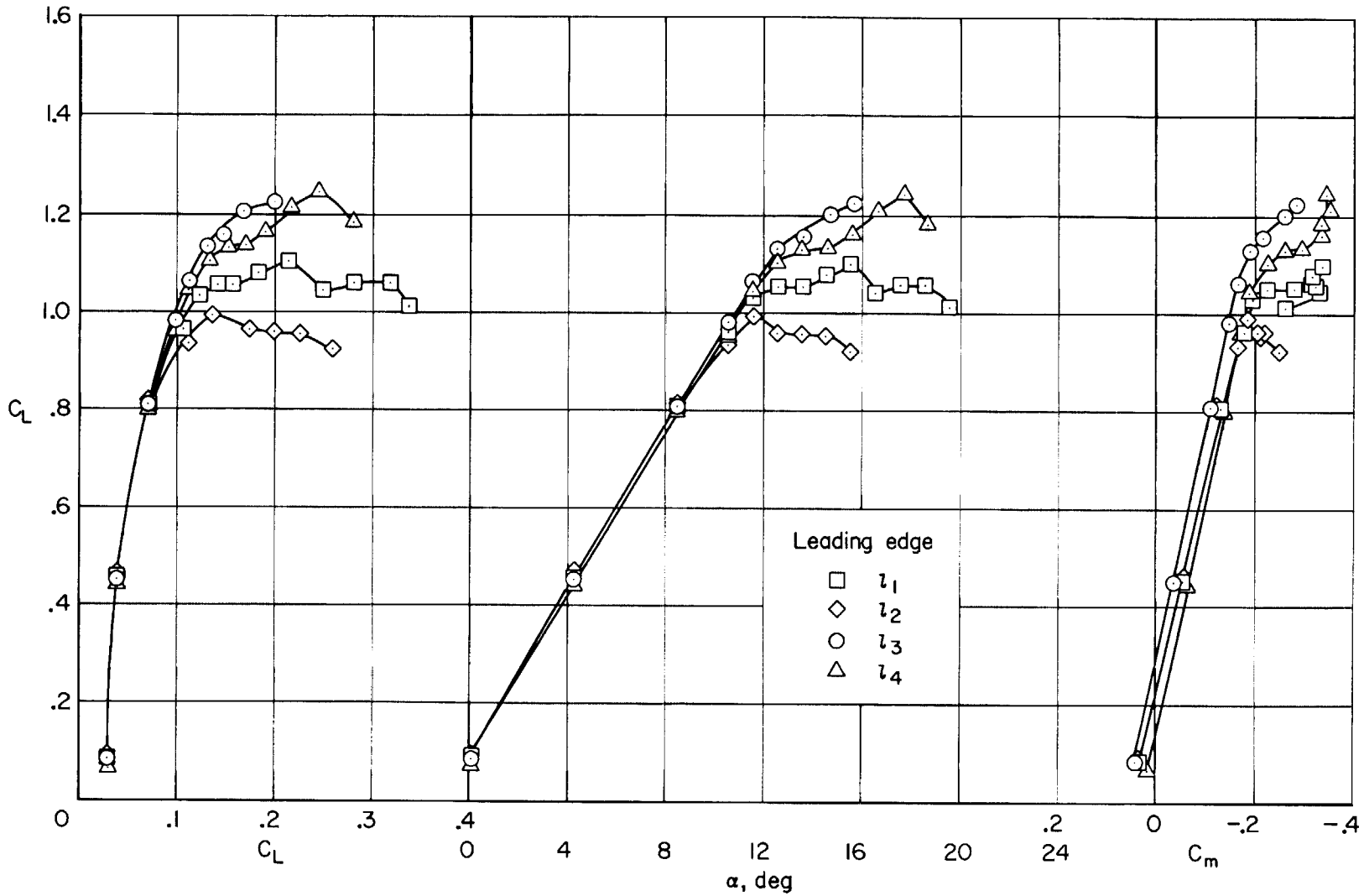

(a) $\delta_f = 0°$

Figure 13.- Comparison of four leading-edge modifications; $R = 8.7 \times 10^6$, $i_t = 0.4°$.

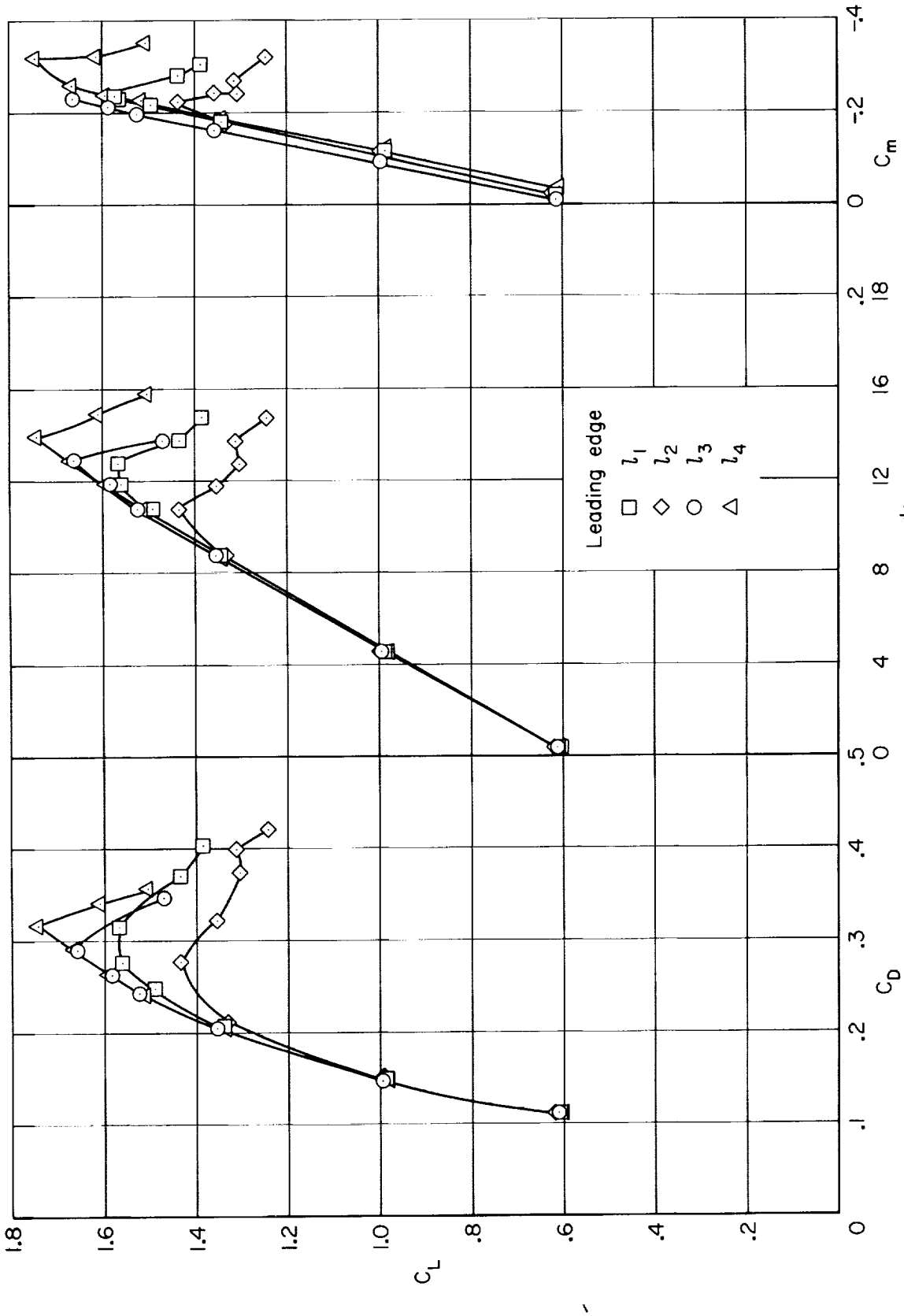

(b) $\delta_f = 38°$

Figure 13.- Concluded.

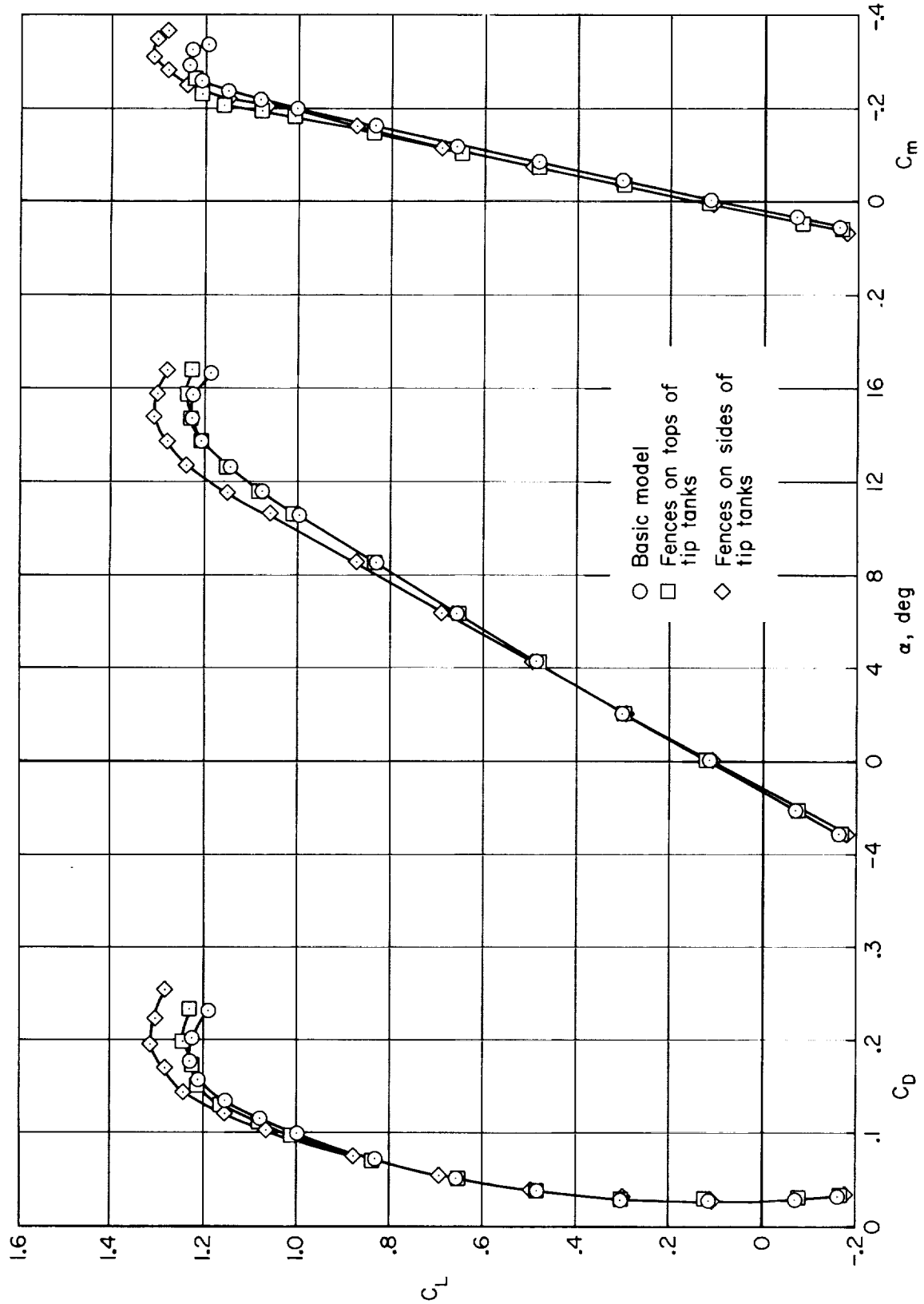

(a) Longitudinal data.

Figure 14.- Effect of fences on tip tanks; $i_t = 2.4°$, $\delta_f = 0°$, $R = 8.7 \times 10^6$.

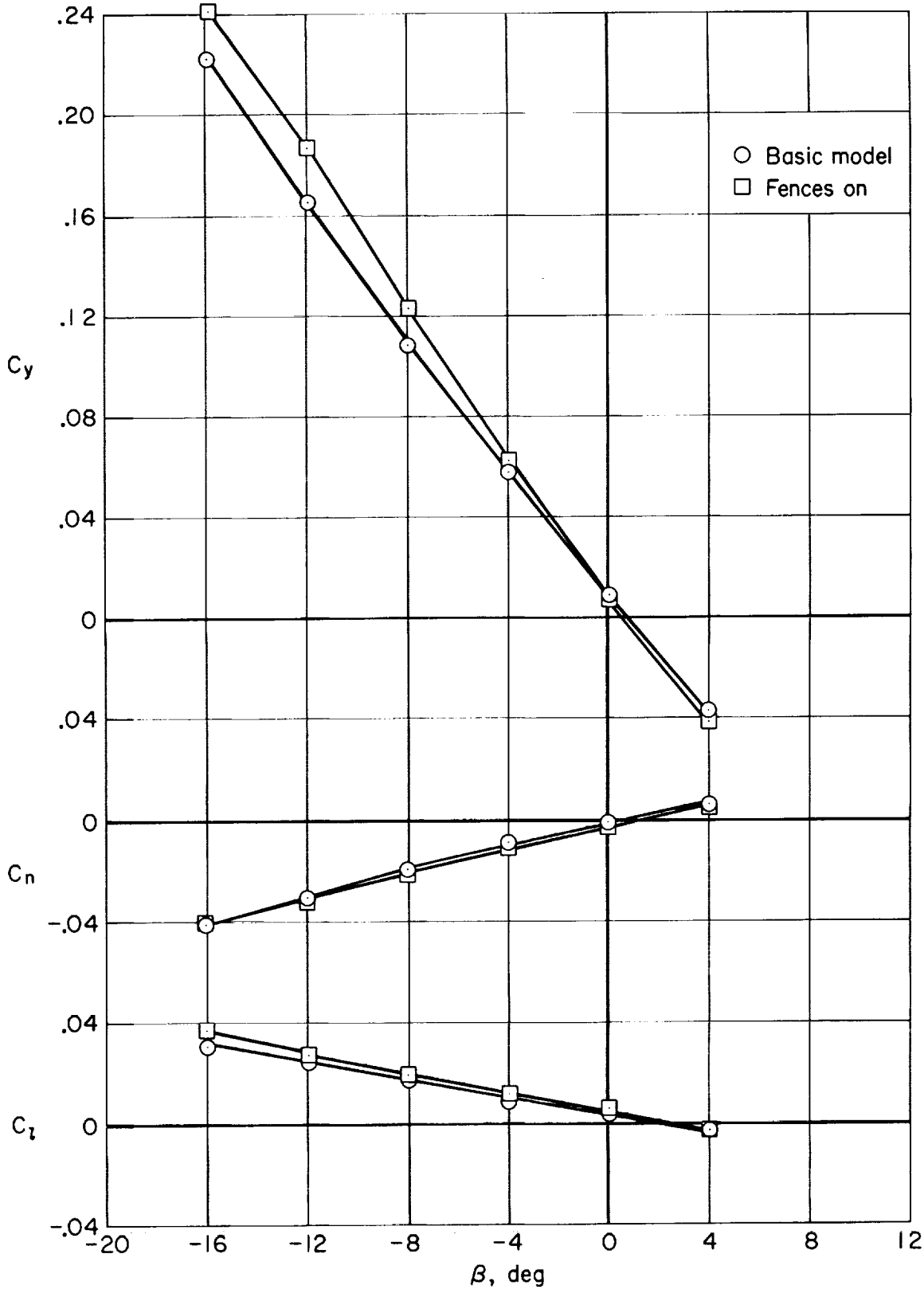

(b) Lateral characteristics with fences on tops of the tip tanks; $\alpha = 0°$.

Figure 14.- Concluded.

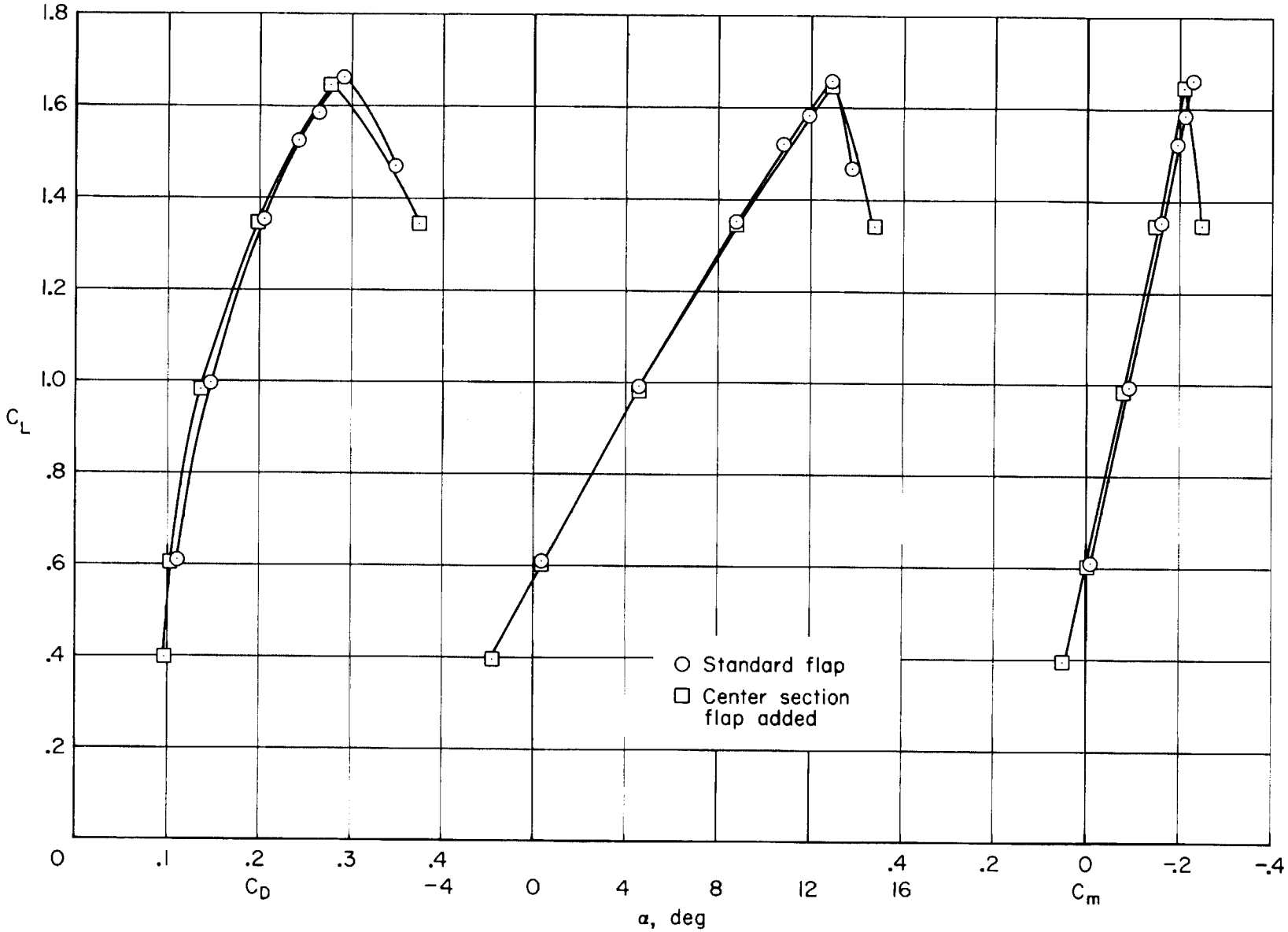

Figure 15.- Effect of standard flap with and without center section flap; $R = 8.7 \times 10^6$, $\delta_f = 38°$.

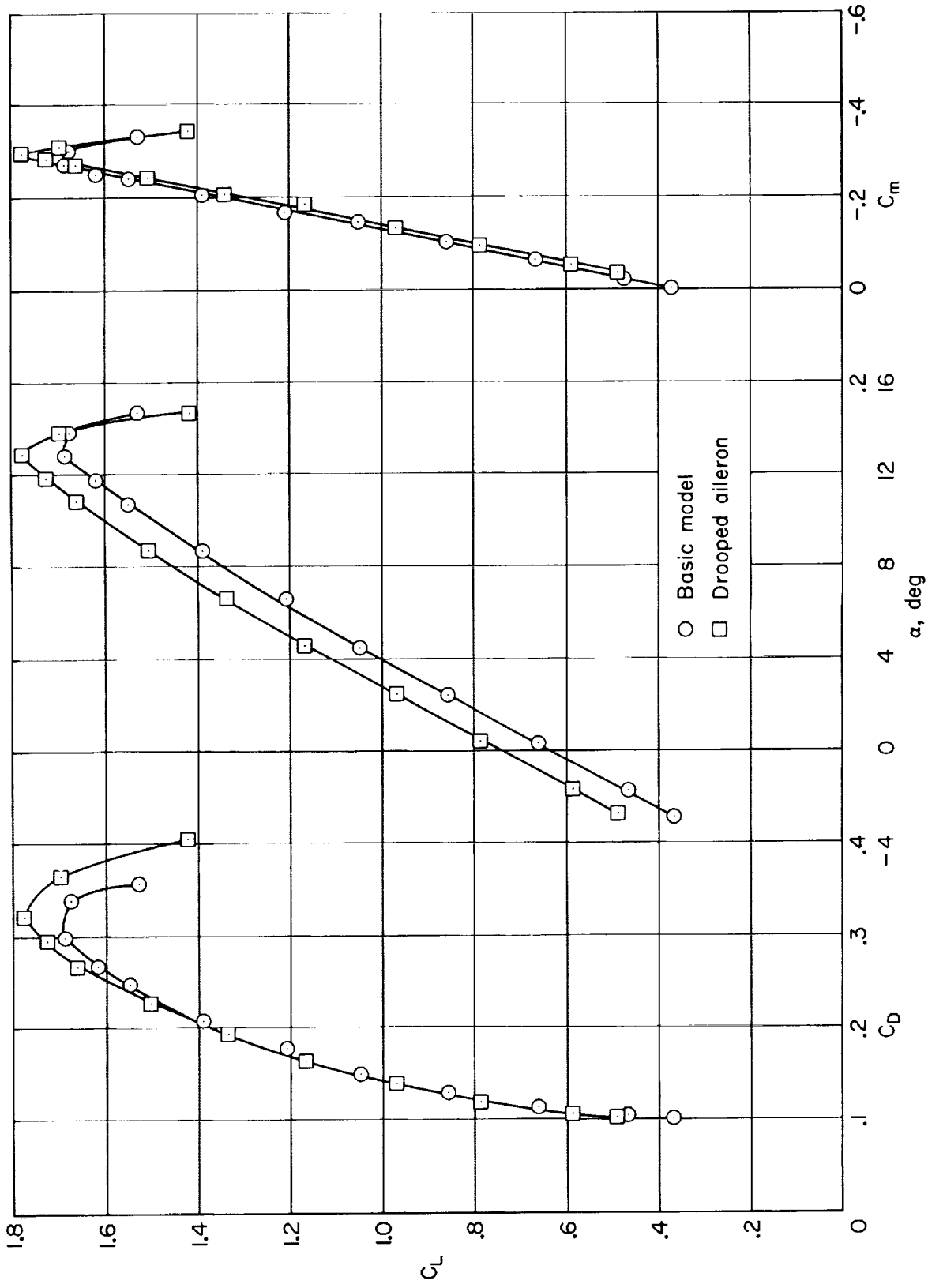

Figure 16.- Longitudinal characteristics with both ailerons drooped 13.7°, $\delta_f = 38°$, $R = 8.7 \times 10^6$, $i_t = 2.4°$.

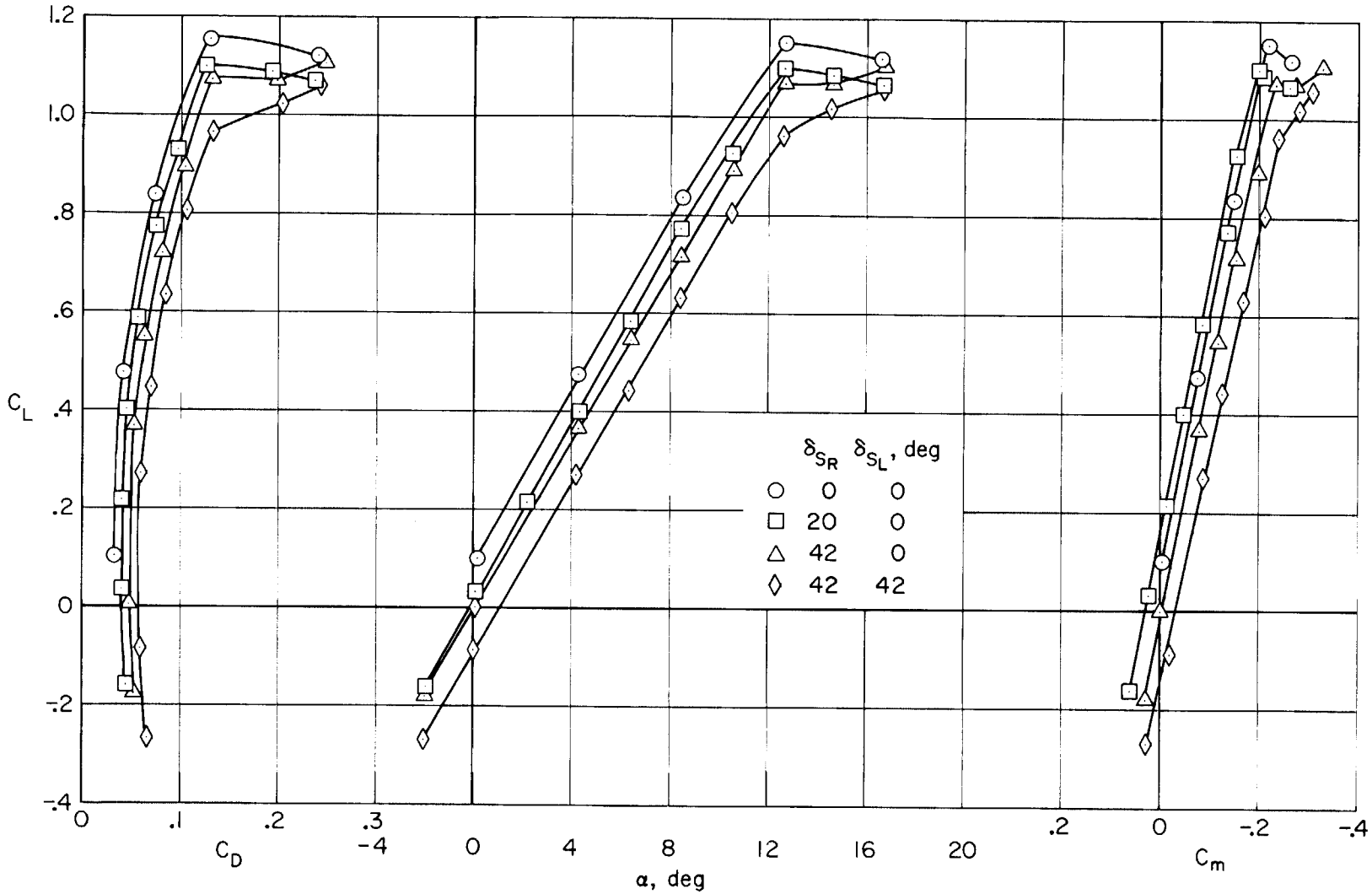

(a) $\delta_f = 0°$, $R = 5.8 \times 10^6$, $i_t = 0.4°$, basic spoiler.

Figure 17.- Effect of spoiler on longitudinal characteristics.

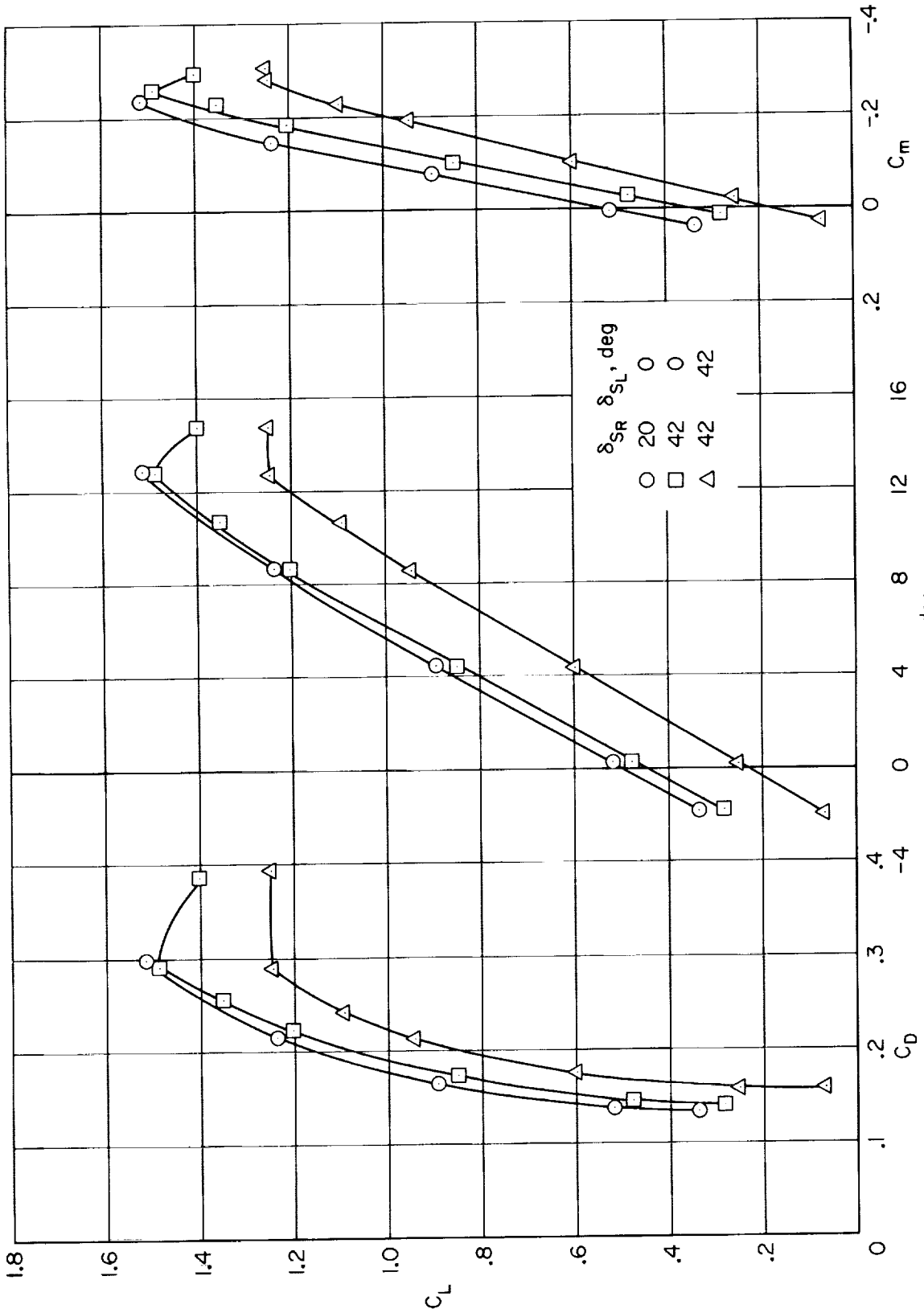

(b) $\delta_f = 40°$, R = 5.8X10^6, basic spoiler.

Figure 17.- Continued.

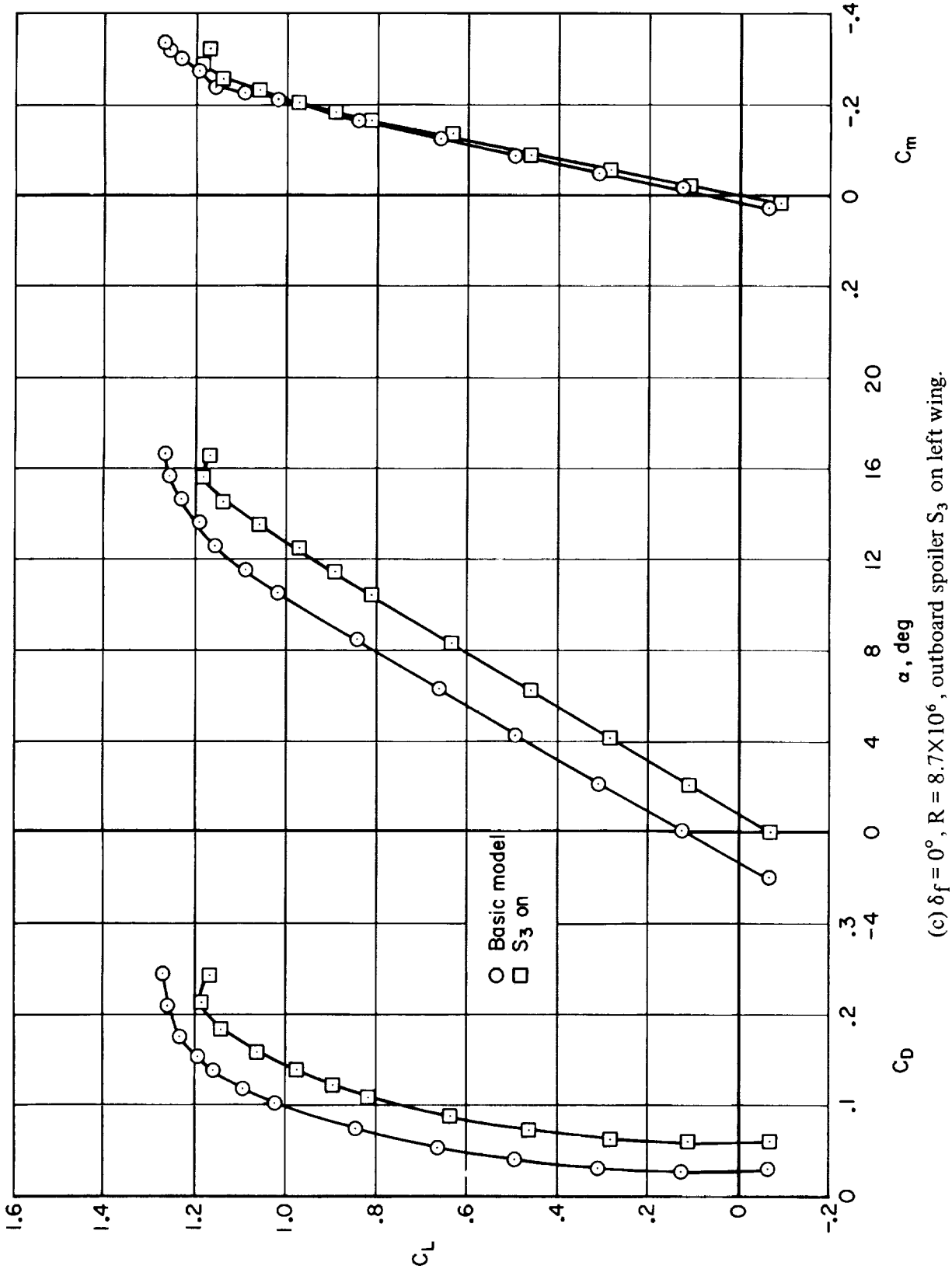

(c) $\delta_f = 0°$, R = 8.7X10^6, outboard spoiler S_3 on left wing.

Figure 17.- Concluded.

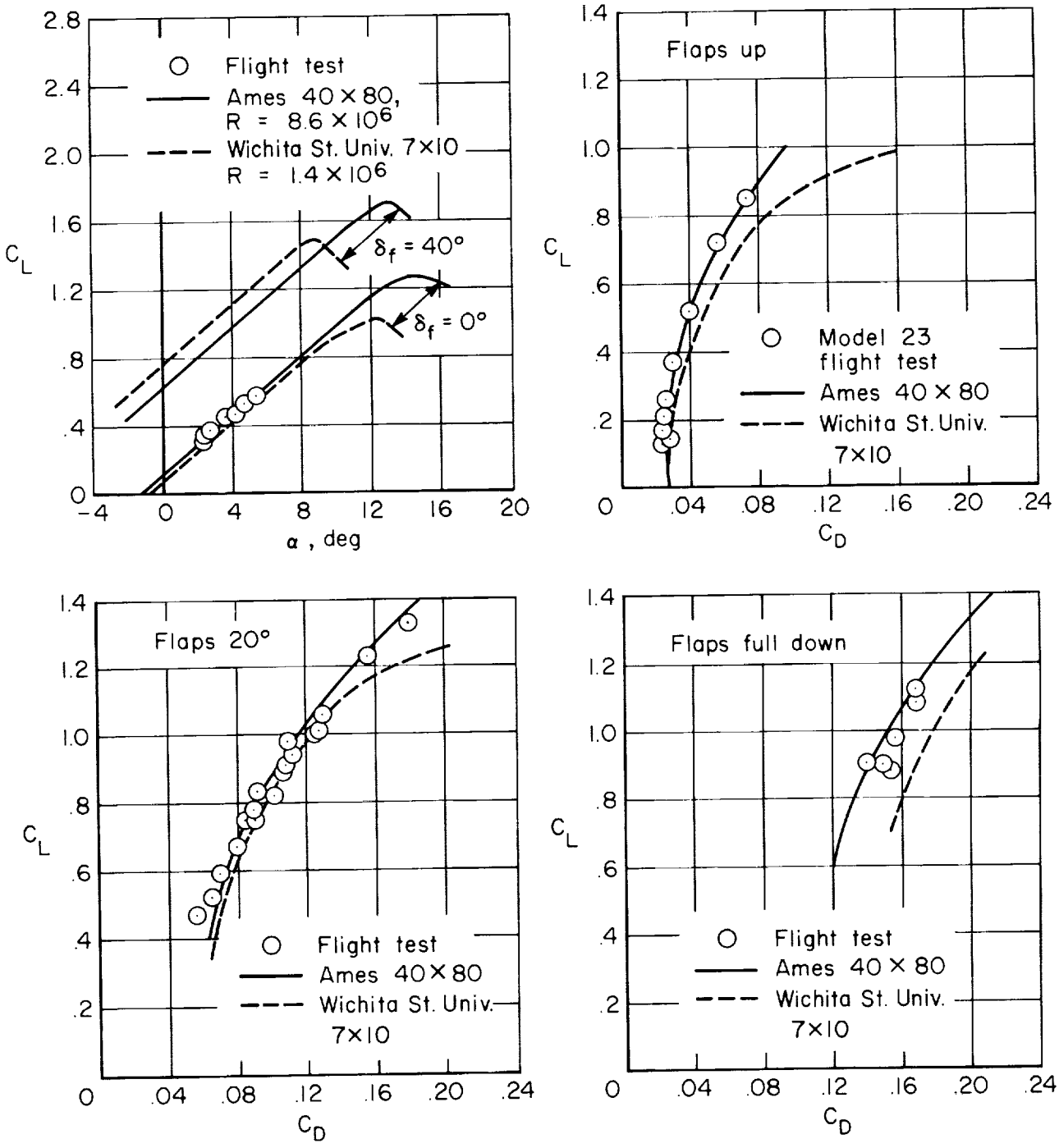

(a) Lift and drag characteristics.

Figure 18.- Comparison of wind-tunnel and flight-test data (taken from ref. 6).

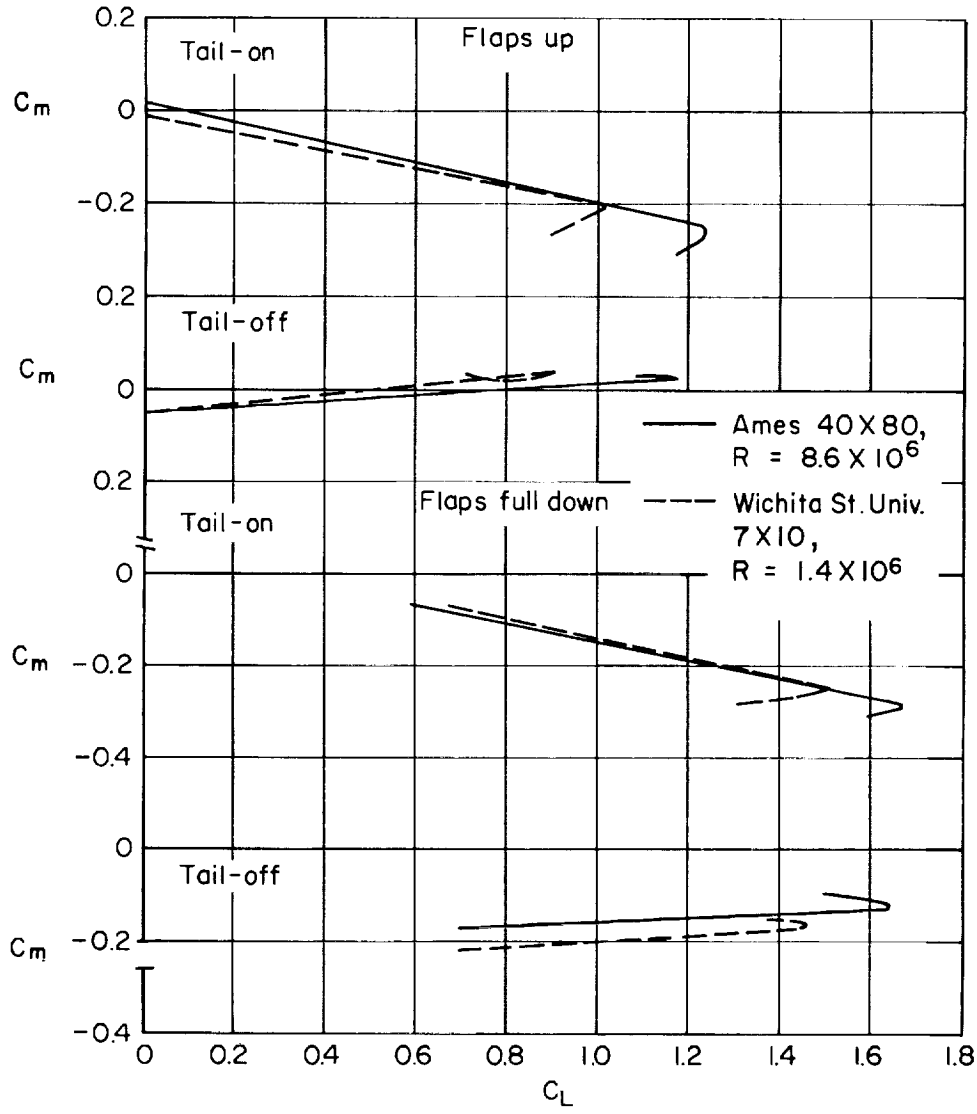

(b) Pitching-moment characteristics.

Figure 18.- Concluded.

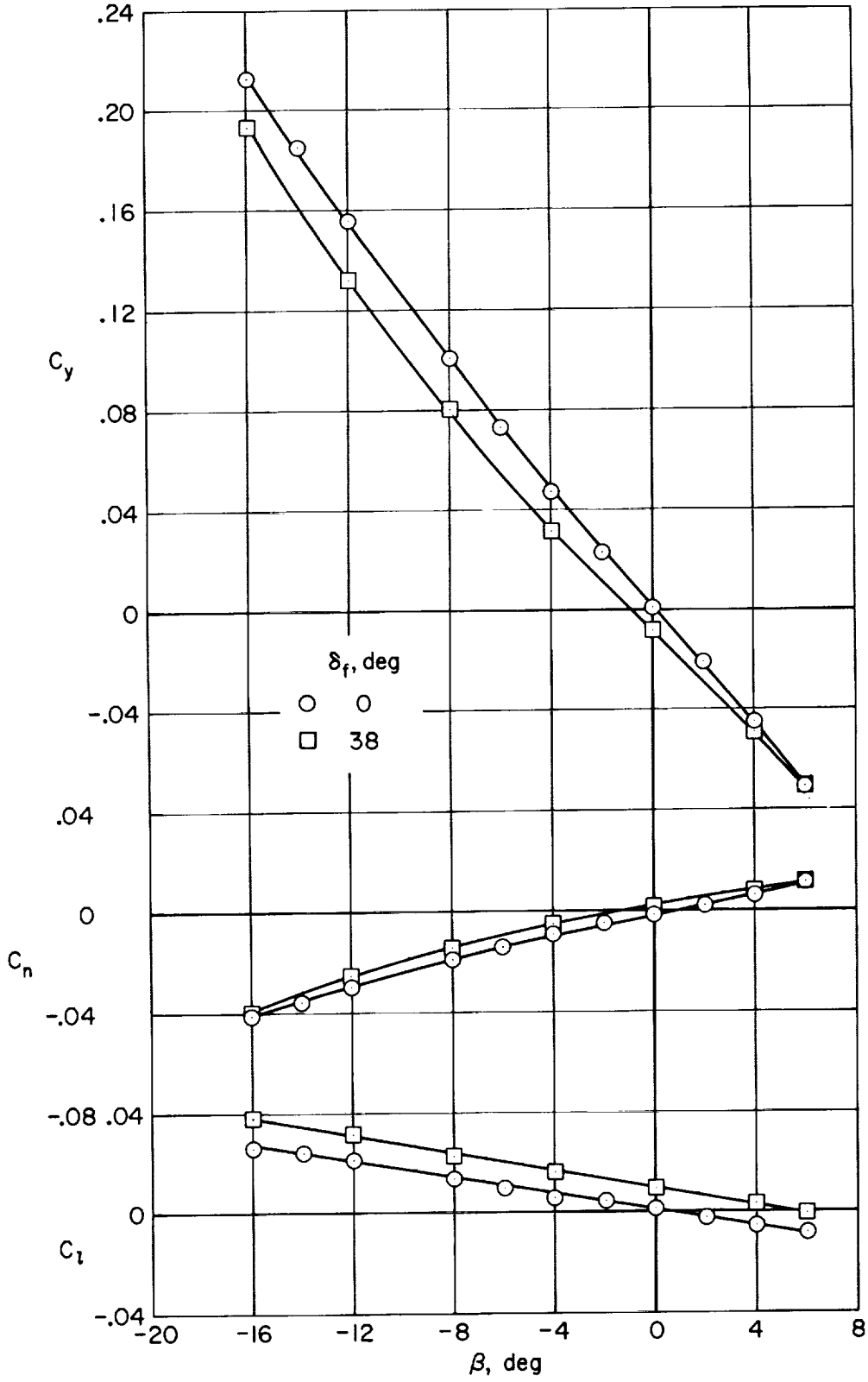

(a) $\alpha = 0°$, R = 8.7×10^6, flaps 0° and 38°

Figure 19.- Lateral characteristics of basic configuration in sideslip.

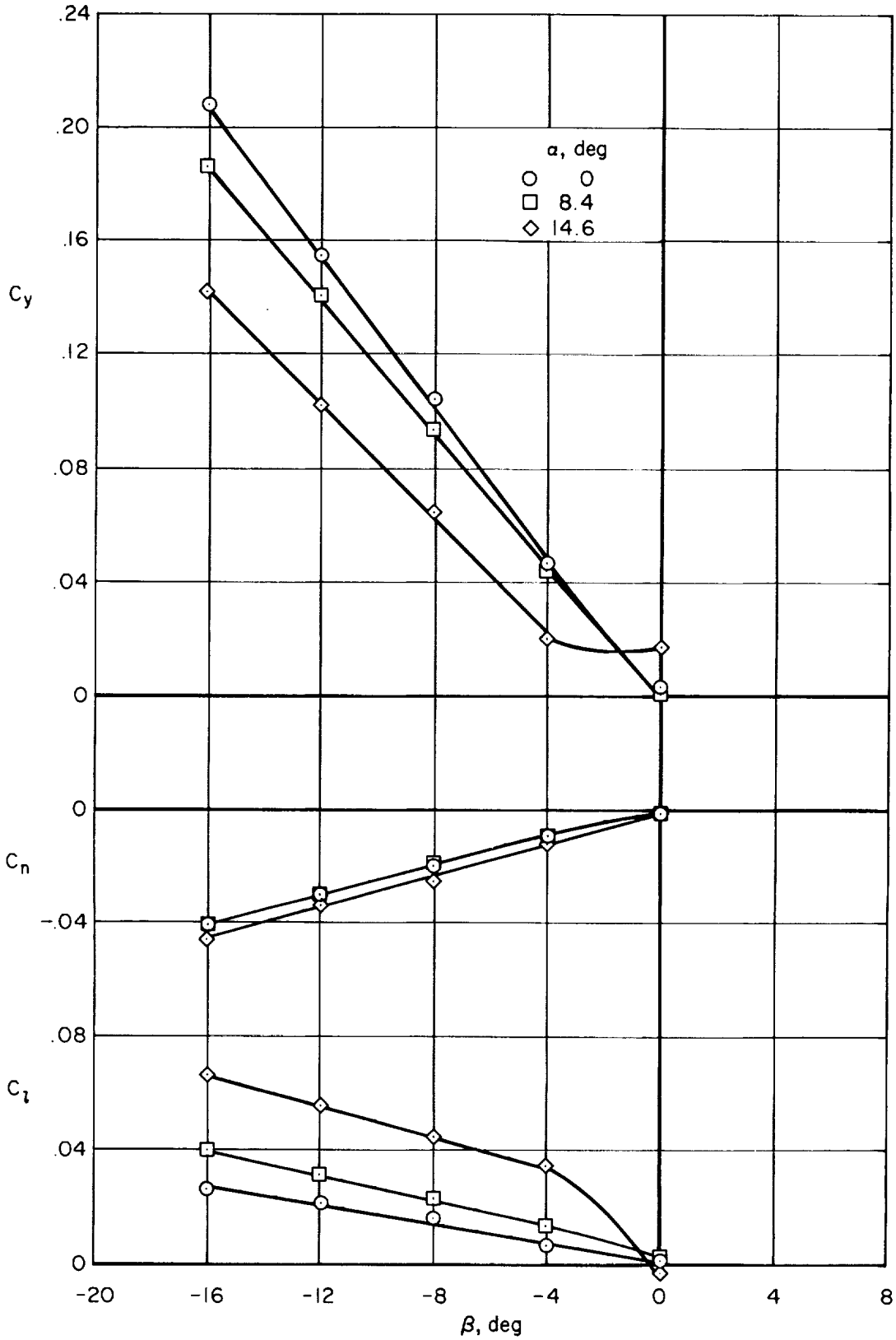

(b) $\delta_f = 0°$, R = 8.7X10^6, $\alpha = 0°$, 8.4°, and 14.6°.

Figure 19.- Continued.

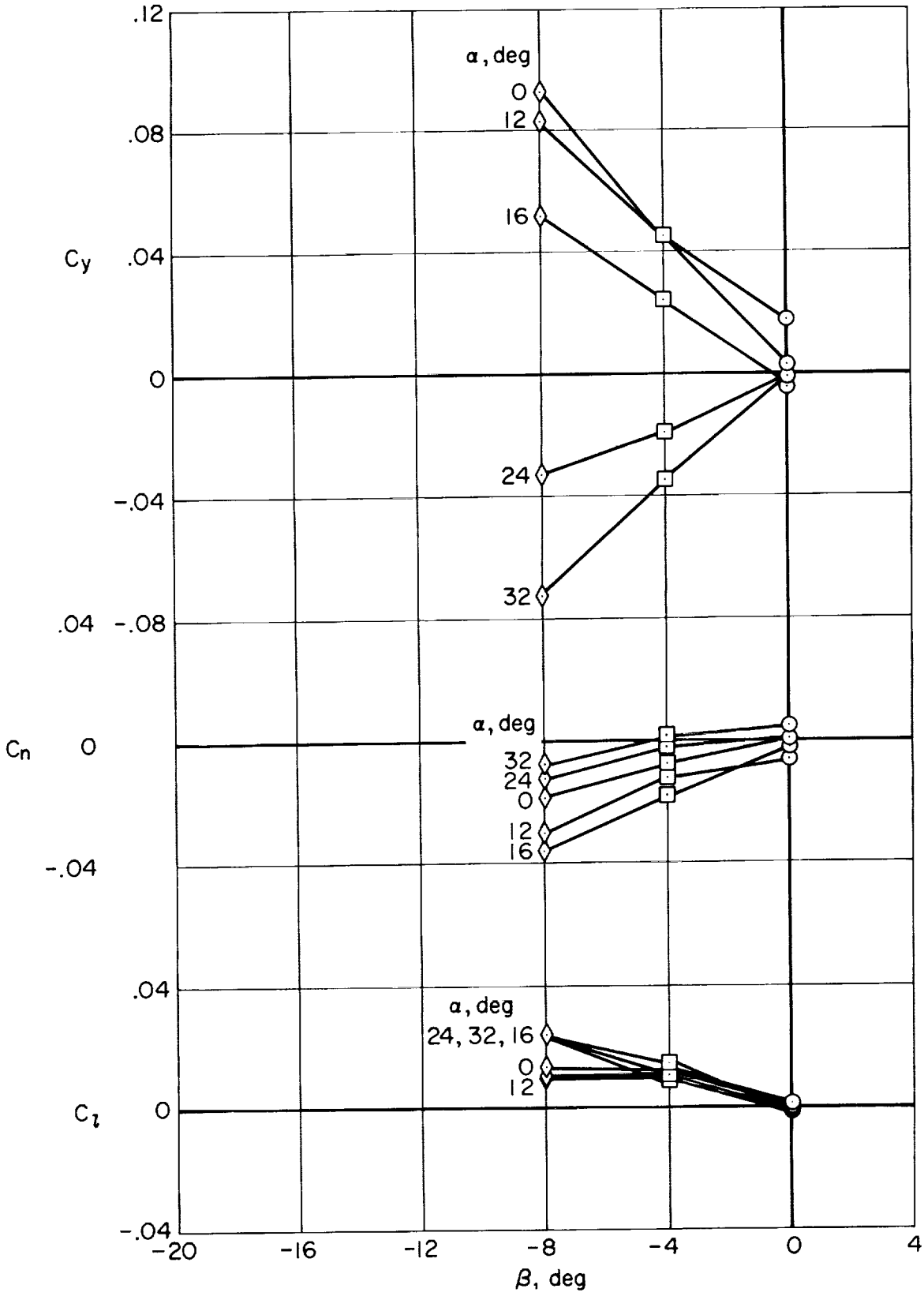

(c) $\delta_f = 0°$, R = 4.1×10^6, $\alpha = 0°, 12°, 16°, 24°, 32°$

Figure 19.- Concluded.

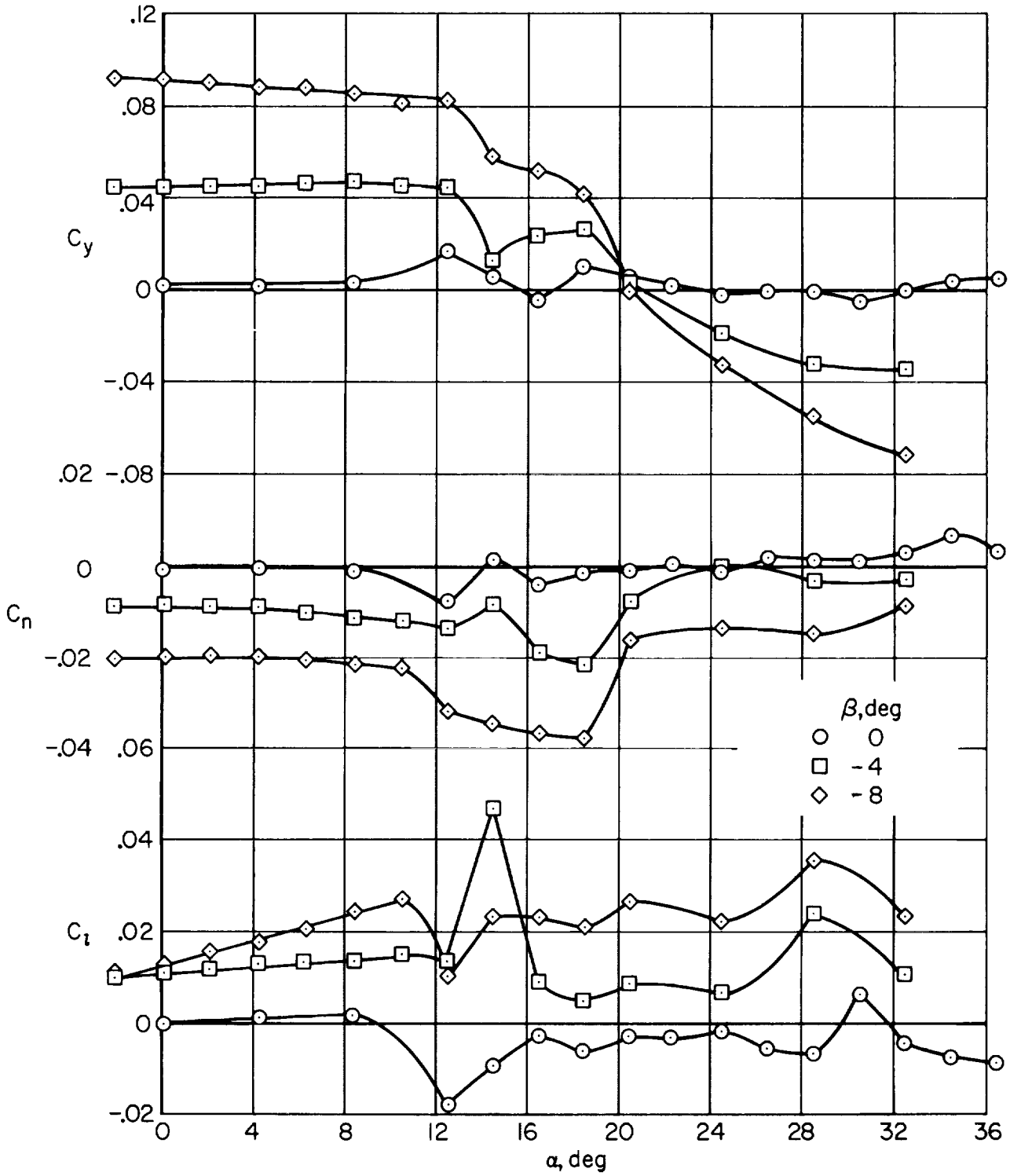

(a) $\delta_f = 0°$, $R = 4.1 \times 10^6$, $\beta = 0°, -4°, -8°$

Figure 20.- Lateral characteristics of basic configuration versus angle of attack.

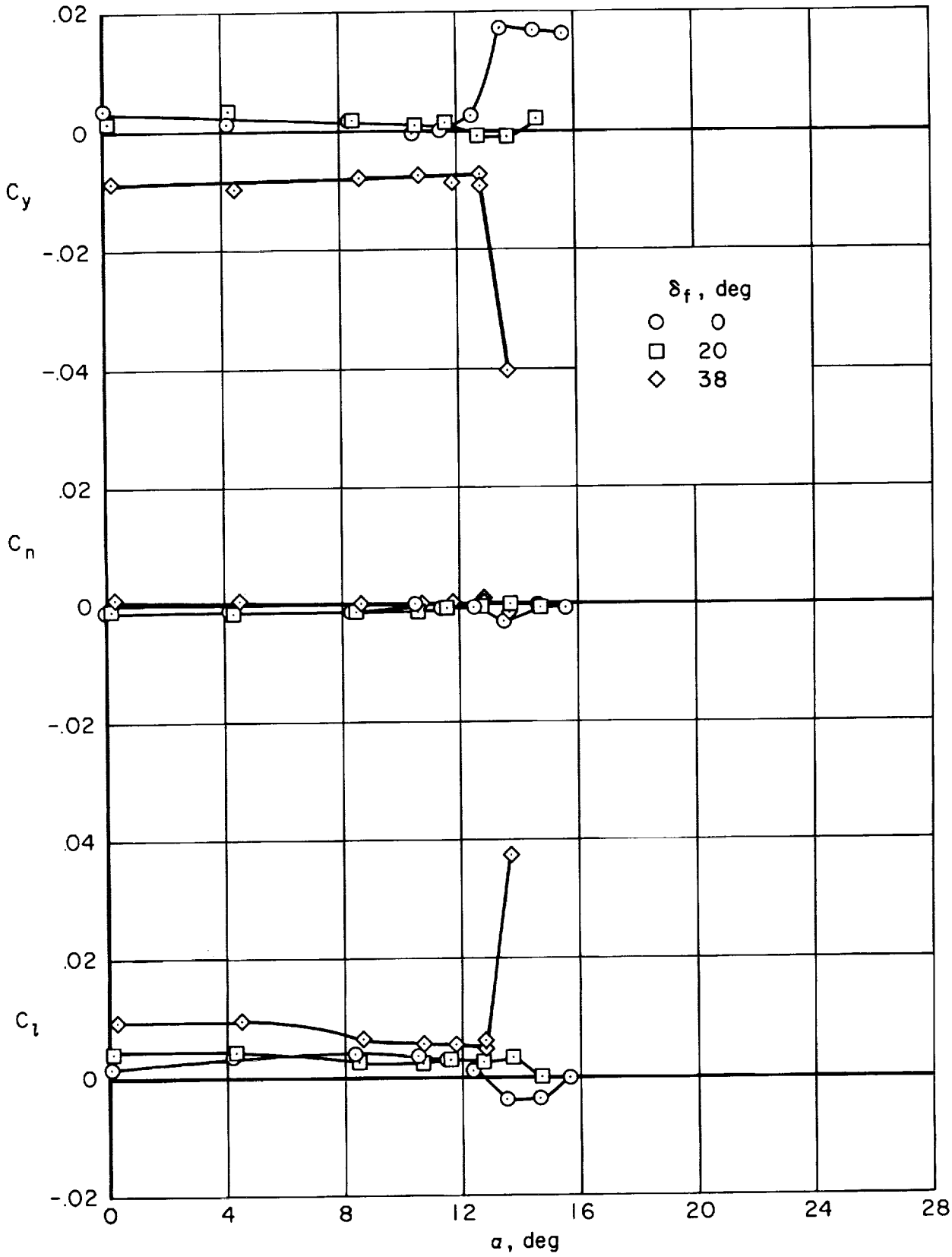

(b) R = 8.7X10^6, $\beta = 0°$, $\delta_f = 0°, 20°, 38°$

Figure 20.- Concluded.

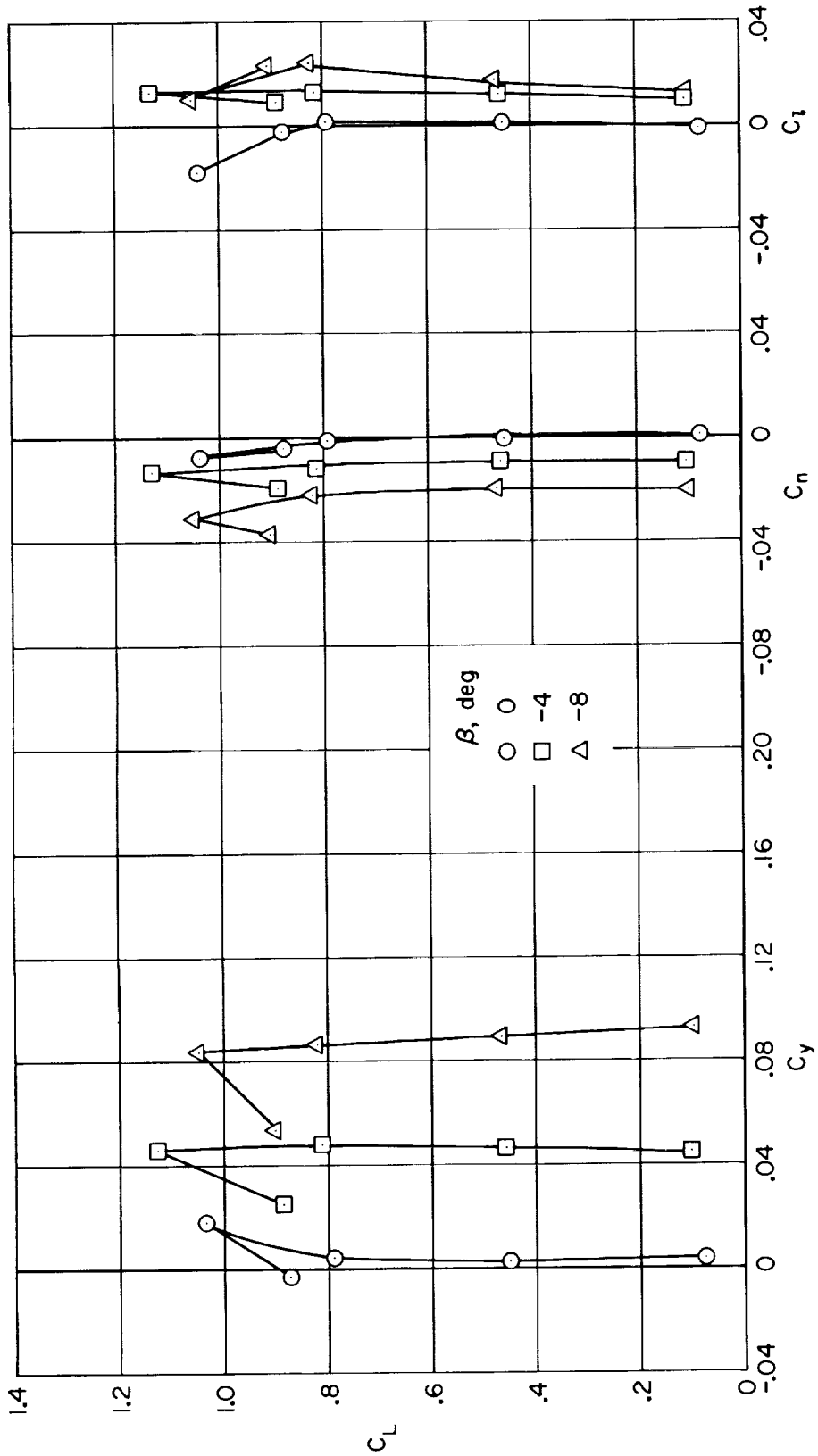

Figure 21.- Lateral characteristics of basic configuration versus lift coefficient; $\delta_f = 0°$, $R = 4.1 \times 10^6$, $\alpha = 0°$.

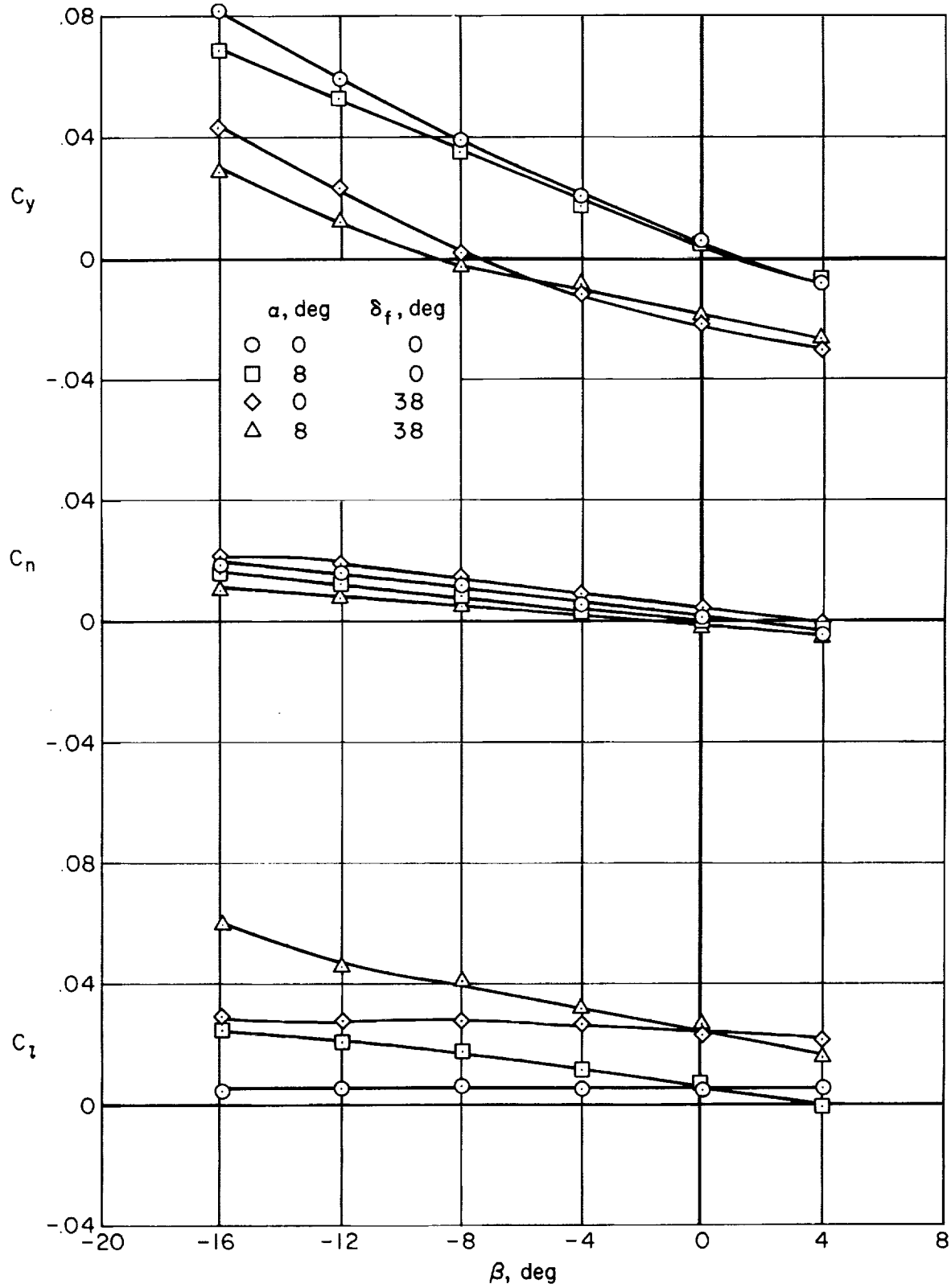

Figure 22.- Lateral characteristics of the model in sideslip with the empennage removed; $R = 8.7 \times 10^6$.

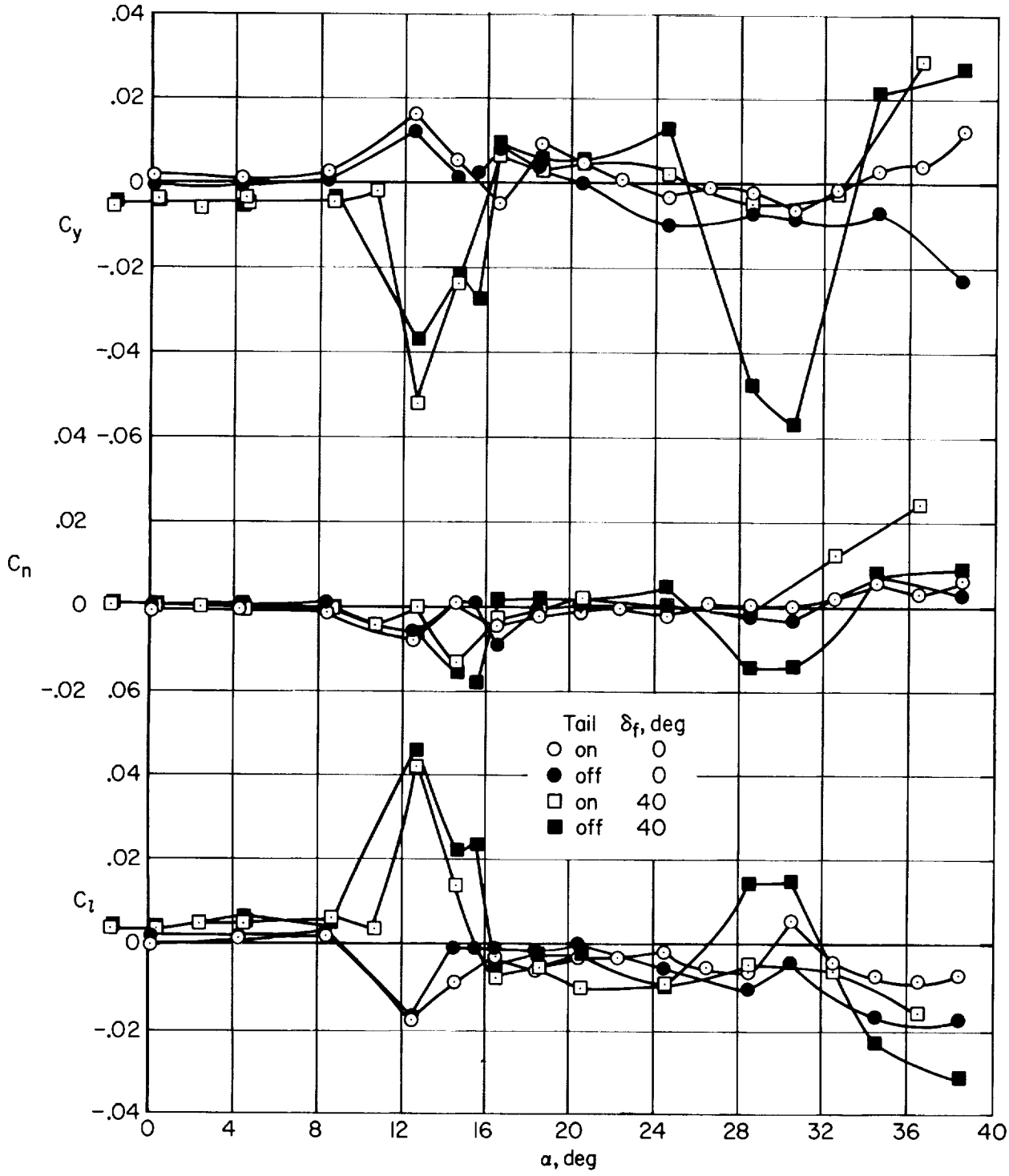

Figure 23.- Lateral characteristics versus angle of attack, tail on and off; $\delta_f = 0°$ and 40°, $R = 4.1 \times 10^6$.

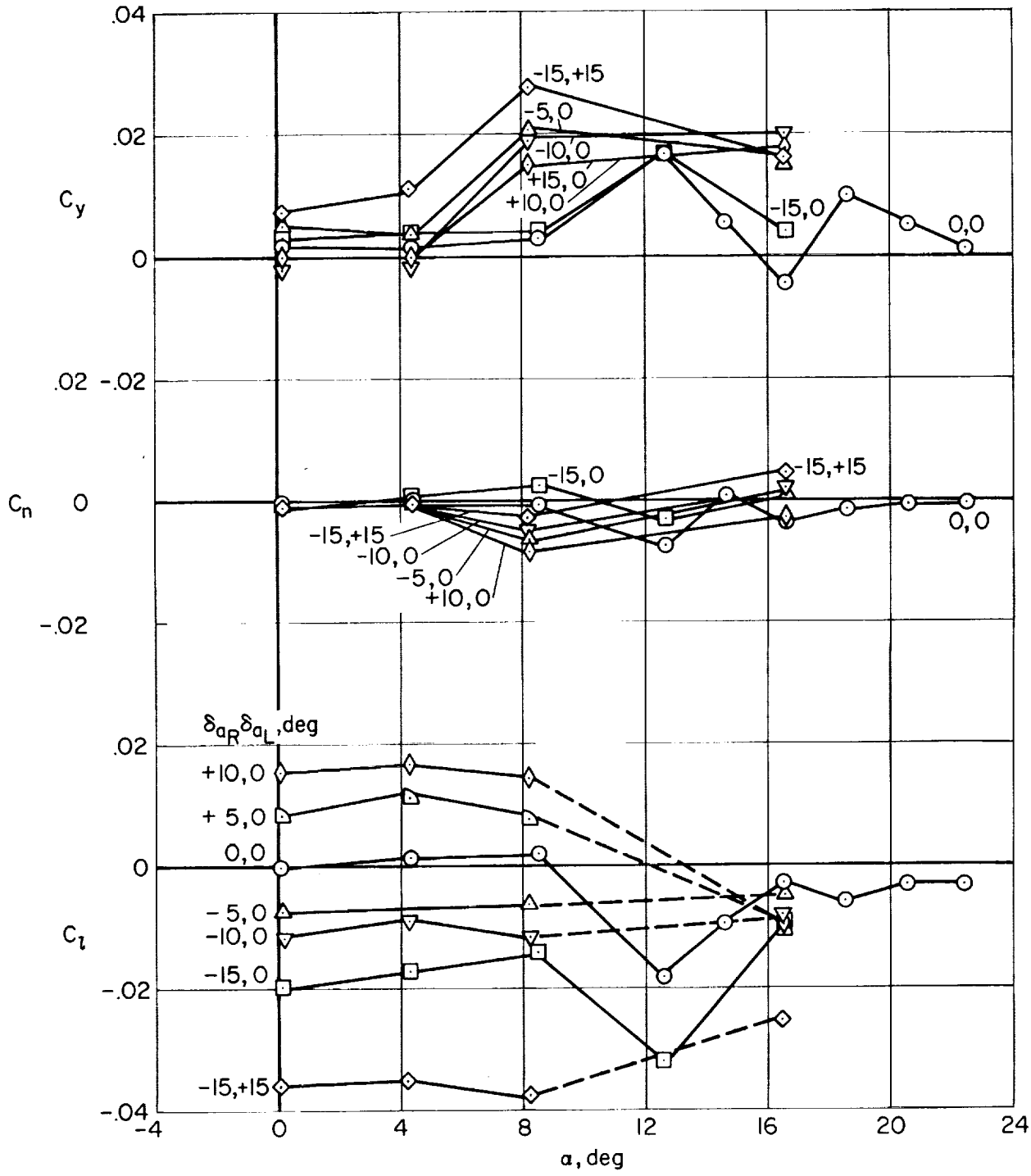

(a) $\delta_f = 0°$, R = 4.1X10^6

Figure 24.- Aileron effectiveness.

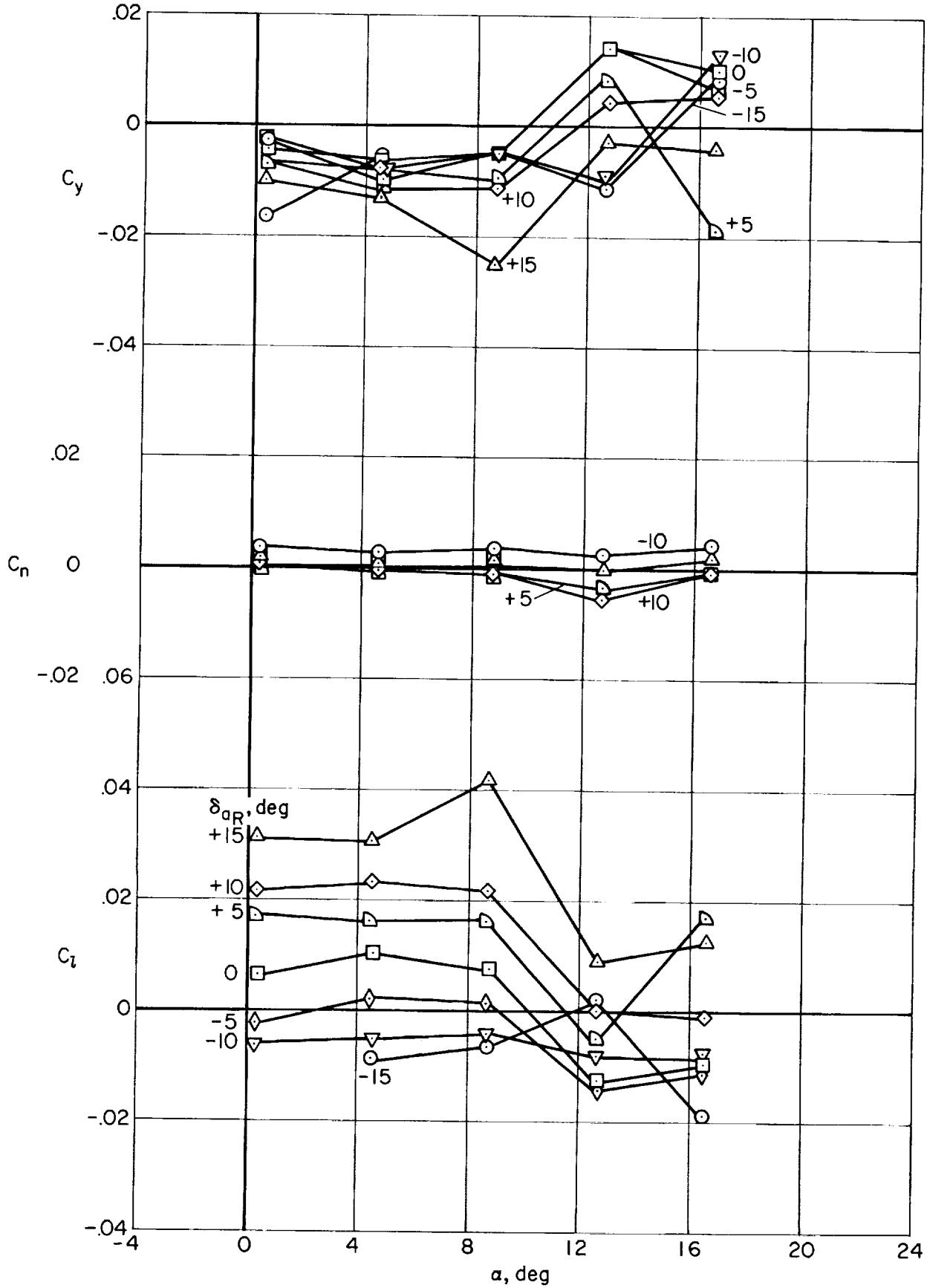

(b) $\delta_f = 40°$, R = 4.1X10⁶

Figure 24.- Continued.

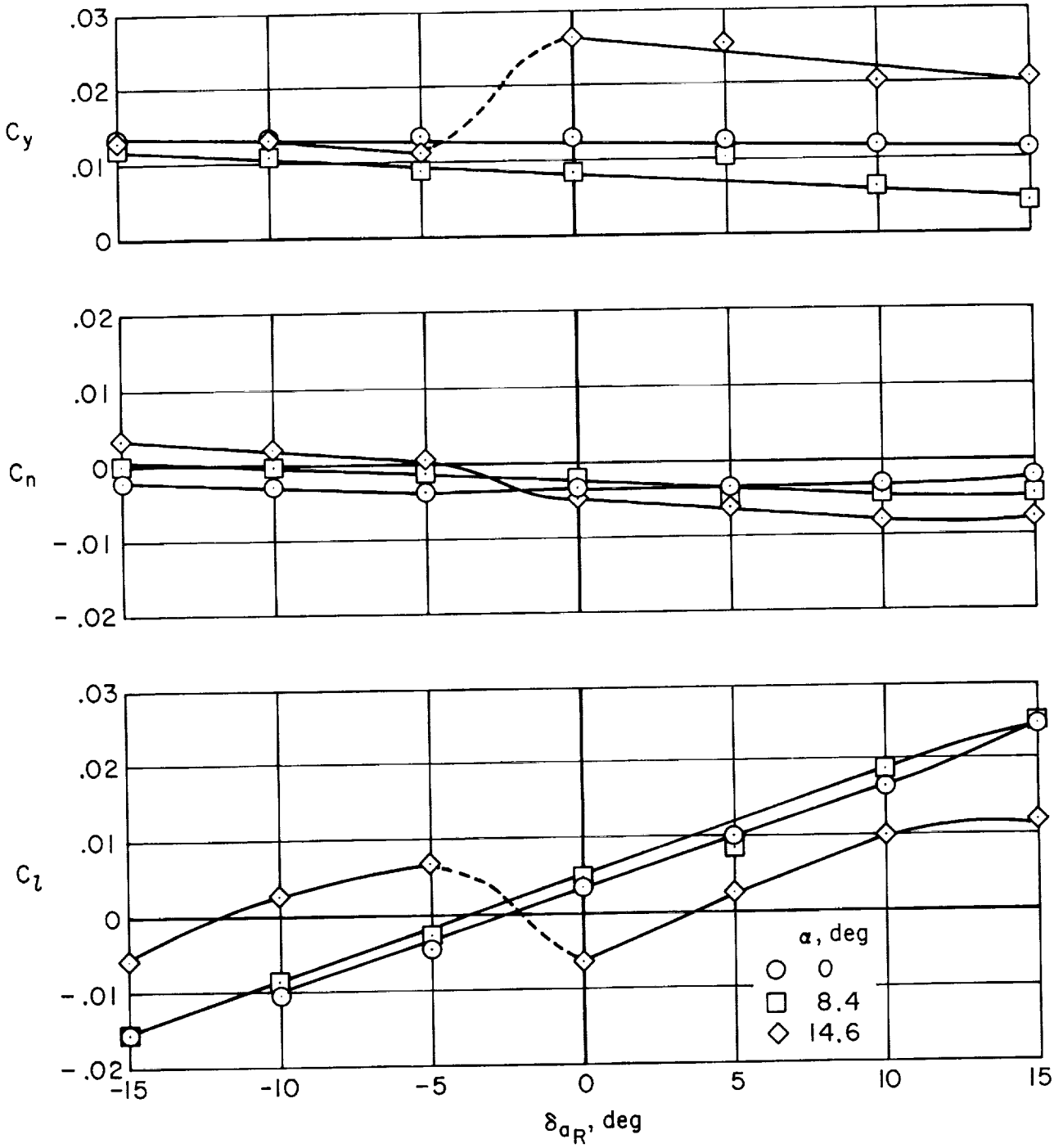

(c) $\delta_f = 0°$, R = 8.7X10^6

Figure 24.- Continued.

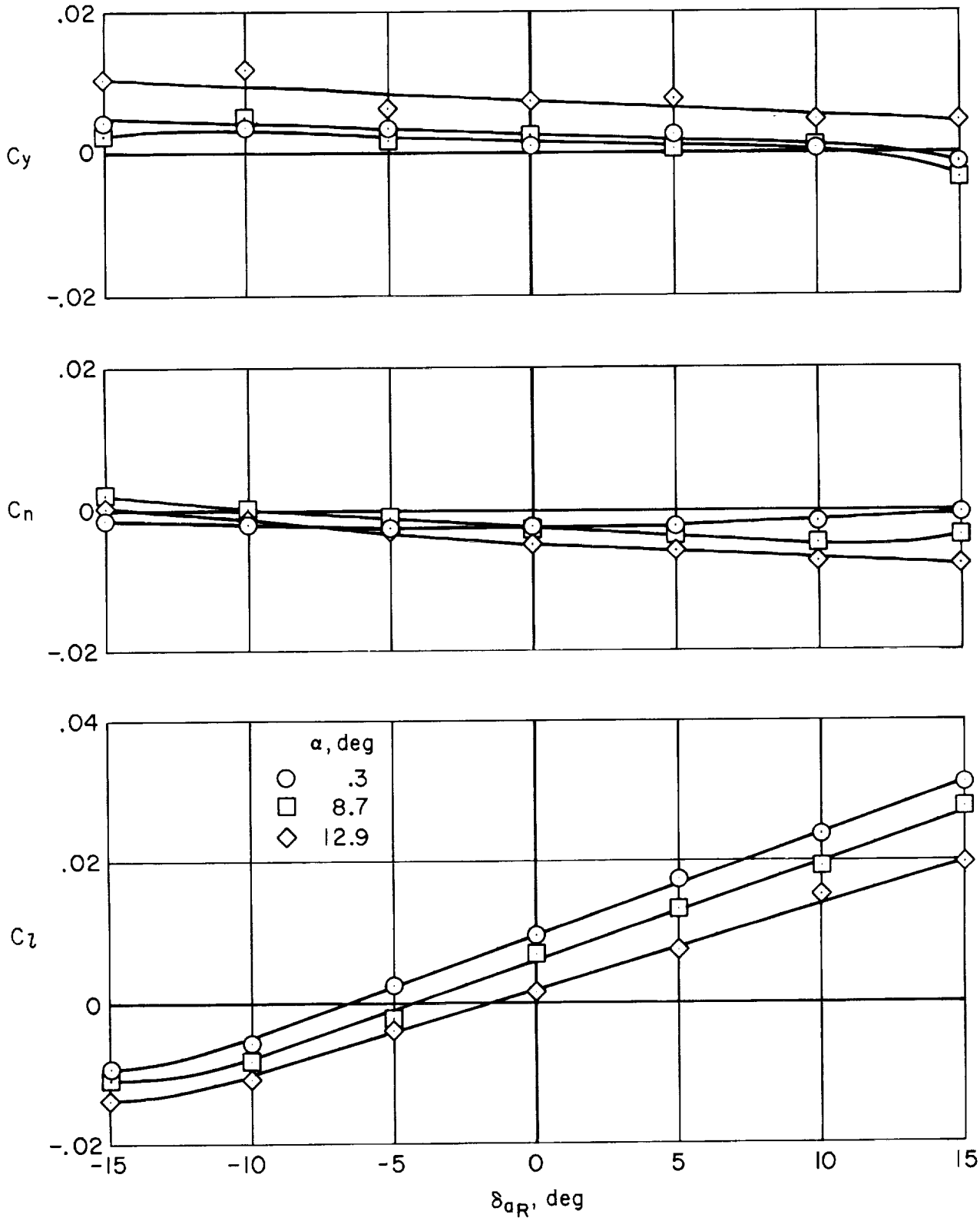

(d) $\delta_f = 38°$, $R = 8.7 \times 10^6$

Figure 24.- Concluded.

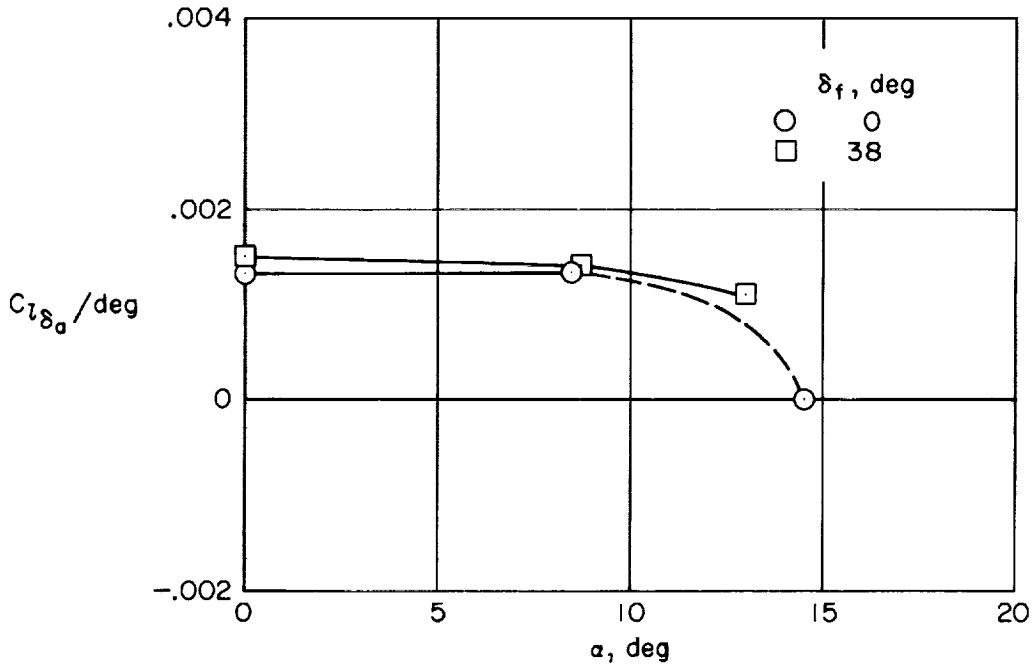

Figure 25.- $C_{l_{\delta_a}}$ for right aileron versus angle of attack (measured at $\delta_{a_R} = 0°$); R = 8.7X10^6.

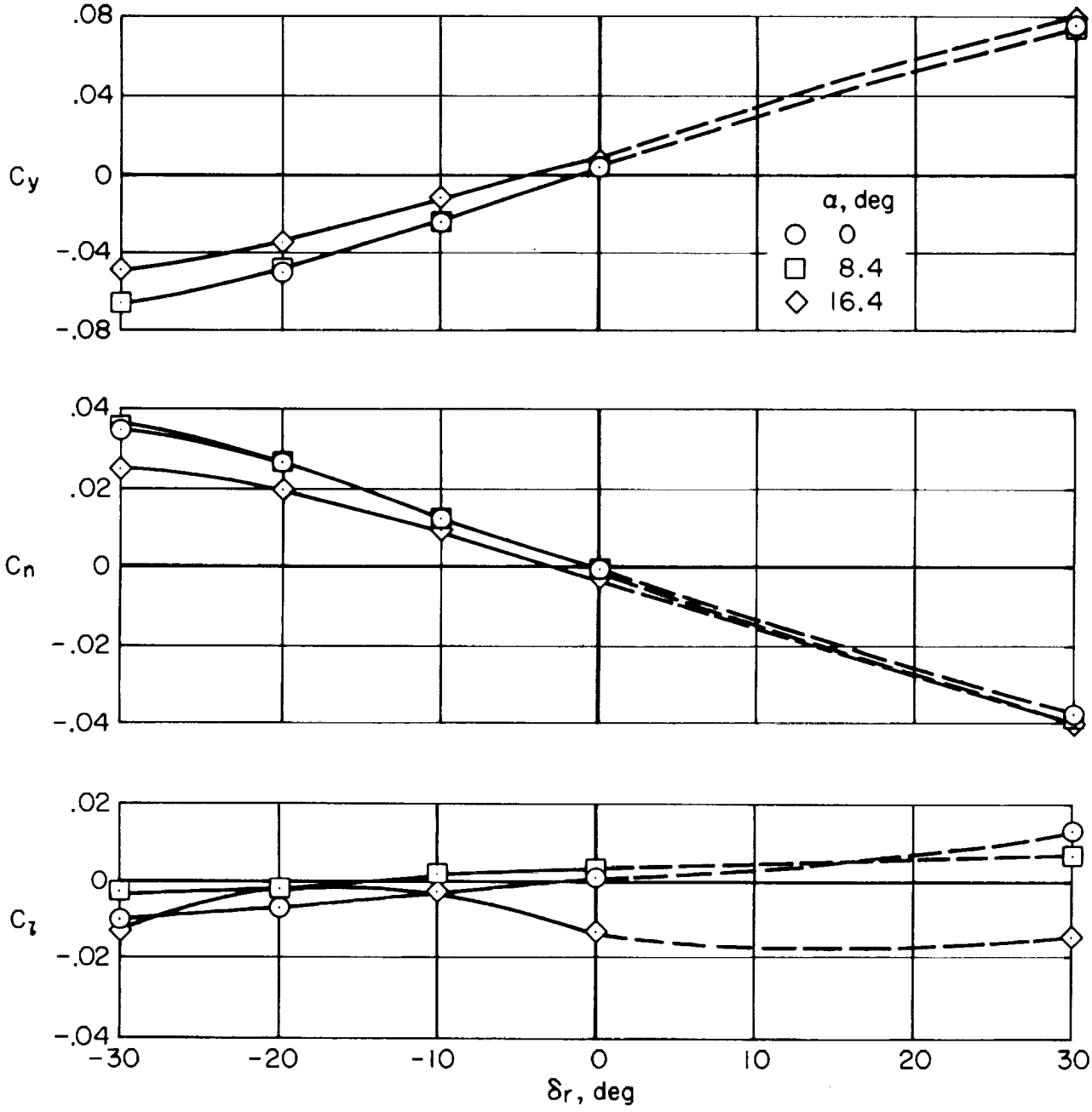

(a) $\delta_f = 0°, \beta = 0°$, R = 4.1×10^6

Figure 26.- Effect of rudder deflection on directional characteristics.

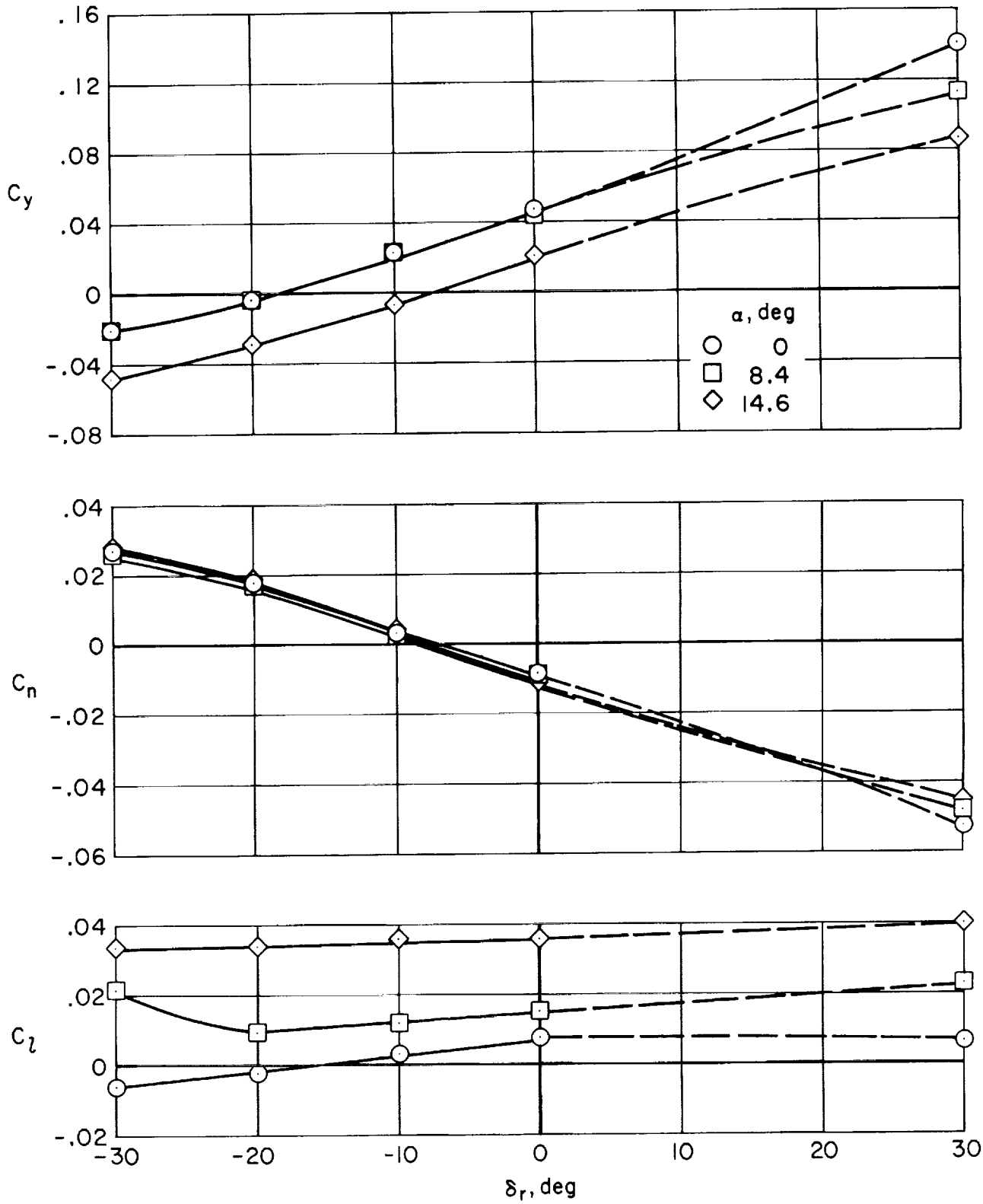

(b) $\delta_f = 0°$, $\beta = -4°$, R = 8.7×10^6

Figure 26.- Continued.

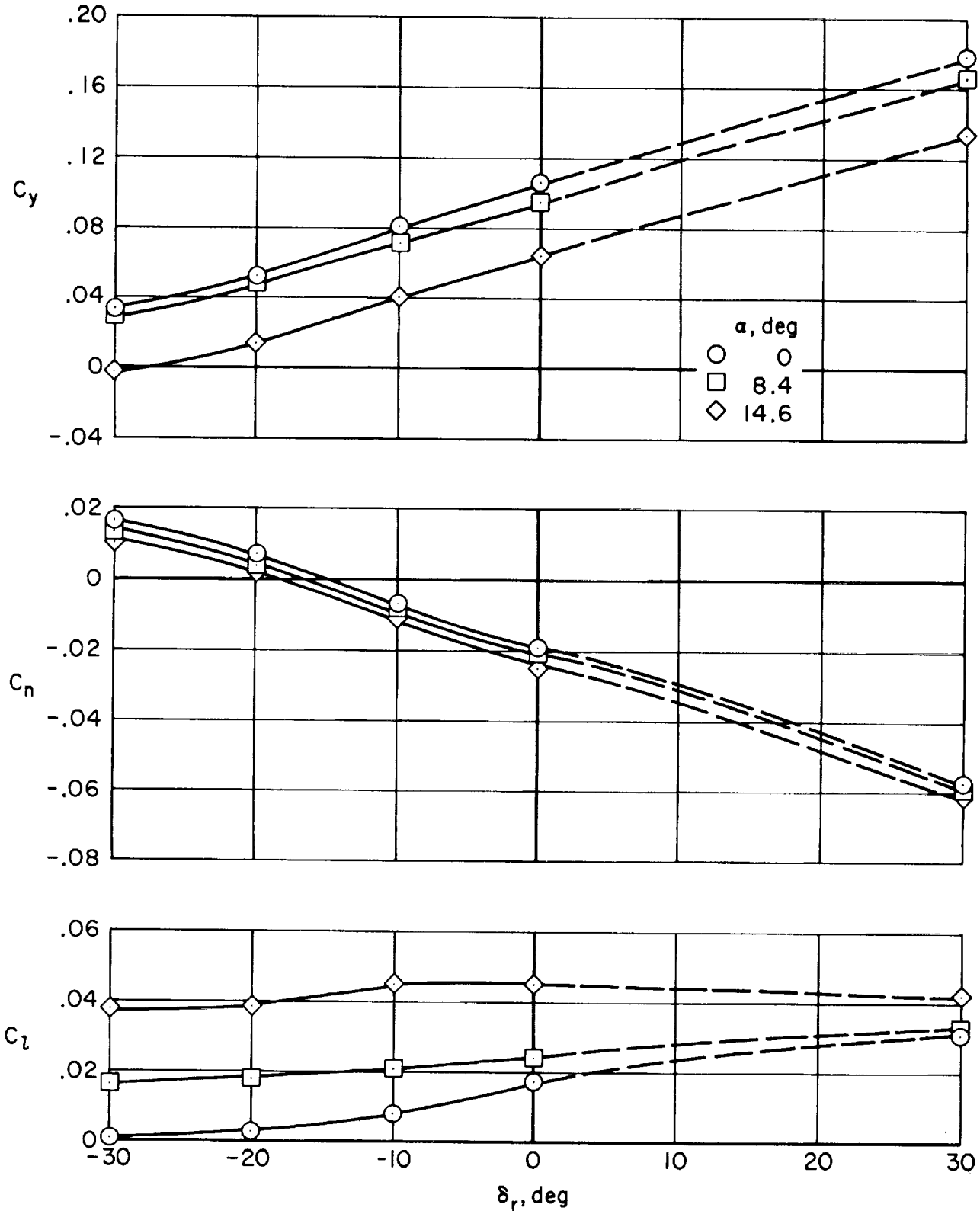

(c) $\delta_f = 0°$, $\beta = -8°$, R = 8.7×10^6

Figure 26.- Continued.

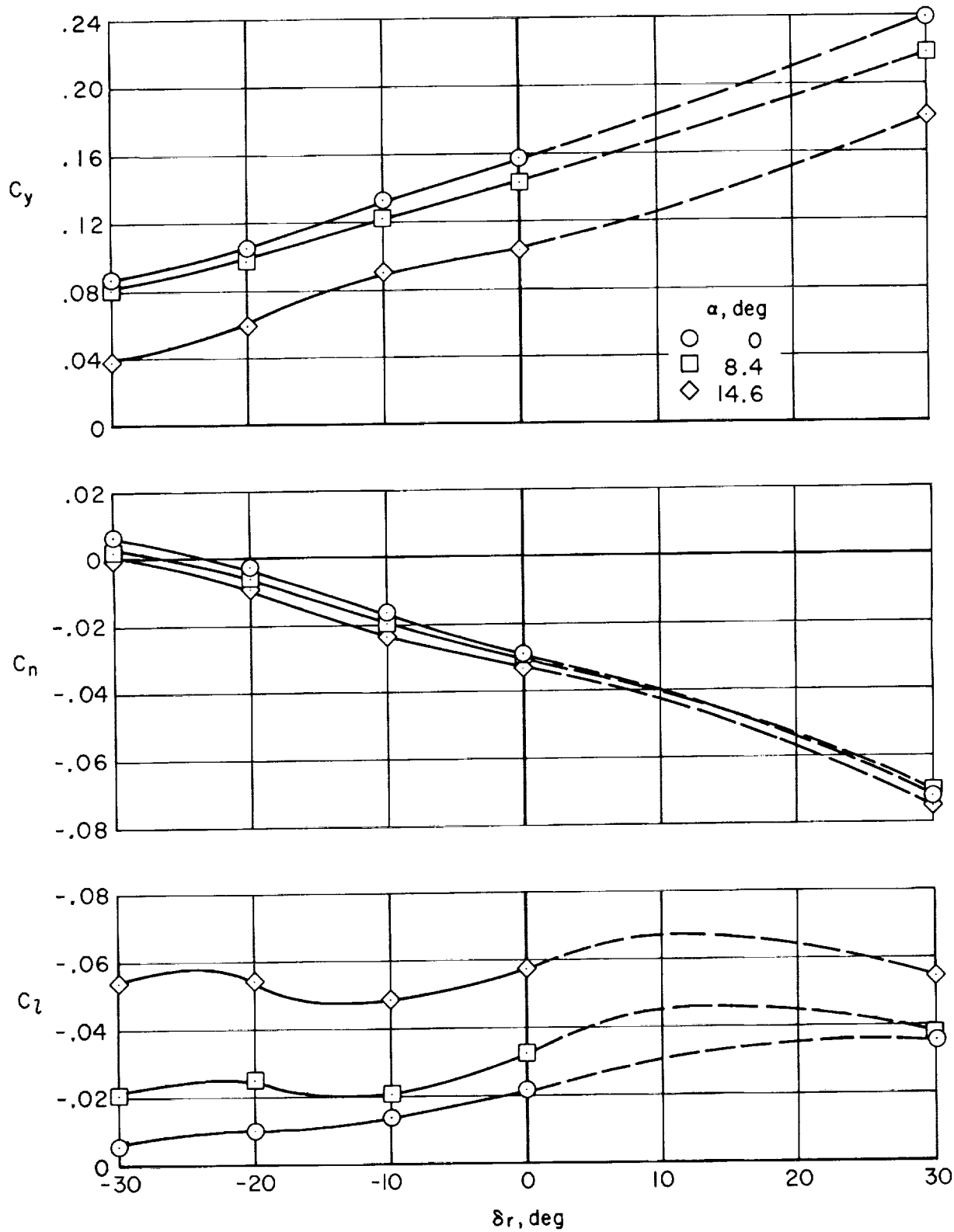

(d) $\delta_f = 0°, \beta = -12°, R = 8.7 \times 10^6$

Figure 26.- Continued.

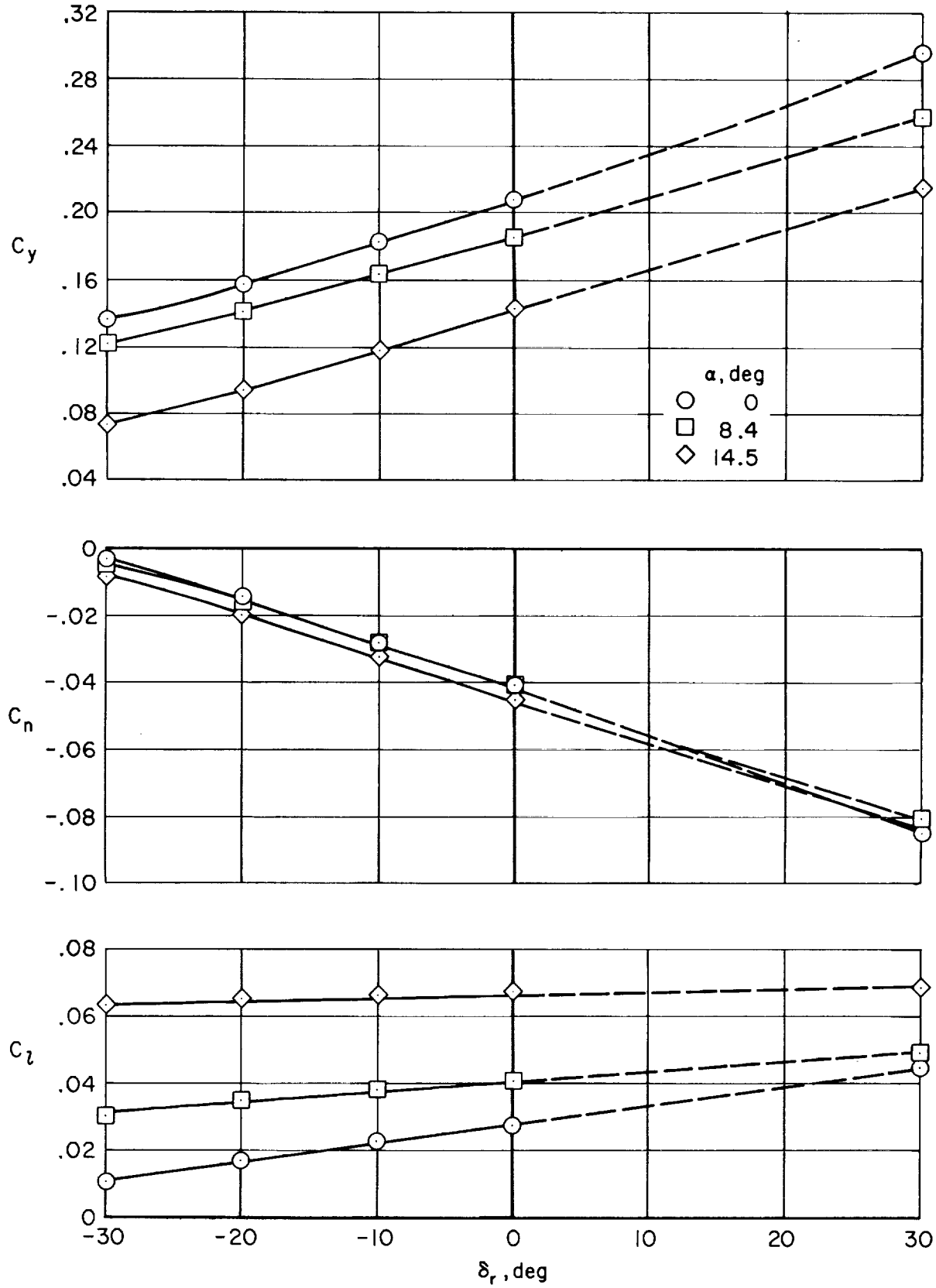

(e) $\delta_f = 0°, \beta = -16°, R = 8.7 \times 10^6$

Figure 26.- Continued.

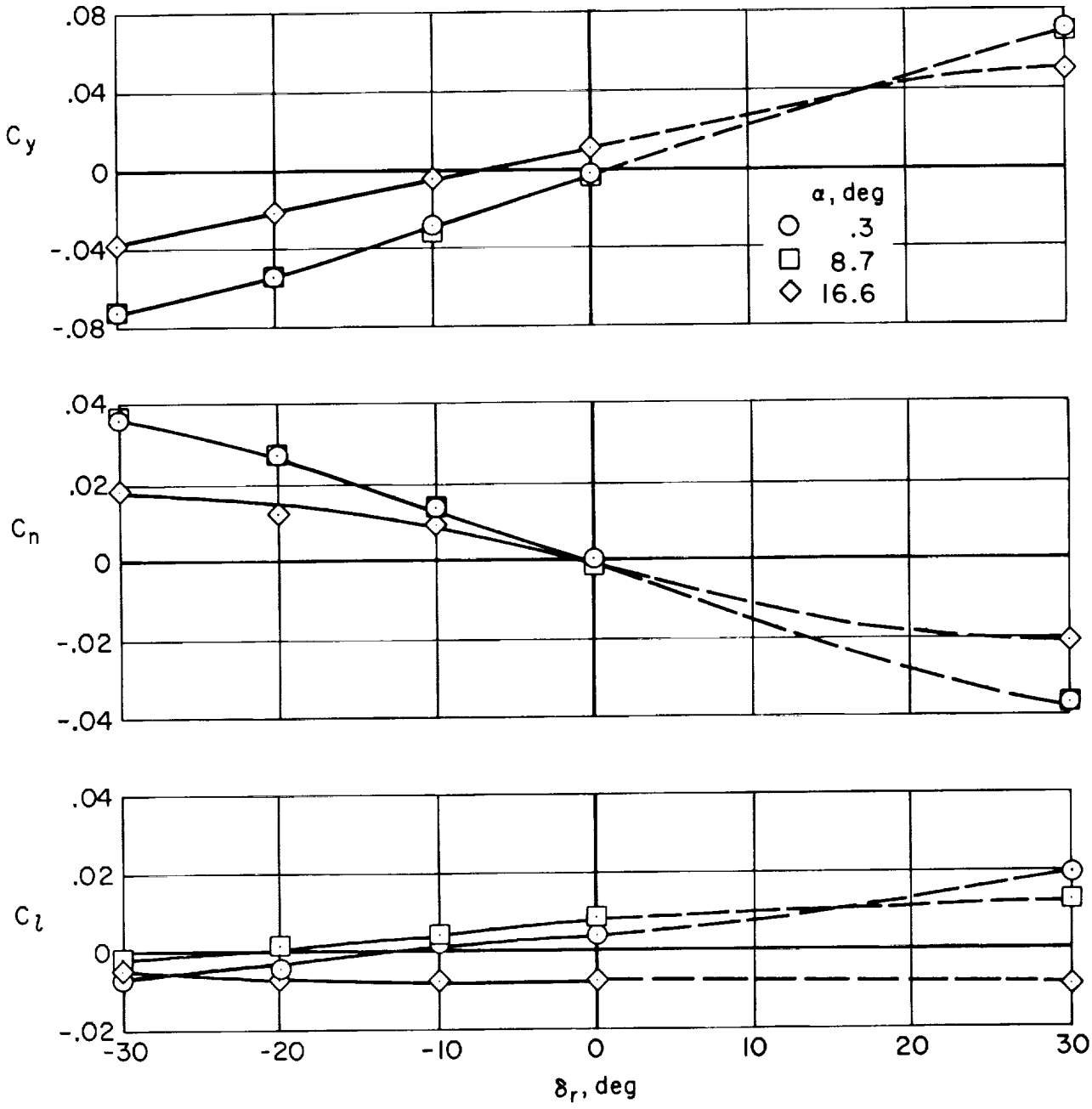

(f) $\delta_f = 40°$, $\beta = 0°$, $R = 4.1 \times 10^6$

Figure 26.- Continued.

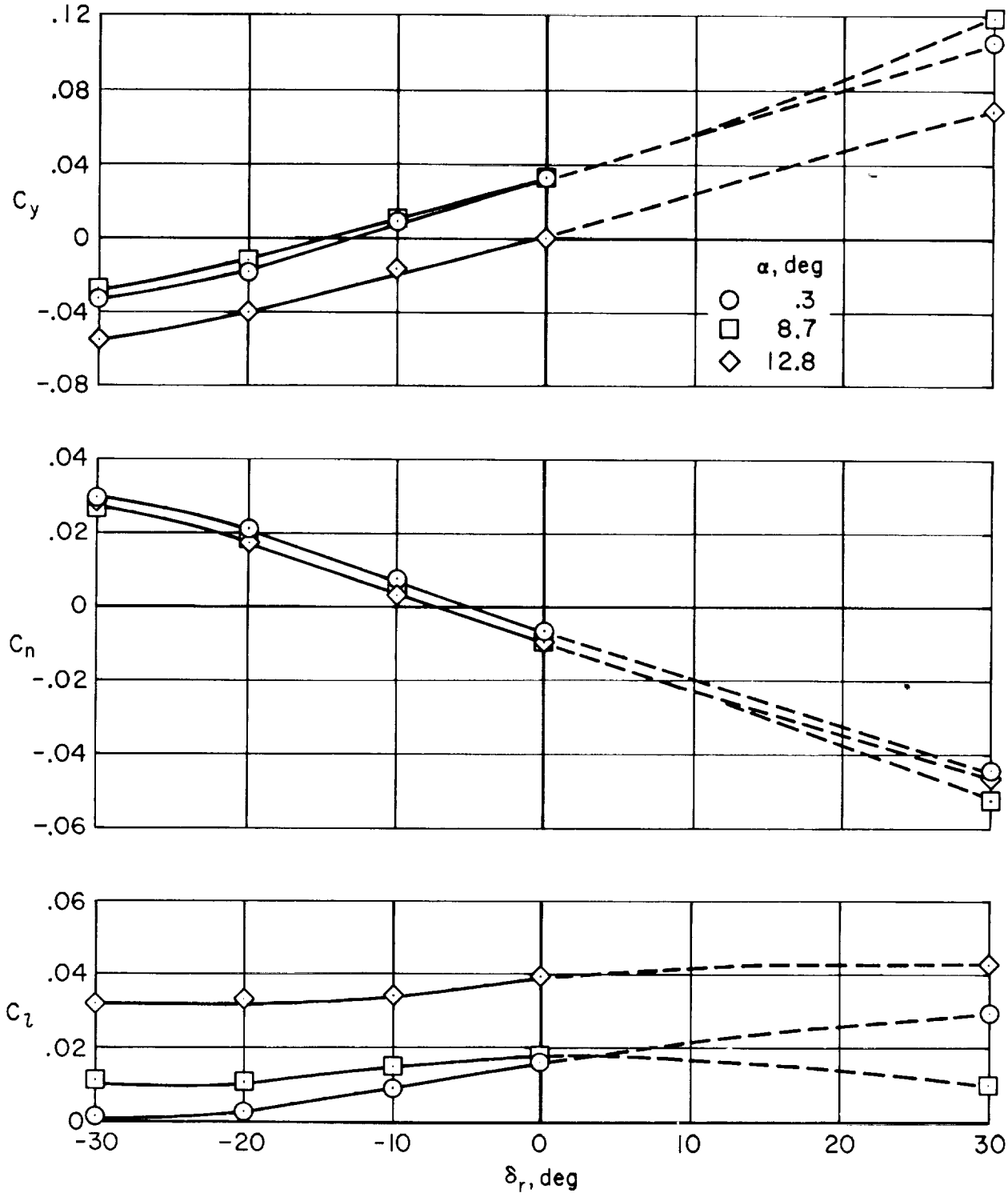

(g) $\delta_f = 38°, \beta = -4°, R = 8.7 \times 10^6$

Figure 26.- Continued.

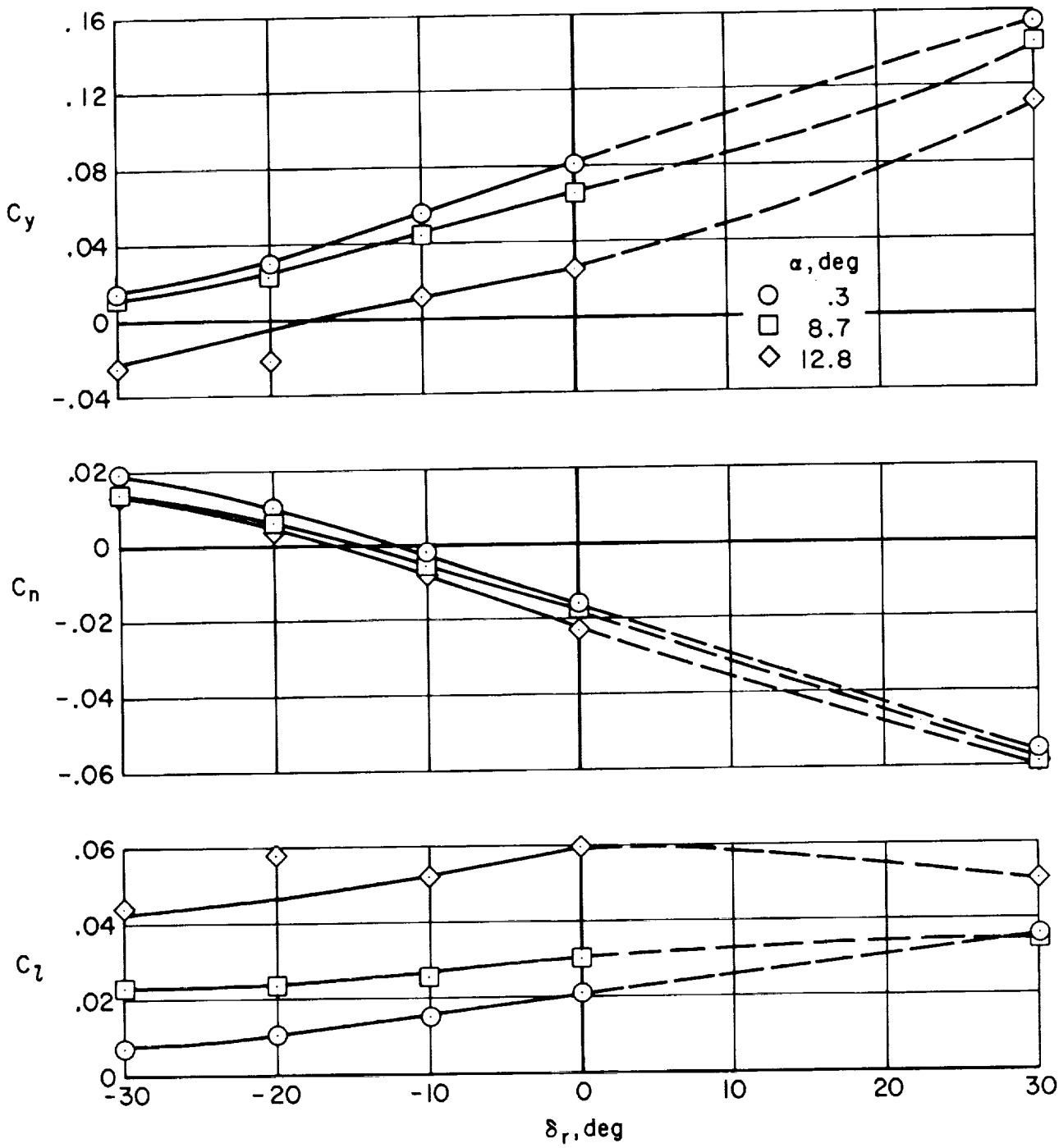

(h) $\delta_f = 38°$, $\beta = -8°$, R = 8.7×10^6

Figure 26.- Continued.

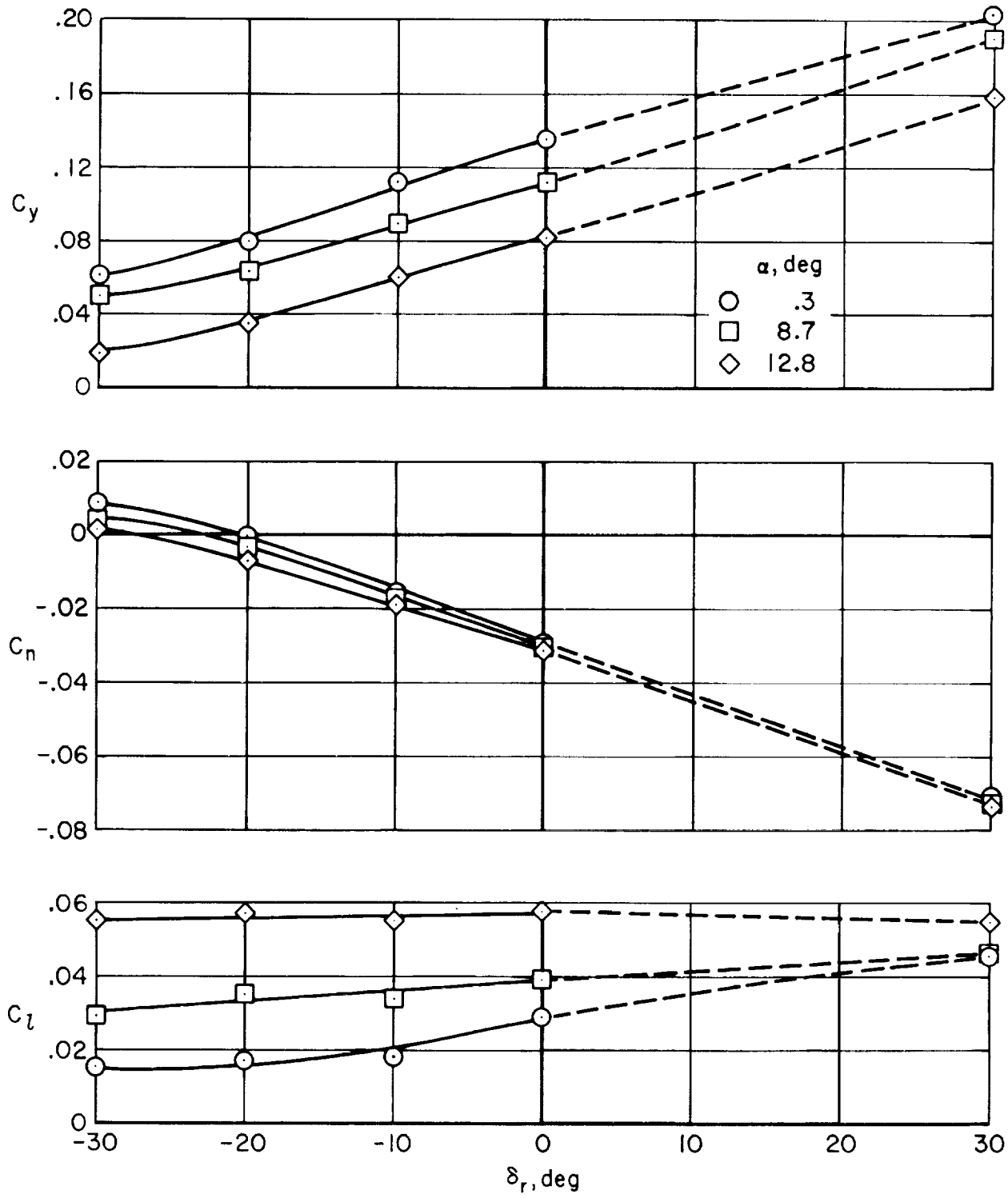

(i) $\delta_f = 38°, \beta = -12°, R = 8.7 \times 10^6$

Figure 26.- Continued.

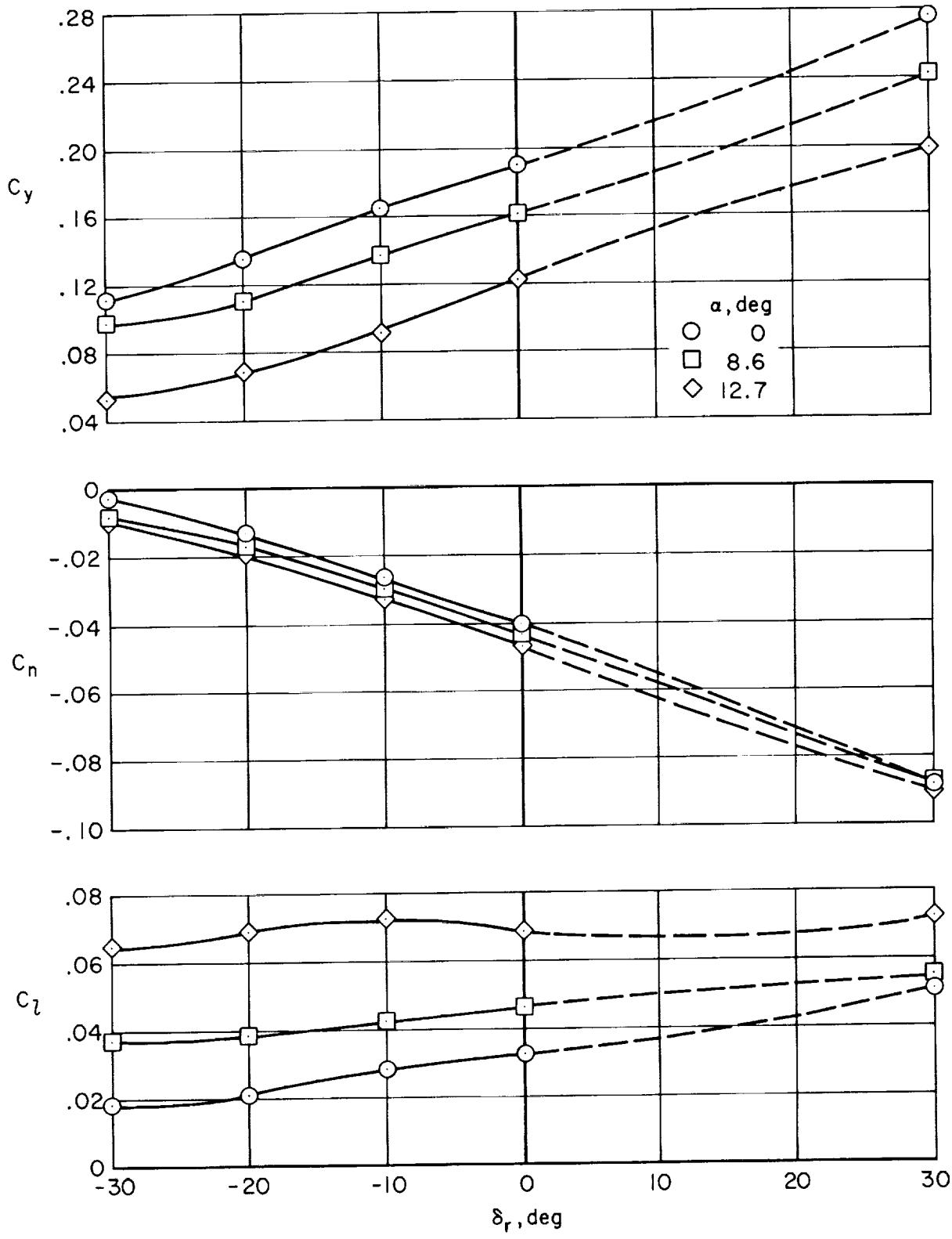

(j) $\delta_f = 38°, \beta = -16°, R = 8.7 \times 10^6$

Figure 26.- Concluded.

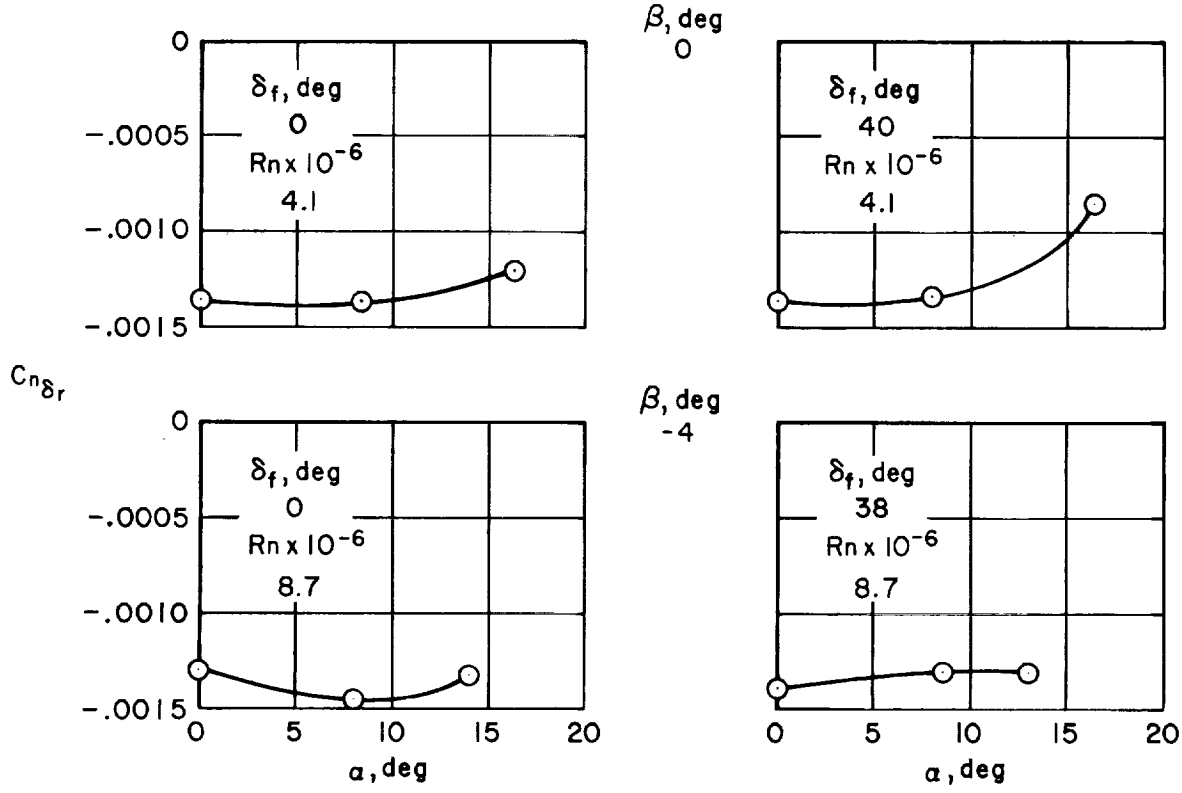

(a) $\beta = 0°$ and $-4°$

Figure 27.- $C_{n_{\delta_r}}$ versus angle of attack for flaps up and down; R = 4.1×10^6 and 8.7×10^6.

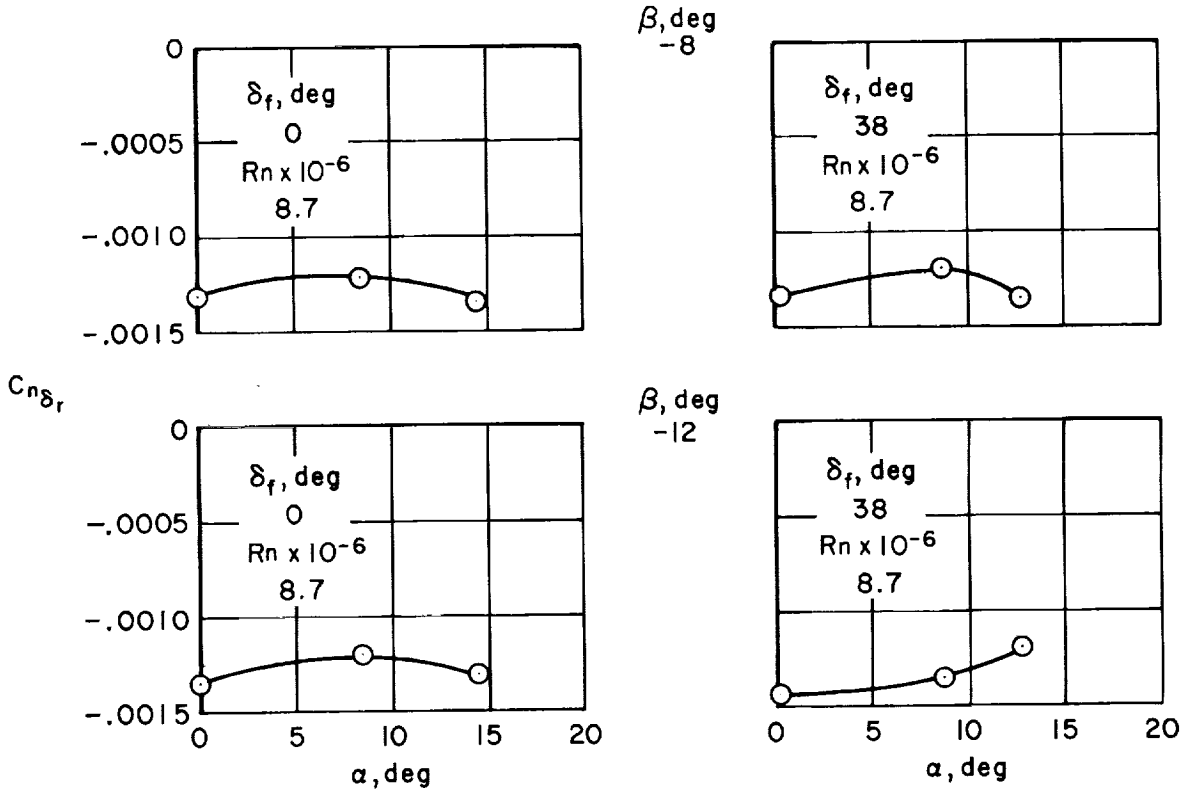

(b) β = -8° and -12°

Figure 27.- Concluded.

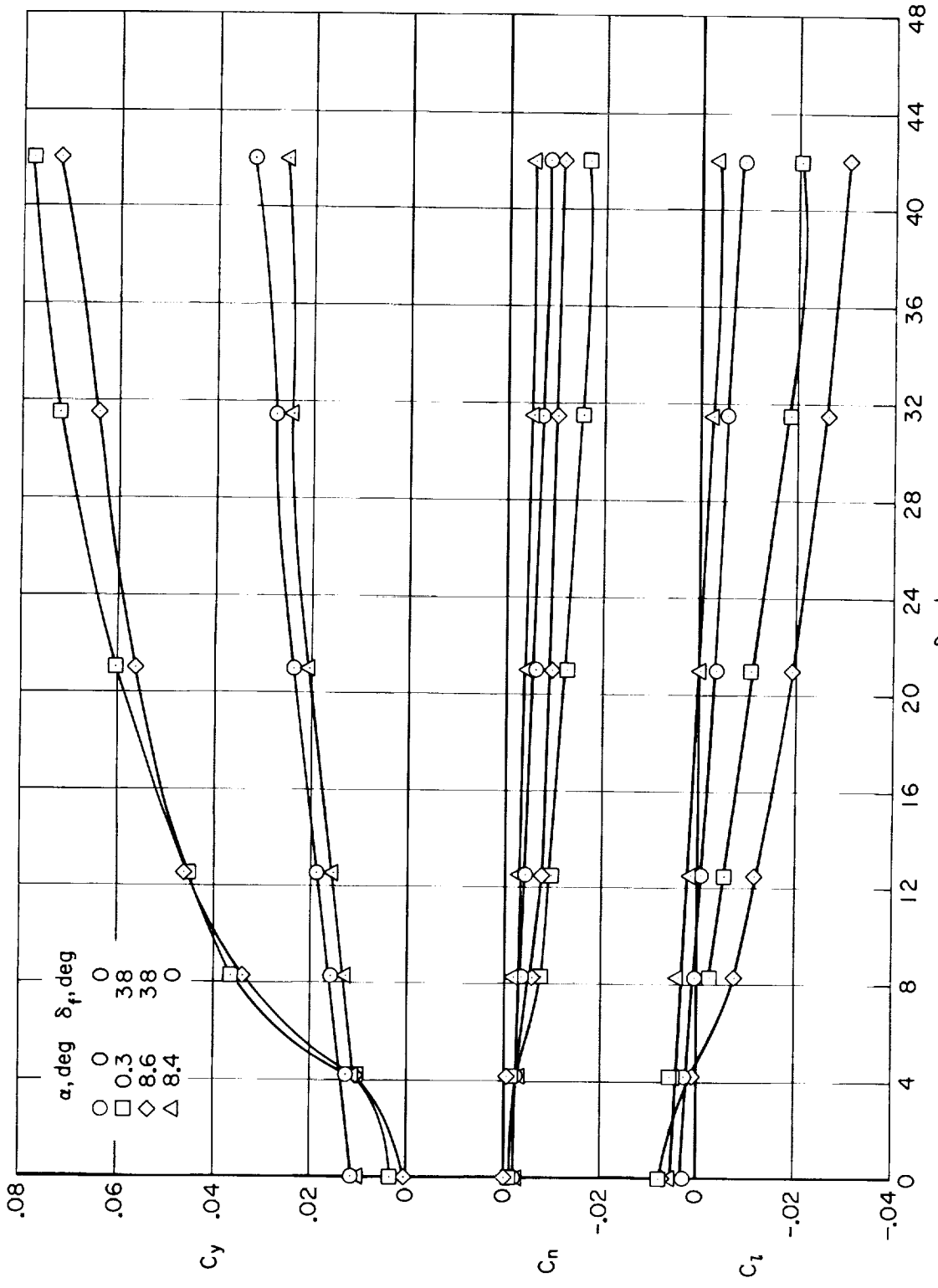

(a) Basic spoiler (inboard).

Figure 28.- Lateral effectiveness of left spoiler; R = 8.7×10^6.

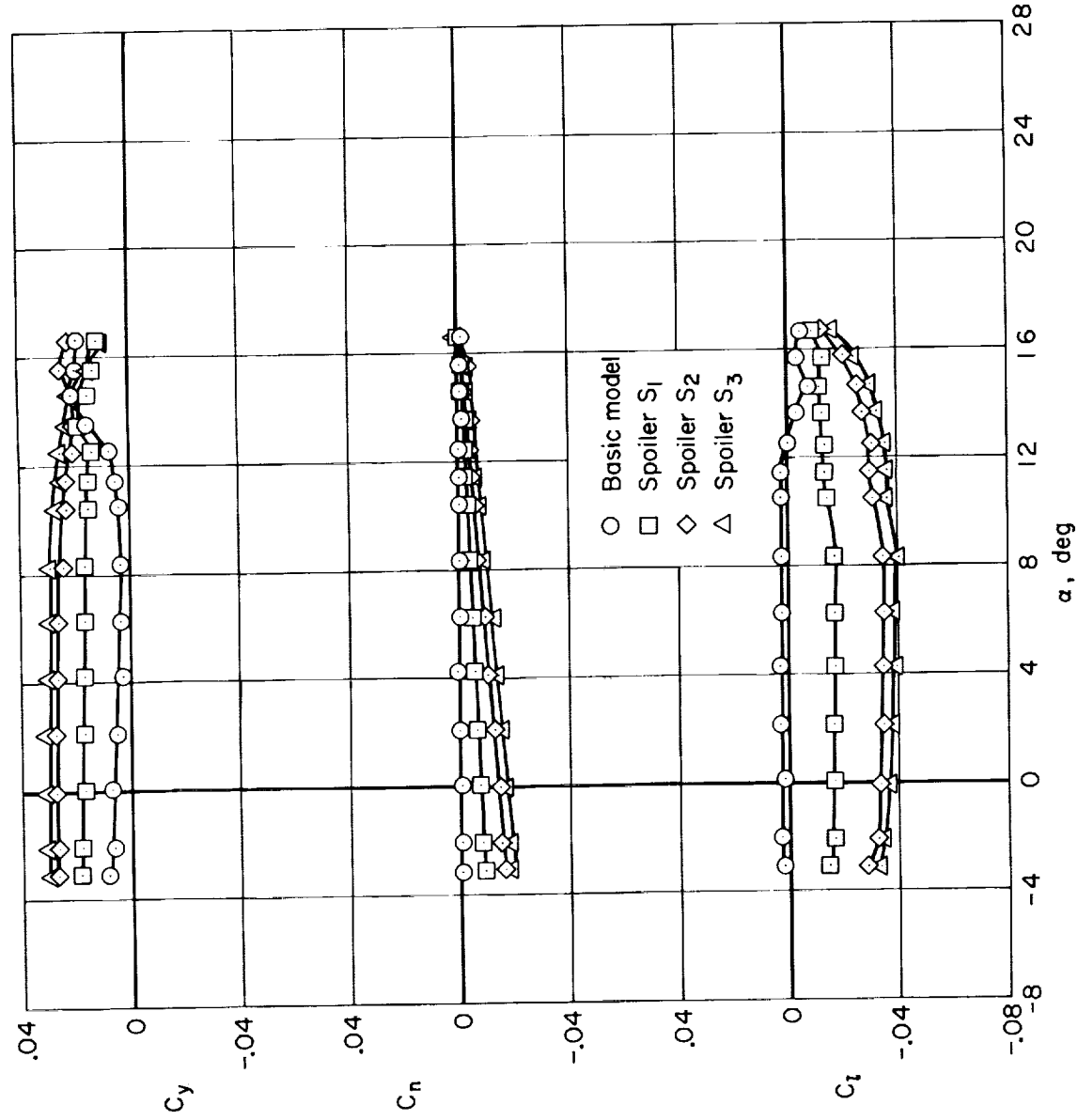

(b) Outboard spoilers on left wing; $R = 8.7 \times 10^6$, $\delta_f = 0°$.

Figure 28.- Concluded.

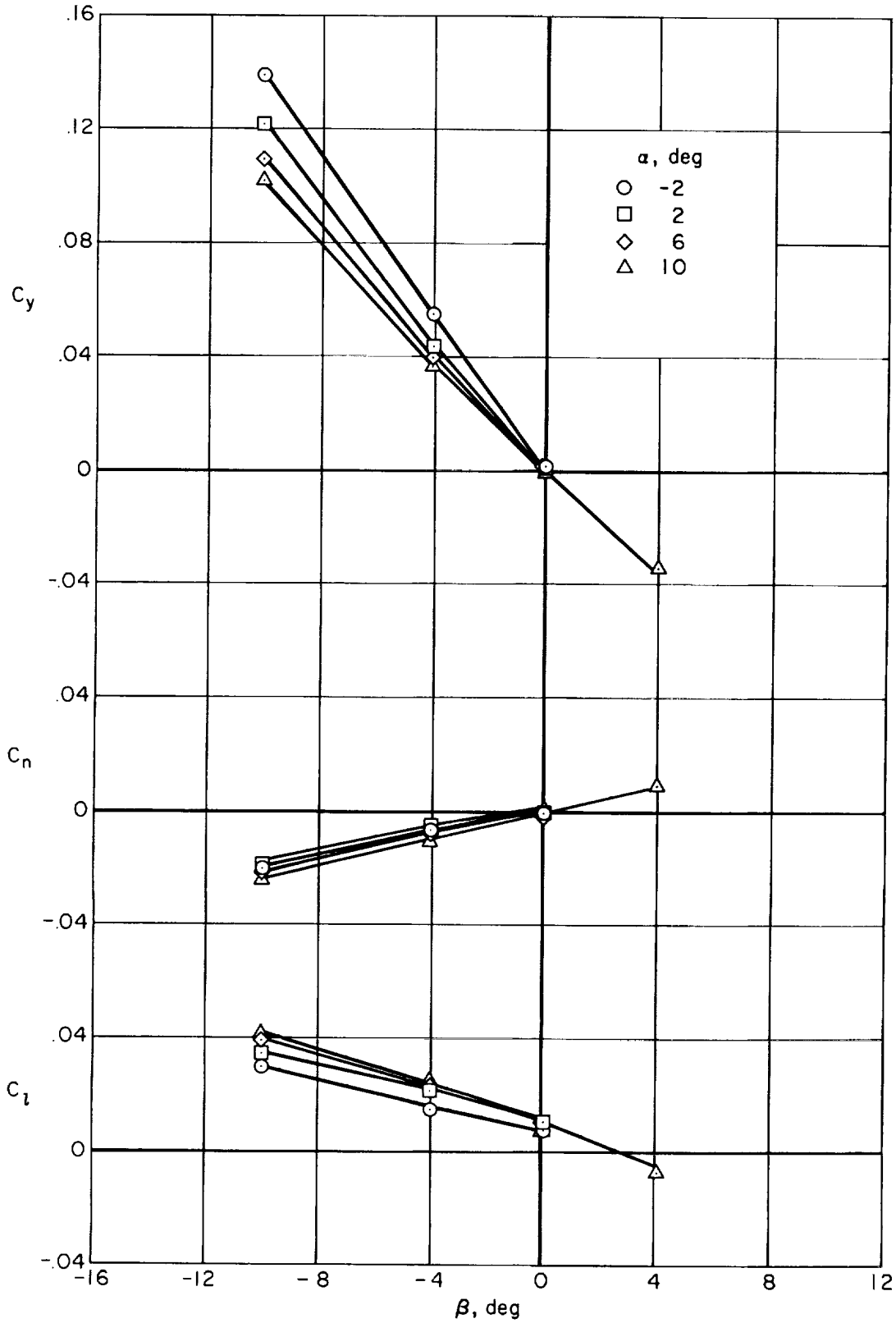

Figure 29.- Lateral characteristics with landing gear down; $R = 8.7 \times 10^6$, $\delta_f = 38°$.

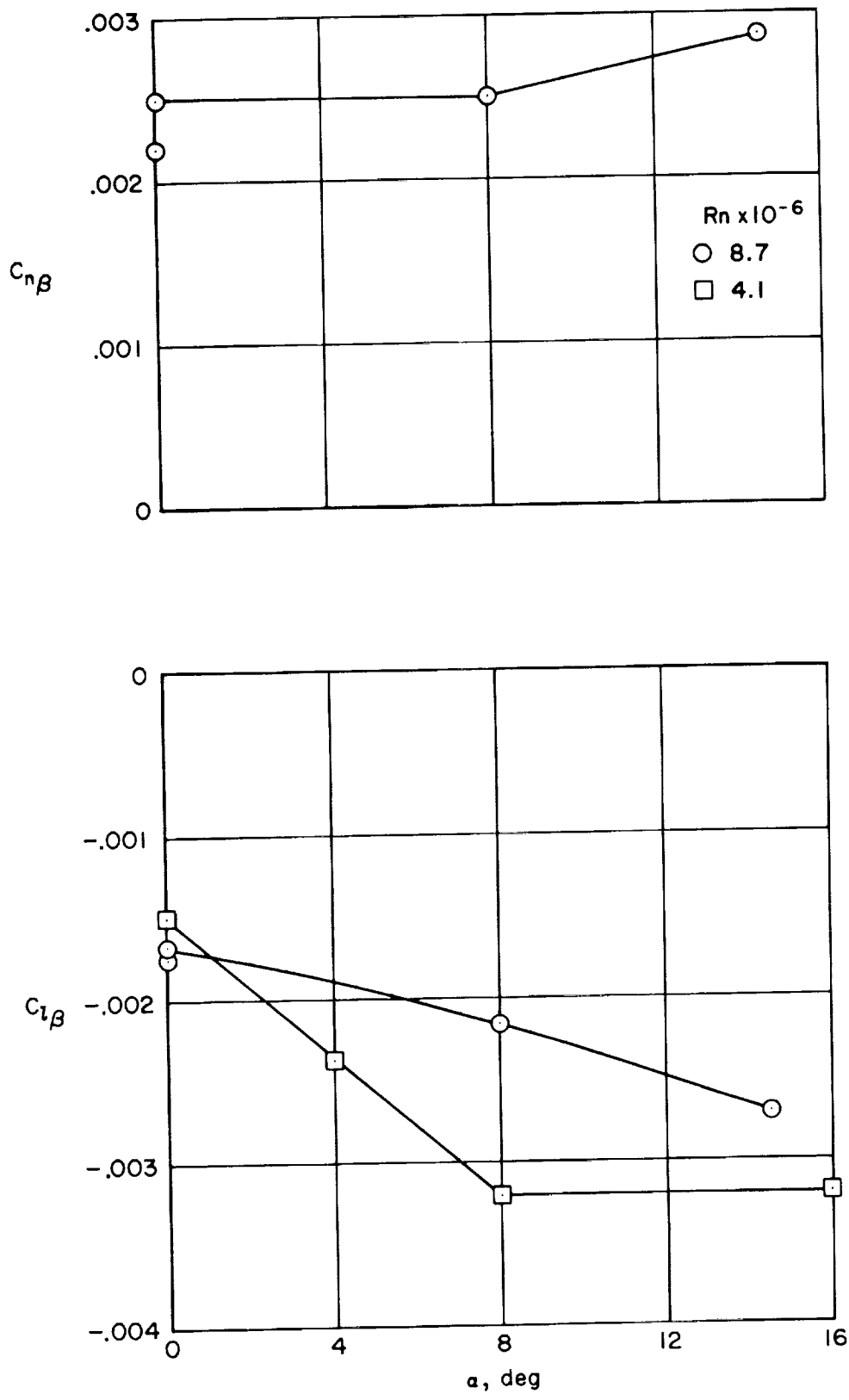

Figure 30.- Stability derivatives C_{n_β} and C_{l_β} versus angle of attack; $\delta_f = 0°$.

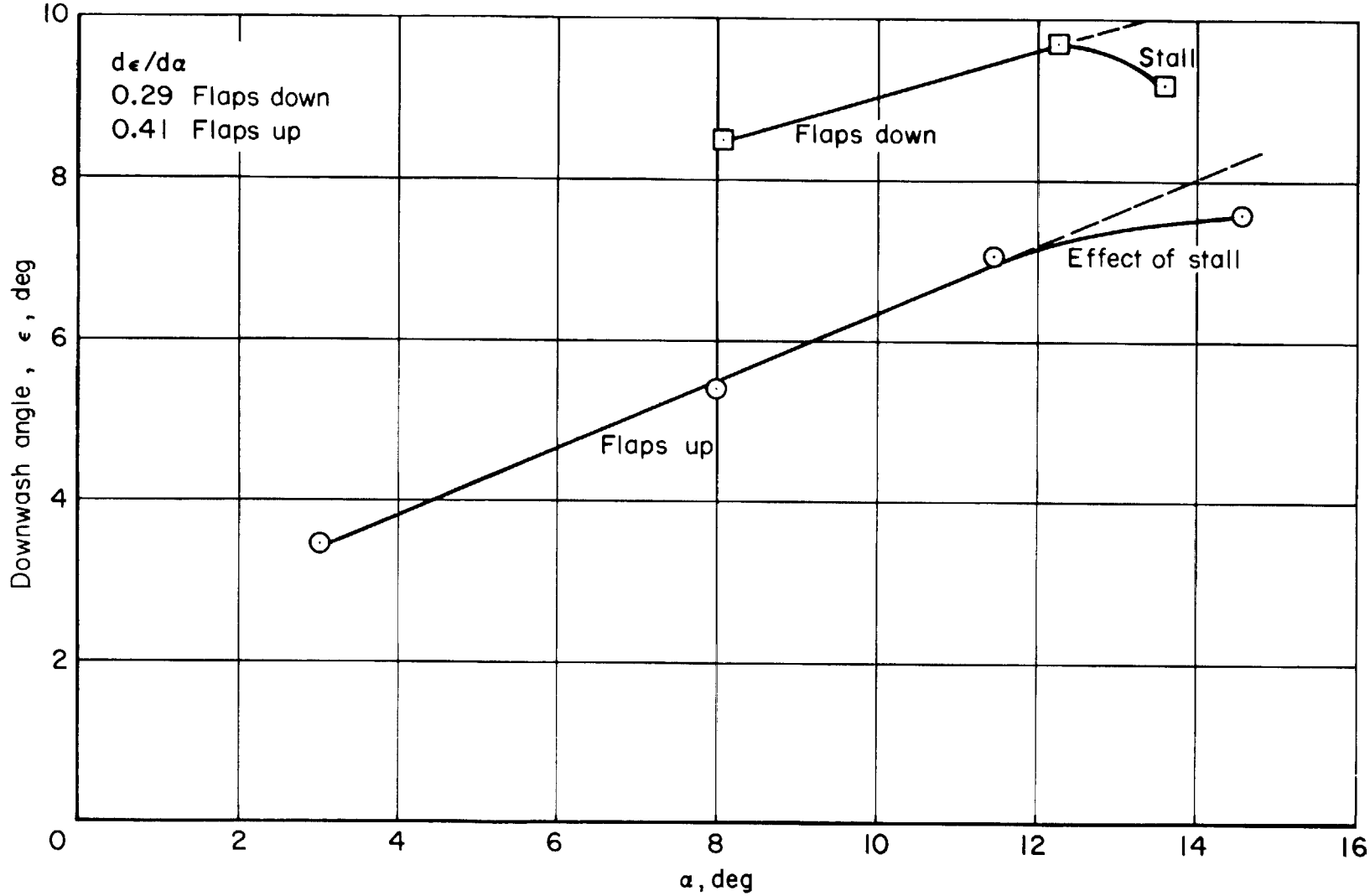

Figure 31.- Average downwash angle at horizontal tail; R = 4.1×10^6 and 8.7×10^6.

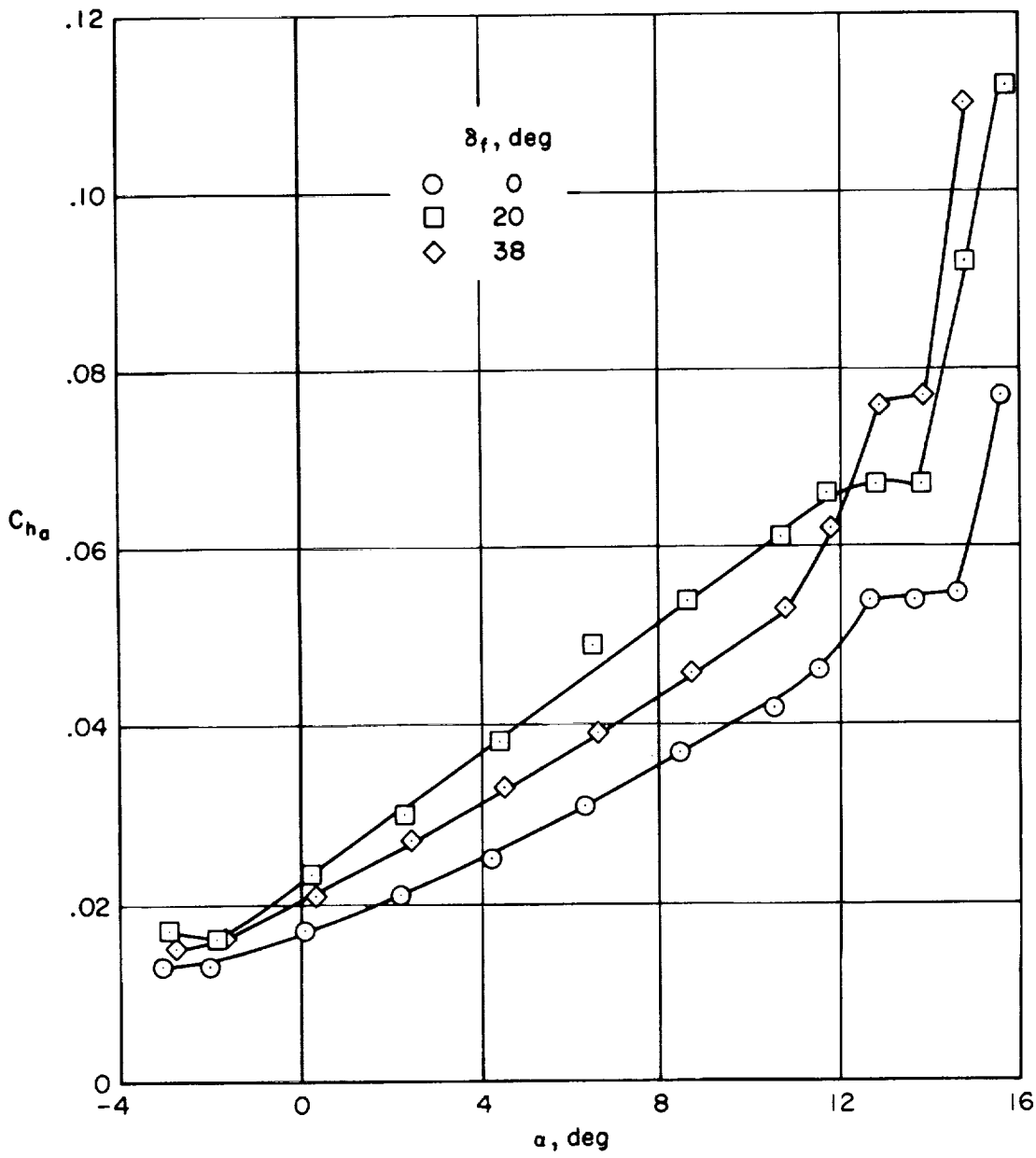

(a) Right aileron hinge-moment coefficient versus angle of attack for three flap angles, $\delta_{a_R} = 0°$.

Figure 32.- Hinge-moment coefficients; R = 8.7×10^6.

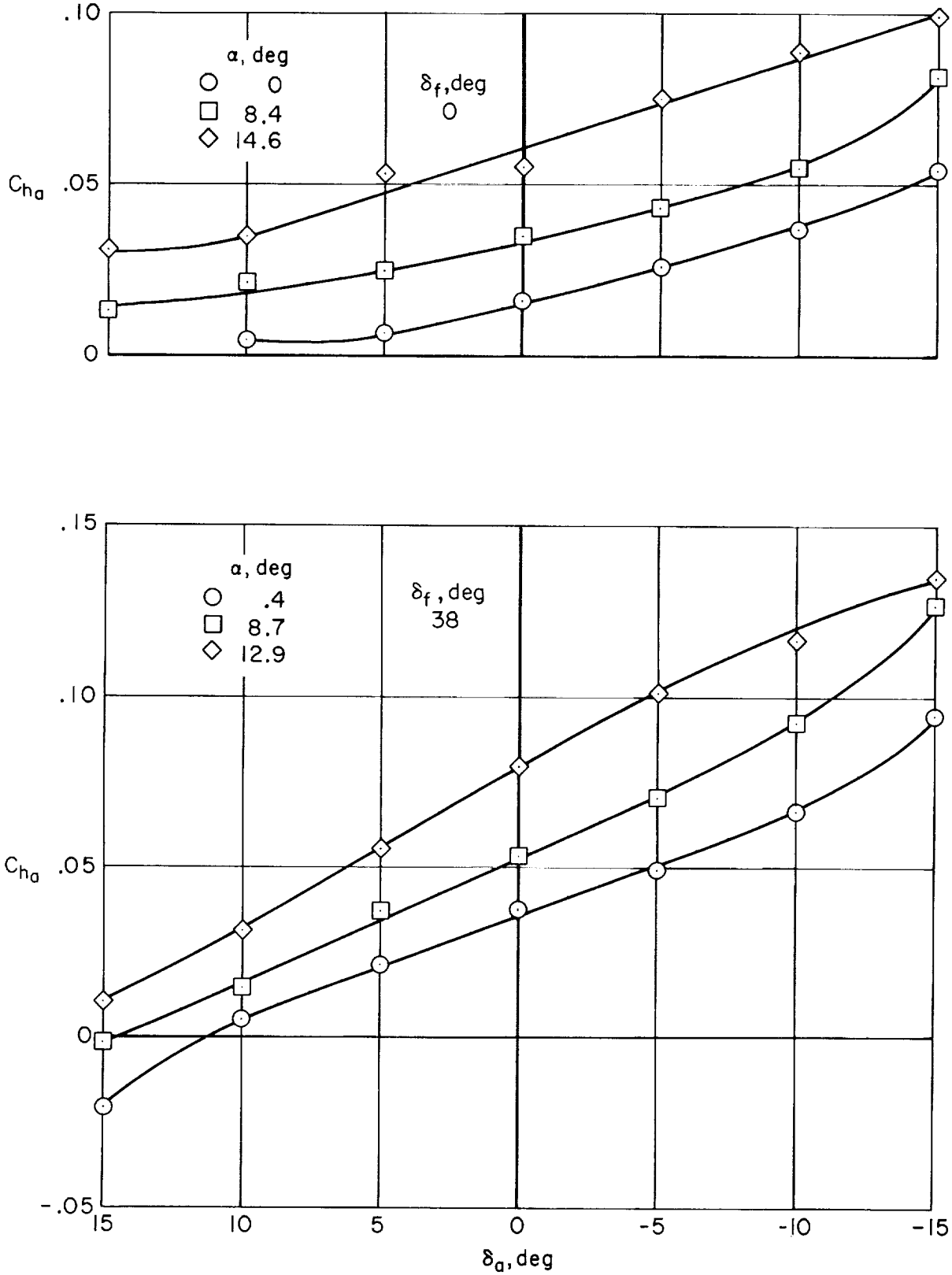

(b) Right aileron hinge-moment coefficient versus aileron angle for $\delta_f = 0°$ (top) and $\delta_f = 38°$ (bottom).

Figure 32.- Continued.

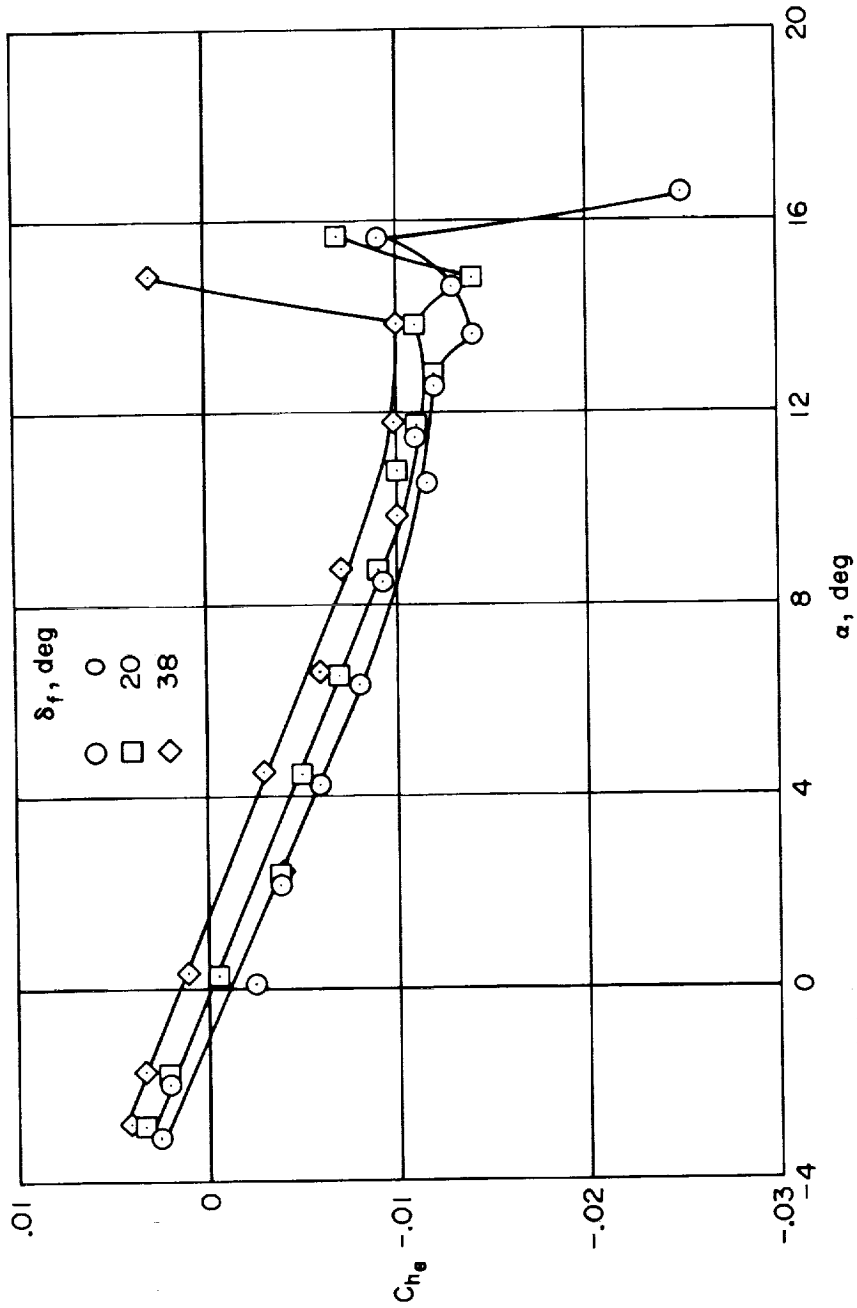

(c) Right elevator hinge-moment coefficient versus angle of attack for three flap angles; $\delta_e = 0°$.

Figure 32.- Continued.

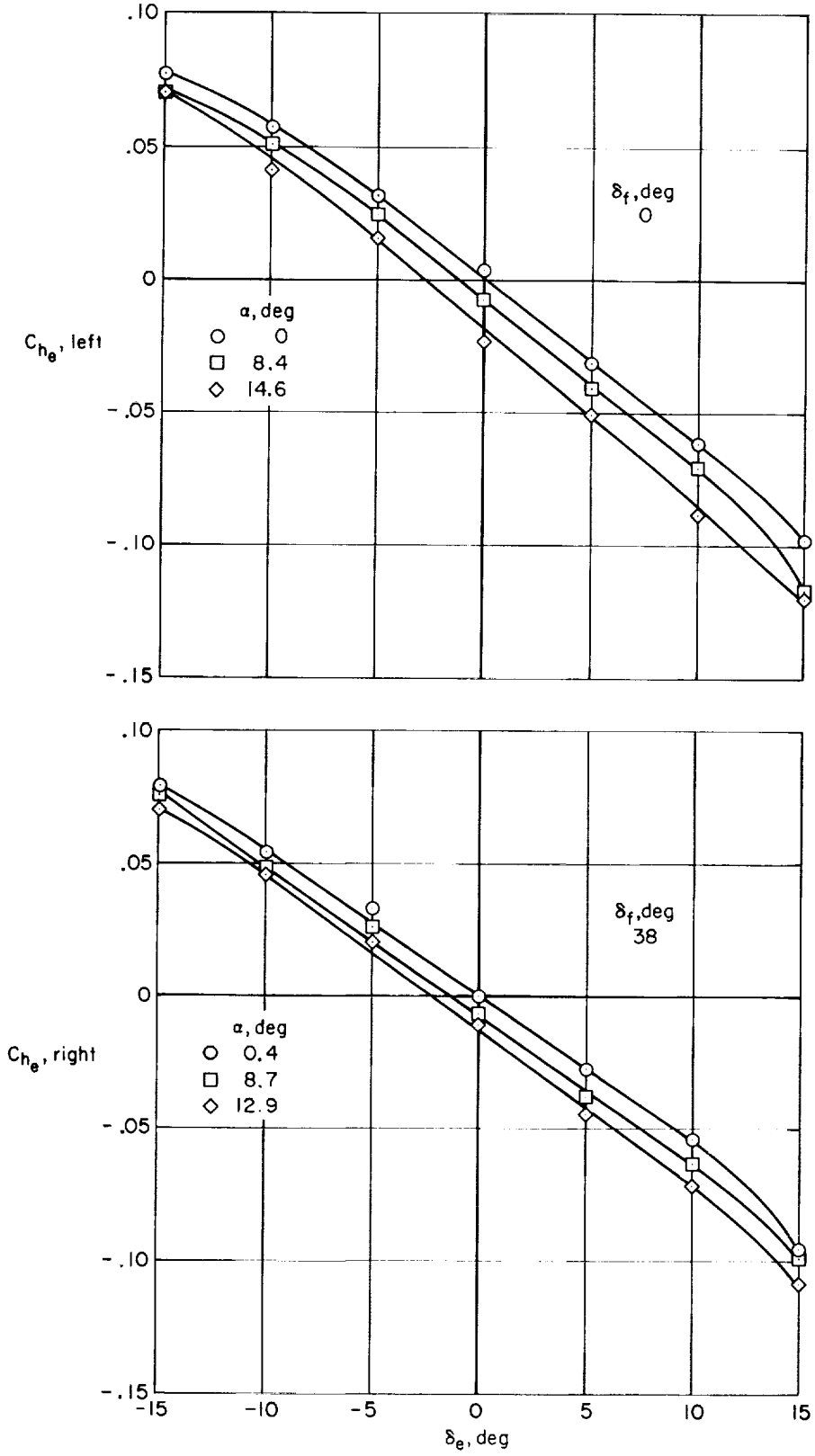

(d) Elevator hinge-moment coefficient versus elevator angle for $\delta_f = 0°$ (top) and $\delta_f = 38°$ (bottom).

Figure 32.- Continued.

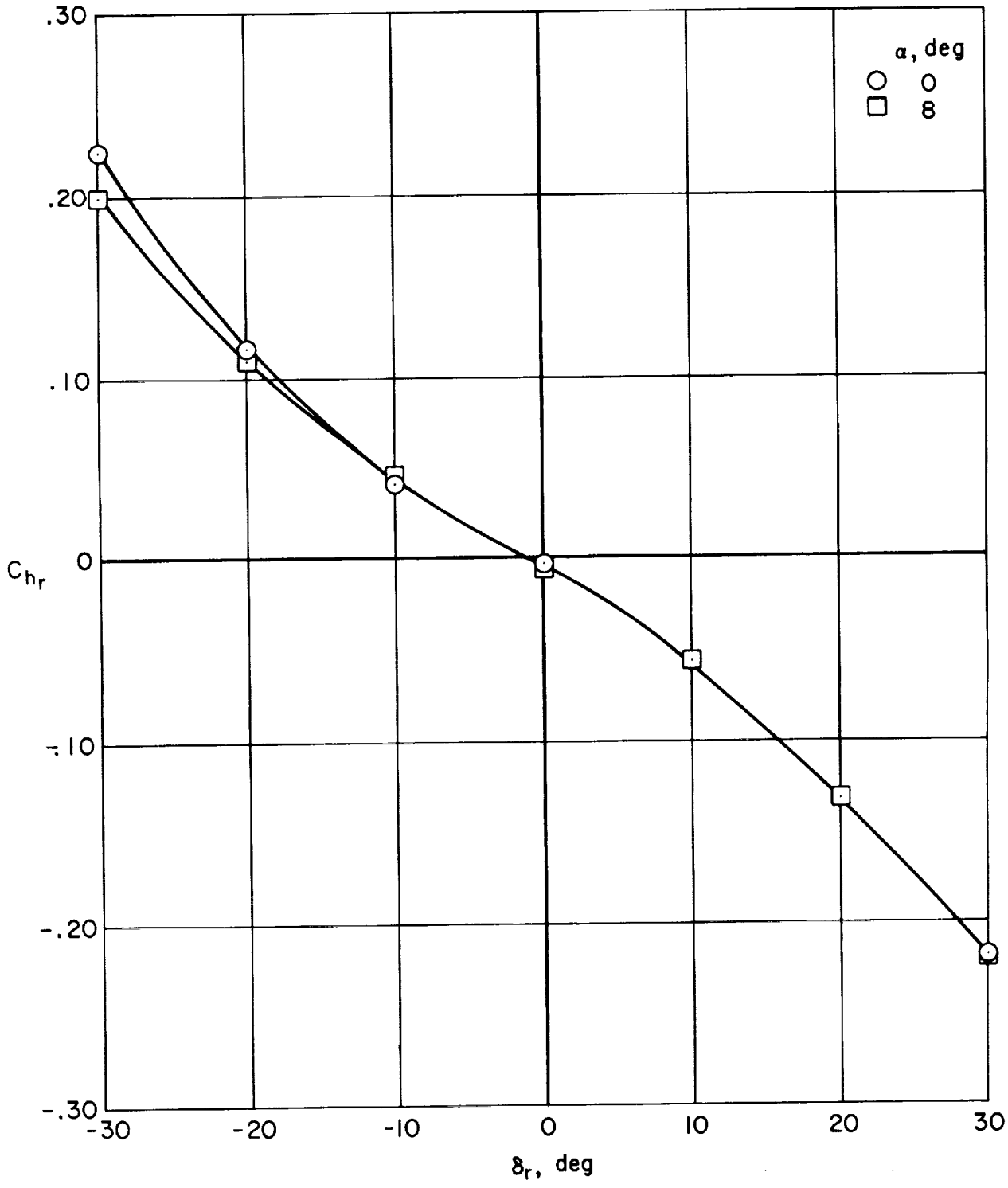

(e) Rudder hinge-moment coefficient versus rudder angle at two angles of attack; $\delta_f = 0°$.

Figure 32.- Continued.

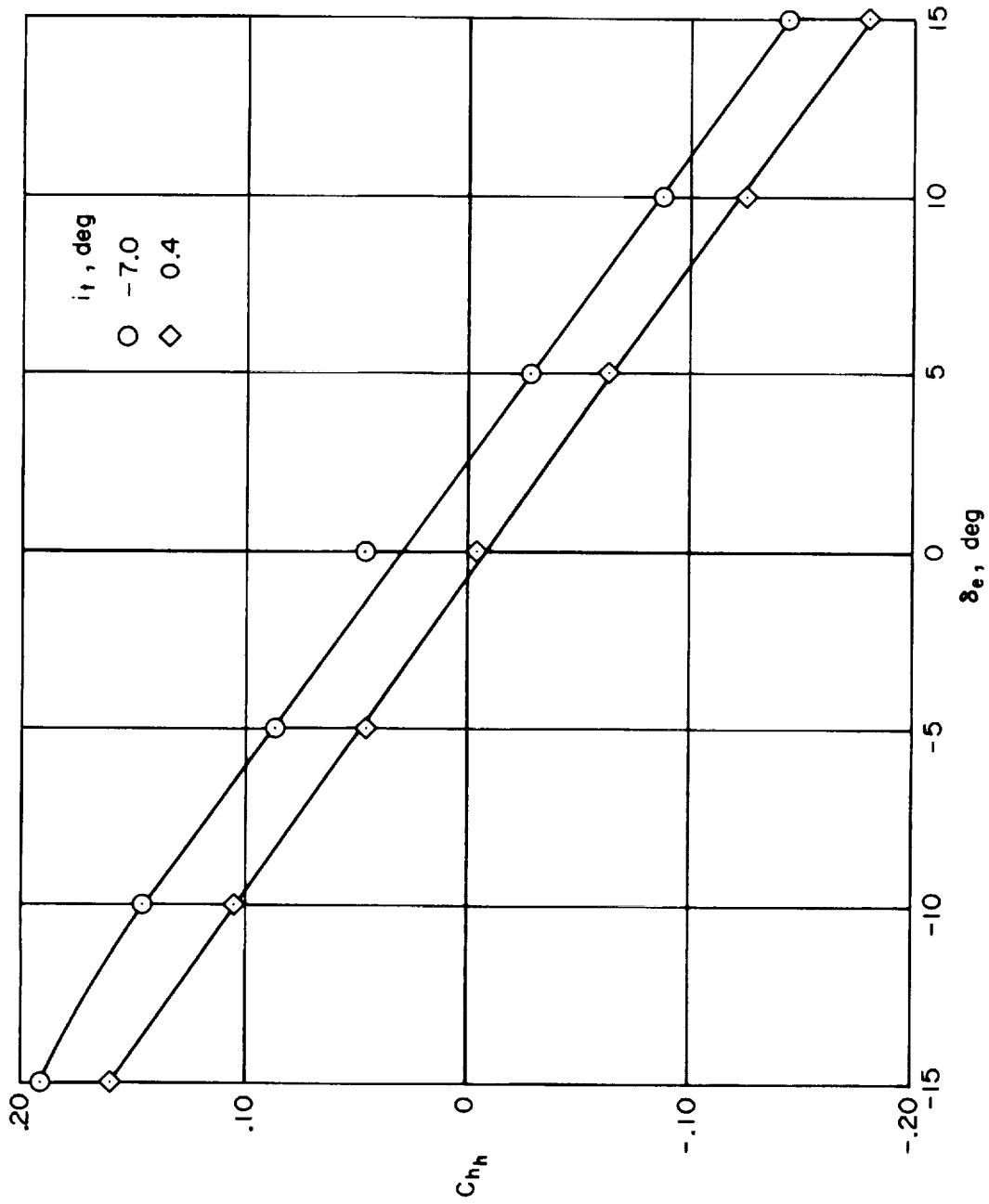

(h) Horizontal stabilizer hinge-moment coefficient versus elevator angle at two tail incidence angles; $\delta_f = 0°$.

Figure 32.- Concluded.

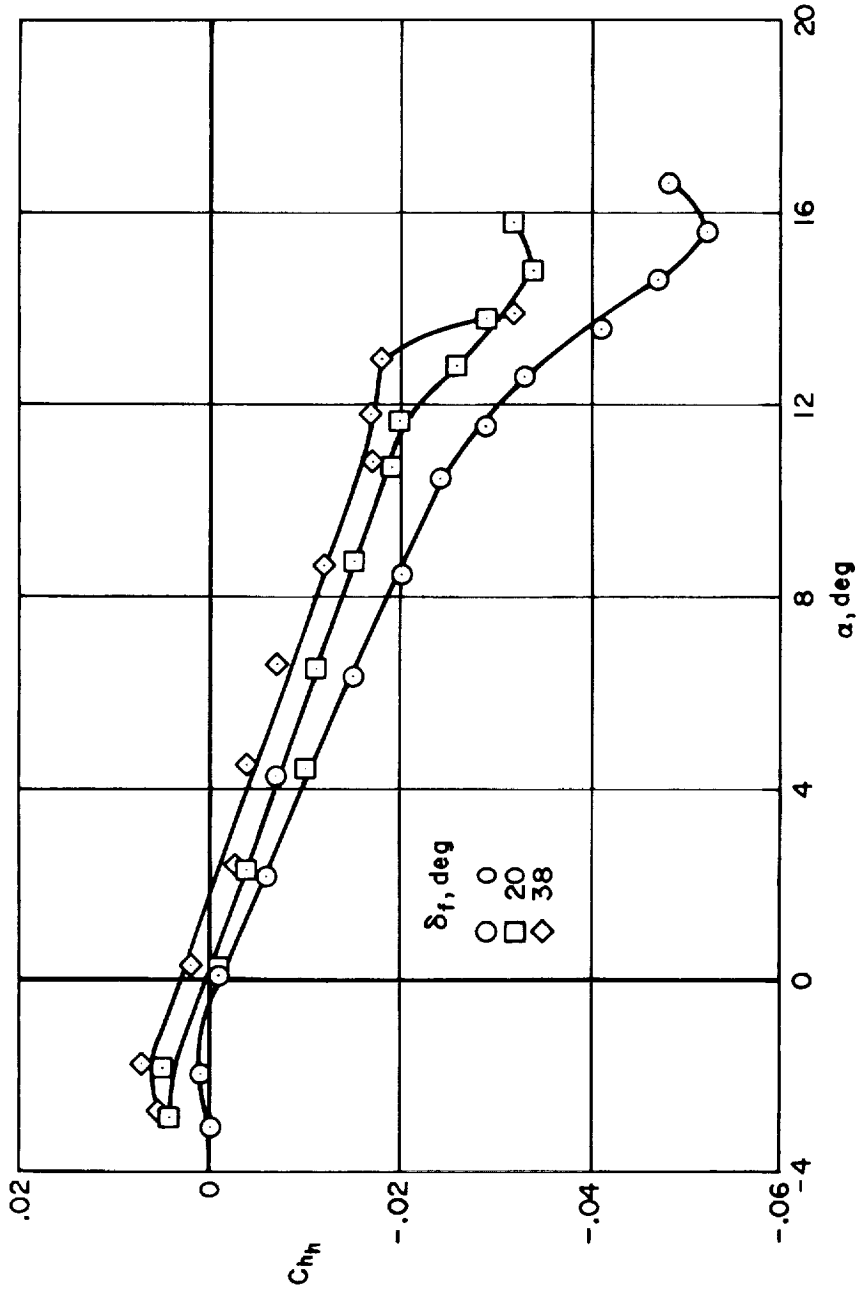

(g) Horizontal stabilizer hinge-moment coefficient versus angle of attack at three flap angles.

Figure 32.- Continued.

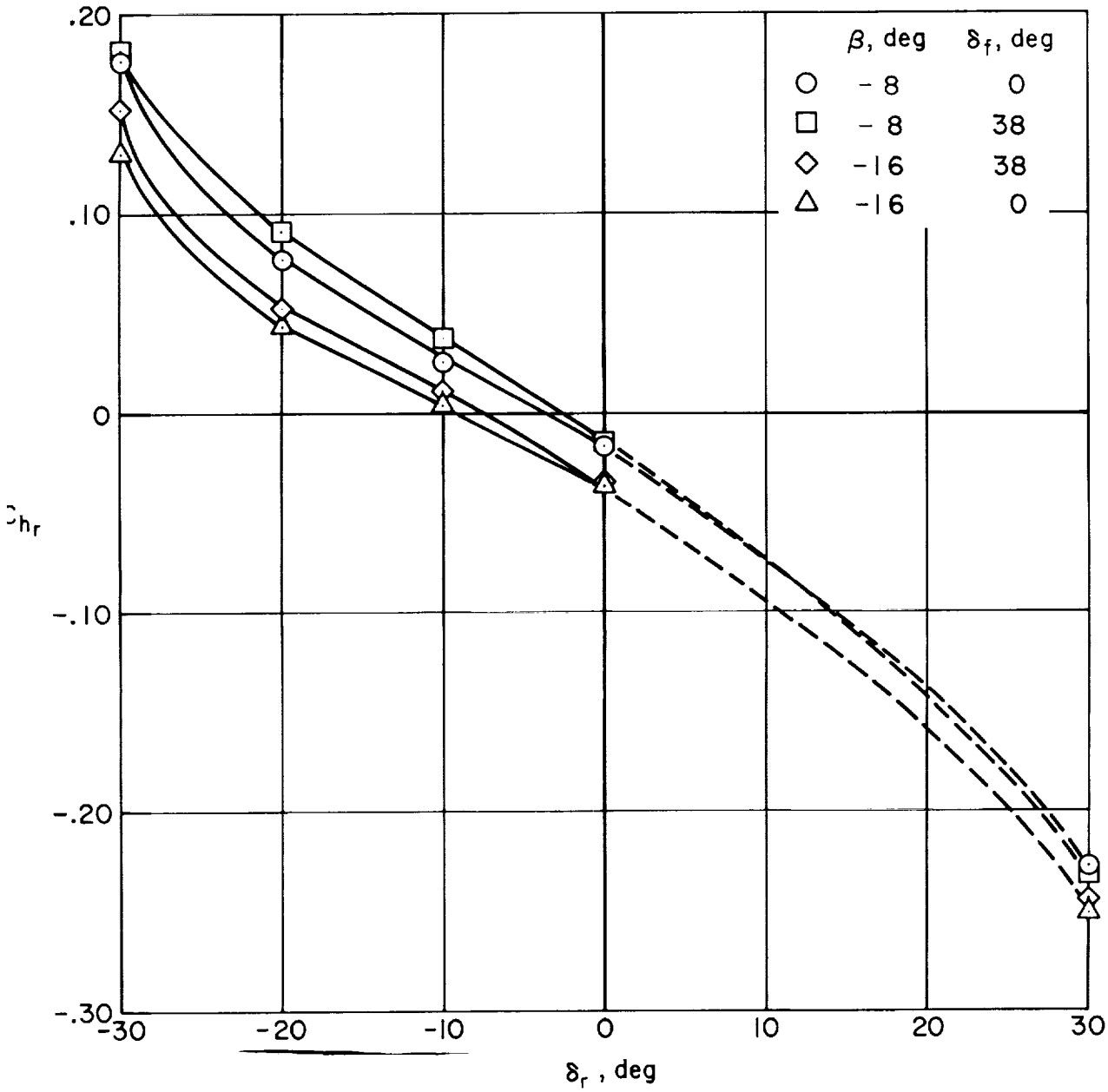

(f) Rudder hinge-moment coefficient versus rudder angle at two sideslip angles and two flap angles; $\alpha = 0°$.

Figure 32.- Continued.

NATIONAL AERONAUTICS AND SPACE ADMISTRATION
WASHINGTON, D.C. 20546

OFFICIAL BUSINESS
PENALTY FOR PRIVATE USE $300

FIRST CLASS MAIL

POSTAGE AND FEES PAID
NATIONAL AERONAUTICS AND
SPACE ADMINISTRATION

U.S.MAIL

POSTMASTER: If Undeliverable (Section 158 Postal Manual) Do Not Return

"The aeronautical and space activities of the United States shall be conducted so as to contribute . . . to the expansion of human knowledge of phenomena in the atmosphere and space. The Administration shall provide for the widest practicable and appropriate dissemination of information concerning its activities and the results thereof."

—NATIONAL AERONAUTICS AND SPACE ACT OF 1958

NASA SCIENTIFIC AND TECHNICAL PUBLICATIONS

TECHNICAL REPORTS: Scientific and technical information considered important, complete, and a lasting contribution to existing knowledge.

TECHNICAL NOTES: Information less broad in scope but nevertheless of importance as a contribution to existing knowledge.

TECHNICAL MEMORANDUMS: Information receiving limited distribution because of preliminary data, security classification, or other reasons.

CONTRACTOR REPORTS: Scientific and technical information generated under a NASA contract or grant and considered an important contribution to existing knowledge.

TECHNICAL TRANSLATIONS: Information published in a foreign language considered to merit NASA distribution in English.

SPECIAL PUBLICATIONS: Information derived from or of value to NASA activities. Publications include conference proceedings, monographs, data compilations, handbooks, sourcebooks, and special bibliographies.

TECHNOLOGY UTILIZATION PUBLICATIONS: Information on technology used by NASA that may be of particular interest in commercial and other non-aerospace applications. Publications include Tech Briefs, Technology Utilization Reports and Technology Surveys.

Details on the availability of these publications may be obtained from:

SCIENTIFIC AND TECHNICAL INFORMATION OFFICE

NATIONAL AERONAUTICS AND SPACE ADMINISTRATION

Washington, D.C. 20546